UNIVERSITÀ
DEGLI STUDI
FIRENZE

Interference Management in Next Generation Wireless Systems: Cognitive and Coordinated Approaches

Marco Pucci

Submitted to the Department of Information Engineering
in partial fulfillment of the requirements for the degree of

DOCTOR OF PHILOSOPHY

in Computer Science, Systems and Telecommunications
Cycle XXVII, Disciplinary Scientific Area ING-INF/03

January 2015

Author .....
Department of Information Engineering

Certified by .....
Prof. Romano Fantacci, Internal Thesis Supervisor

.....
Dr. Dania Marabissi, Internal Thesis Supervisor

.....
Prof. Khaled Ben Letaief, External Thesis Supervisor

.....
Prof. Giuliano Benelli, External Thesis Supervisor

.....
Eng. Giampiero Francavilla, External Thesis Supervisor

Accepted by .....
Prof. Luigi Chisci, Ph. D. Coordinator

Years 2012/2014

Interference Management
in Next Generation Wireless Systems:
Cognitive and Coordinated Approaches

by

Marco Pucci

Submitted to the Department of Information Engineering
on January 7, 2015, in partial fulfillment of the
requirements for the degree of
DOCTOR OF PHILOSOPHY

Abstract

In recent years, we have witnessed a rapid evolution of wireless communication technologies to meet the ever increasing demand of diversified mobile services. It is expected that mobile traffic volume will continue to increase in the following years with a massive diffusion of connected devices and a wide range of quality of service requirements. This represents a challenge for future wireless systems, which shall guarantee high-quality and high-data rate services into limited spectrum.

OFDMA femtocells have been pointed out by the industry as a good solution not only to overcome the indoor coverage problem but also to deal with the growth of traffic within macrocells. However, the deployment of a new femtocell layer may have an undesired impact on the performance of the macrocell layer. The resource allocation and the avoidance of electromagnetic interference are some of the more urgent challenges that operators face before femtocells become widely deployed.

Following the *primary/secondary* paradigm, low power nodes shall have *cognitive* capabilities in order to monitor the network status and optimize their transmission reducing the interference to the primary licensed system. Otherwise, some types of coordination are often used to manage each transmission and to avoid that set of issues. This is possible when both systems are aware of the presence of the other transmission point and a control channel is available to each other.

The use of multiple antennas for wireless communication systems has gained overwhelming interest during the last decade - both in academia and industry. Multiple antennas can be utilized in order to accom-

plish a multiplexing gain, a diversity gain, or an antenna gain, thus enhancing the bit rate, the error performance, or the signal-to-noise-plus-interference ratio of wireless systems, respectively. These techniques, and beamforming in particular, offer an extra degree of freedom to eliminate the interference in cognitive paradigm networks.

This thesis recaps the works done throughout the Ph.D. course. Each chapters include parts and excerpts of publications.

Chapter 1 provides a general introduction to the interference in wireless systems. Initially, a interference characterization is presented and then the interference management techniques in 4G and 5G systems are discussed. The need of heterogeneous scenarios leads to different issues and offers new solutions. In this context, the role and potentiality of the antenna arrays are treated.

In the Chapter 2 primary/secondary paradigm is described in detail. In particular, the problem of interference management by a small-cell equipped with antenna array in an actual scenario is investigated. Then, the problems that arise both during the acquisition step of the angular information or during the antenna pattern modeling are discussed. In the last part, some resource allocation algorithms are proposed in order to improve the performance of secondary systems, keeping the interference on primary under control.

In the Chapter 3, the interference management is approached from a coordinated point of view. Thus, macro-cell and small-cells cooperate to reduce the interference experienced by each user. Initially, the control link is exploited only to convey the network signaling information, useful to co-allocate users of each system on the same time-frequency elements and increase the total system efficiency. With regard to this, a resource management algorithm is proposed which exploits the knowledge of the angular distances among users by using an antenna array to shape the digital radio pattern. Subsequently, the behavior of the network is investigated when coordination increases. In this case, more transmission points can be used to convey information to users in order to increase the data-rate of the users at cell-edge and to relieve congestion of the more saturated cells.

Finally, future directions and conclusions are drawn.

Internal Thesis Supervisor:

Prof. Romano Fantacci, Full Professor
University of Florence

Dr. Dania Marabissi, Assistant Professor
University of Florence

External Thesis Supervisor:

Prof. Khaled Ben Letaief, Full Professor
Hong Kong University of Science and Technology (HKUST)

Prof. Giuliano Benelli, Full Professor
University of Siena

Eng. Giampiero Francavilla, Innovation and Software Director
Thales Italia

List of Publications

[1] G. Bartoli, R. Fantacci, D. Marabissi, and M. Pucci, "Resource Allocation schemes for Cognitive LTE-A Femto-cells using Zero Forcing Beamforming and User Selection," in *Proc. IEEE Global. Telecommun. Conf. (GLOBECOM)*, Austin, US-TX, Dec. 2014.

[2] G. Bartoli, R. Fantacci, D. Marabissi, and M. Pucci, "Coordinated Scheduling and Beamforming Scheme for LTE-A HetNet Exploiting Direction of Arrival," in *Personal Indoor and Mobile Radio Communications (PIMRC), 2014 IEEE 22nd International Symposium on*, Sept 2014.

[3] G. Bartoli, R. Fantacci, D. Marabissi, and M. Pucci, "Angular Interference Suppression in Cognitive LTE-A femtocells," in *International Wireless Communications and Mobile Computing Conference (IWCMC2014)*, Nicosia, Cyprus, Aug. 2014.

[4] G. Bartoli, R. Fantacci, D. Marabissi, and M. Pucci, "Adaptive muting ratio in enhanced Inter-Cell Interference Coordination for LTE-A systems," in *International Wireless Communications and Mobile Computing Conference (IWCMC2014)*, Nicosia, Cyprus, Aug. 2014.

[5] G. Bartoli, R. Fantacci, B. K. Letaief, D. Marabissi, N. Privitera, M. Pucci, and J. Zhang, "Beamforming for Small Cells Deployment in LTE-Advanced and Beyond," *IEEE Wireless Commun. Mag.*, vol. 21, no. 2, Apr. 2014.

[6] G. Bartoli, R. Fantacci, D. Marabissi, M. Pucci, C. Armani, and L. Niccolai, "Cognitive suppression of Multipath Interference in Angular Domain," in *Wireless Innovation Forum European Conference on Communication Technologies and Software Defined Radio (WInnComm)*, Munich, Germany, Jun 2013.

[7] G. Bartoli, R. Fantacci, D. Marabissi, and M. Pucci, "Physical Resource Block clustering method for an OFDMA cognitive femtocell system," *Physical Communications*, Oct. 2013.

[8] G. Bartoli, R. Fantacci, D. Marabissi, and M. Pucci, "LTE-A femto-cell interference mitigation with MuSiC DOA Estimation and Null Steering in an Actual Indoor Environment," in *Proc. IEEE Int. Conf. Commun. (ICC)*, Budapest, Hungary, Jun. 2013, pp. 2707–2711.

Acknowledgements

First of all, I would like to thank Prof. Romano Fantacci for the doctorate formative opportunity. In particular, the chance to face with international contexts and different academic institutions: it was an essential part of my personal growth. Sincere thanks.

In addition, I am grateful to Dania, who coordinated and addressed the work done in these three years. Her contribution has been proved several times being essential and decisive: as when she could give us a good reason to get on board on that flight.

A special thanks to colleagues and friends of the Lab with whom I shared great philosophical discussions, tiring work breaks and refreshing cocktails. Thanks to their Oriental Survival Kit, I was able to return home safe and sound in order to write this thesis.

I would also like to spend a few lines for a friend who went along with me throughout the PhD. course. With Giulio, we studied, joked around, designed source code and tittle-tattled. I'm sure a day will come when he will try again to explain to me the matrix product... Waiting for that moment, I seize the opportunity to thank him for everything else.

Finally, as every day, the last thoughts are with my lady.
As a matter of fact, there were a lot of opportunity to thank Claudia, but I just wish to tell her once again.

I dedicate this thesis to her.

Contents

List of Figures

Chapter 1

Interference in Wireless Systems

1.1 Introduction

Wireless communication has witnessed a heavy growth in term of transmitted information as a result of mobile internet, new wireless services and smart phones traffics. New radio access technologies (RAT) provide new services and high data rate everywhere. In the wireless communication systems the information is sent over radio frequency bands that may be characterized by their carrier frequency, bandwidth, propagation conditions, and interference conditions.

The radio spectrum is a common resource and hence the use of it is strictly regulated by national governments and agencies like the International Telecommunication Union (ITU). The regulation is needed to ensure that the different systems may coexist without interfering with each other. The drawback of such regulation is that spectrum allocations are rigid. Regulation is done over large geographical areas and, in particular, over long time periods, whereas spectrum is accessed locally and over short time periods. In this context, the cost of obtaining new frequency bands to exclusive use is high.

If the rules of accessing radio spectrum would be more flexible such bands could taken into secondary use locally. Such secondary use could coexist with the primary if the interference among the two is managed dynamically and locally. As the usage of wireless systems keeps increasing at a rapid rate both in terms of the data rate per user and in number of users, the wireless systems need to be continuously developed further to keep up with capacity demand. In general, higher system capacity may be achieved by improving the spectral efficiency, increasing the bandwidth, and deploying more base stations. New frequency bands are searched for in higher frequencies as well.

However, these improvements come with a cost. Higher spectral efficiency at the physical layer through e.g. use of multiple antenna techniques and spectrally efficient waveforms increases the cost of the devices. The same is true for increasing the bandwidth. Supporting multiple frequency bands (also called carrier aggregation) in a device requires careful RF design and it is expensive. Limited availability of new paired frequency bands hinders deployment of new frequency division duplex (FDD) systems. Decreasing reuse factor means that the interference among the reusing radio links increases.

In general, the interference experienced in a system can be classified in different types, since it is caused by different subjects. In a wireless system we can analyze these interferences: self-interference, multiple access interference, co-channel and adjacent channel interference.

Self interference includes interference that occurs among signals that are transmitted from a single transmitter. The specific mechanism and amount of self interference depends on the modulation type. For instance, in OFDM there may be ICI among the subcarriers due to carrier frequency offsets caused by oscillator mismatches, and the doppler effect and fast fading caused by motion of the transceivers. Another source of self interference is the transceiver non-idealities, such as amplifier nonlinearity and IQ imbalance. ISI occurs in OFDM when the delay spread of the channel exceeds the length of the cyclic prefix or guard interval, and also when the receiver is not accurately enough time-synchronized to the transmission. The interstream interference in

a multi-stream MIMO transmission may be also considered as a form of self interference.

Multiple access interference (MAI) is interference among the transmissions from multiple radios utilizing the same frequency resources to a single receiver. When multiple transmissions in cellular uplink take place simultaneously, they are interfering with each other. Even though the physical layer would allow orthogonal (in the time, frequency, code, or spatial domain) multiple access in theory, orthogonality may not be maintained in practice due to synchronization errors, RF circuitry non-idealities, and the effects of wireless propagation channel.

Cellular systems employ several mechanisms in order to maintain sufficient orthogonality in multiple access scenarios. Firstly, power control is essential. Since the terminals transmitting to the BS are distributed over the cell area, there is a large variation in the pathloss between the BS and the terminals. If all terminals would transmit with the same power the difference of the received powers can be high enough for the stronger signals to mask the weaker signals due to the limited dynamic range of the receiver.

In case of frequency division multiple access (FDMA) and OFDMA, the power on the used sub-bands or sub-carriers leaks also on the neighboring sub-bands. The ratio of the power transmitted on the desired sub-band to the power transmitted on the adjacent sub-band is called the adjacent channel power ratio (ACPR, usually given in dB). The ACPR may easily be smaller than the range of the observed uplink pathloss values (in dB) from the terminals to the BS. This means that a FDMA UL needs to be power controlled.

The uplink multiple access may have also a time domain multiple access (TDMA) component whereby there may also be MAI in between consecutive transmissions. The differences in the terminal to BS distances implies that the propagation delay of the transmissions is different among the terminals. This is compensated by a so-called timing advance, where the transmission timing is tuning accordingly.

A more recent addition in wireless systems is spatial domain multiple access (SDMA). In SDMA uplink, several users transmit on the same

time-frequency resources to the base station. When the base station is equipped with a sufficient number of antennas the signals may be separated at the BS in spatial domain. The requirement is that the uplink channels for each simultaneously transmitted symbol are linearly independent. When the channel state is known at the transmitter, the transmission may be precoded such that interference is minimized.

Co-channel interference (CCI) is interference between links that reuse the same frequency band (channel). In cellular systems this is also known as intercell interference. The cellular frequency reuse may be considered as the crucial invention of the cellular wireless communication technology, which dates back to 1945 and to United States Federal Communications Commission (FCC) [1]. In a cellular network employing frequency reuse, the band is divided to a set of orthogonal channels. The number of orthogonal channels is called the *reuse factor* of the system. High reuse factor leads to low CCI on the expense of reduced bandwidth per BS. In order to enable higher peak data rates and mean spectral efficiency, there has been a shift to a reuse factor equal to 1 as a part of the development of 3rd and 4th generation networks.

Such network is called a reuse-one network, and in it all cells may utilize the full system bandwidth and the system becomes interference limited in terms of its capacity. Even though reuse-one networks provide higher average spectral efficiency and maximize the peak spectral efficiency, they have also drawbacks. The cell-edge users will experience very low SINR levels due to the high CCI level. Depending on the scheduling principle, the variance of the SINR distribution translates to either lower average spectrum efficiency or reduced fairness. It is evident that CCI is the dominant factor limiting the performance of reuse-one wireless data networks.

Adjacent channel interference (ACI) is interference between links that communicate geographically close to each other using neighboring frequency bands. For instance, several network operators may deploy their own networks in the same area and operate on frequency bands that are close to each other. Hence, ACI needs to be taken into account in the system specifications so that it will not hamper the system perfor-

mance. In practice, the minimum coupling loss between a transmitter and a receiver on adjacent bands may be estimated and the transceivers may be designed such that ACI remains at a tolerable level. In order to do this the transceivers must utilize adequate filtering on stop-bands. The needed quality of the filters may be controlled by reserving a guard band between the bands.

A related interference type to ACI is coexistence interference (CEI) which occurs among heterogeneous radio access technologies. CEI may arise on the same frequency band or between adjacent frequency bands. Some examples include interferences between 2nd generation and 3rd generation networks and interferences between different systems operating on the unlicensed bands.

1.2 Interference management in 4G

4G cellular standards use heavy spectrum reuse (equal to 1) in order to achieve high system capacity and simplify network planning. The system capacity increase comes at the expense of SINR degradation due to increased intercell interference, which severely impacts cell-edge user capacity and then overall system throughput.

Most 4G systems, including WiMAX 802.16m [2–4] and Third Generation Partnership Program Long Term Evolution (3GPP-LTE) [5], are targeting single-frequency deployments. While the increase in capacity due to the availability of increased bandwidth can typically offset the capacity loss due to SINR degradation, the capacity of users with very weak SINR (cell edge users) still degrades. Hence, interference management schemes are critical to improve the performance of cell edge users. Both 802.16m and 3GPP-LTE, therefore, have focused on several interference management schemes for improving system performance: these techniques include semi-static radio resource management (RRM) through adaptive fractional frequency reuse (FFR) mechanisms, power control, and smart antennas techniques to null interference from other cells. Together, these techniques aim to address the aggressive re-

quirements in cell edge user throughput and absolute spectral efficiency over previous releases [2–5].

1.2.1 DL RRM

Multicellular RRM efficiently partitions resources across cells in order to manage resource interference experienced in each cell. Both 802.16m and 3GPP-LTE have focused on semi-static RRM techniques, which adapt frequency reuse across cells based on user distribution and traffic load. In particular, a mix of high and low reuse frequency resources are allowed in each cell. Resources governed by reuse 1 can be assigned to users that are closer to the center of the cell and experience less interference from other cells. The lower reuse resources are assigned to interference-limited users at the cell edge.

Allowing a combination of frequency reuse patterns overcomes the capacity limitation inherent with lower frequency reuse, while also retaining a low interference environment to retain throughput and coverage for cell edge users. It is very important to notice that the definition of what constitutes cell center vs. cell edge users is an important part of FFR design: this is typically based on SINR metrics rather than actual user location within the cell.

The actual power allocation across the frequency partitions is a function of user distribution across the cell and is optimized cooperatively by cells based on their user feedback. Resource power allocation across the sectors results in an associated cost for each partition, which captures the spectral efficiency (SE) penalty implied by lower reuse. For example, a resource belonging to a hard reuse 3 partition will use three times the cell bandwidth when compared to one in a reuse 1 partition, hence will incur three times the cost in terms of lowered spectral efficiency. This cost-weighted spectral efficiency associated with a resource is referred to as the normalized spectral efficiency and is computed as

$$Normalized\ SE\ (resource) = \frac{Expected\ SE\ (resource)}{Resource\ Metric\ (partition)}.$$

The resource metric indicates the cost or spectral efficiency penalty associated with the soft reuse factor of the partition. The normalized spectral efficiency indicates the true spectral efficiency of a given partition, and is used to determine the preferred FFR partition (PFP), corresponding to the maximum average normalized SE, for each user. Dimensioning of the FFR partitions and the associated resource metrics is based on cooperative sharing of the PFP by all users in the system. Various optimization schemes may be used to derive the optimal FFR parameters from these reports. The exact algorithm is implementation-dependent.

In 802.16m, the initial FFR partitions and the corresponding Resource Metrics are available to users as broadcast information. Upon network entry, the user measures the average SINR on each frequency partition and computes an average normalized SE. It then computes the maximum normalized SE across all FFR partitions and reports the corresponding partition as its PFP. These PFP reports are aggregated across base stations in the system to update the FFR configuration, including partitions size and power level. The user will also report channel quality indicator (CQI) metrics on the best M resources in the preferred FFR partition. These metrics are used by the BS for dynamic resource allocation among users in a cell. The BSs can adjust the resource metrics periodically to ensure adequate use of resources across partitions. Such updates may happen locally at the BS level unless a consistent trend in use of a particular partition is observed. The BS may report this trend to the central RRM function for it to make the necessary changes in the FFR partition configuration. Thus, the FFR configuration may be managed through faster but localized updates of the resource metrics coupled with a slower but more system-wide change to the FFR partitions and configuration.

The 3GPP LTE standard allows for very generic FFR schemes to be implemented in the DL, depending on the distribution of mobiles or traffic load. The basic mechanism is the use of a relative narrowband transmit power (RNTP) indicator, which is exchanged between BSs on the X2 interface [6]. The RNTP is a per physical resource block (PRB)

indicator which conveys a transmit power spectral density mask that will be used by each cell. This feature results in arbitrary soft reuse patterns being created across the system. The idea would be that each cell would have a specific sub-band for which it will generate low interference with its reduced transmit spectral density. The DL scheduler can exploit this induced frequency selective interference in one of two ways. First, if frequency selective sub-band CQI reporting is used, these CQI reports will inform the scheduler that there is a particular sub-band which has low interference and hence improved CQI. Second, if wideband CQI reporting is used to reduce the uplink overhead, the scheduler can be made aware of the identity of the strongest interfering cell for a particular mobile it is serving. Based on knowledge of which cell is causing the dominant interference in the DL, the scheduler can consult the RNTP report from this cell to see which sub-band is being transmitted at reduced power and hence generating less interference, and can choose to schedule mobile in that sub-band so that it experiences higher SINR.

1.2.2 UL Power Control and FFR

Orthogonal frequency-divison multiple access (OFDMA) systems operate with tight synchronization across cells, and the main source of interference is intercell interference. Power control is not typically used in the DL in order to avoid dynamic fluctuation in signal power across resources. However, uplink power control is crucial for managing intercell interference.

Open loop power control is used for data transmission in 802.16m: in this case power levels are adjusted to track long-term fading while fast fading variations are tracked through adjustments in adaptive modulation and coding. Closed loop power control is enabled only for control channels. Open loop uplink power control in 802.16m is designed to manage the average interference in the system to some desirable interference over thermal (IoT) level. Specifically, the power update algorithm is derived based on the concept of maximum sector throughput,

in which power is increased for a user if the gain in spectral efficiency is greater than the net spectral efficiency loss in other cells due to the increased interference.

The uplink power control specification in 3GPP LTE allows for a wide variety of power control modes to be utilized. In 3GPP LTE, the baseline uplink power control method for transmissions on the PUSCH is an open loop power control but aperiodic closed loop power control corrections can be sent by the BS in the uplink scheduling grant.

The closed loop power control rate is typically chosen to be much faster for the PUCCH due to the tight QoS constraints and lack of HARQ. The power control mode can be set to accumulate commands received over multiple subframes [7]. For example, the uplink scheduler can maintain an internal uplink target SINR for mobile, and based on the SINR measured on the uplink, the uplink scheduler can send closed loop power control corrections in the accumulated mode to adjust the mobiles transmit power achieving the target SINR. However, unlike 802.16m, the LTE specification does not allow the DL SINR to be used as part of the open loop power control set-point. Instead, a longterm DL SINR measure can be inferred from long-term averages of the CQI. One advantage of the DL-SINR-based method over the fractional power control (FPC) method is that it allows differentiation of mobiles that may have low path loss but generate a high amount of interference, such as mobiles located to close the BS but near the sector boundary. One disadvantage of the DL-SINR-based method in the 3GPP LTE context is that it depends on the CQI feedback from the mobile, and there may be notable variability in the CQI measurement reports for the same radio frequency (RF) condition from different mobile manufacturers.

Finally, in 3GPP LTE a high interference indicator (HII), which is defined per PRB, can be exchanged between cells via the X2 interface [8] to implement uplink FFR. A HII bit set to 1 for a particular PRB means that this PRB has high sensitivity to uplink interference for this cell; when the HII bit is set to 0 for a particular PRB, it signifies that this PRB has low sensitivity to uplink interference. The exchange of HII reports between cells allows the creation of fractional reuse patterns

through uplink scheduling and power control. In this way, the uplink scheduler in a given cell can intelligently choose to schedule mobiles that generate lower interference to this neighbor cell only in those PRBs for which the HII report high sensitivity.

1.3 Interference management in 5G

As 4G cellular systems deployment densify, co-channel interference becomes a major source of obstacles to cell throughput improvement. Although some network-side solutions for co-channel interference management have been introduced in current 4G standards, it turns out that most of those solutions yield only poor gains in realistic environments. Network-side interference management needs to be complemented by UE-side interference management to realize true factor-one reuse.

Among all the limitations of 4G systems, high co-channel interference in the downlink is one of the biggest concerns, as the densely overlaid heterogeneous network deployment with full resource reuse is considered inevitable in future cellular systems. As a matter of fact, co-channel interference management has driven recent LTE releases, and two important features such as intercell interference coordination (ICIC) and coordinated multipoint (CoMP) communication have been introduced. Basically, the interference management in 4G LTE is mostly a network-side operation and transparent to receivers. Network-side interference management is beneficial to ensure backward compatibility with legacy users and easy to deploy by extending the legacy network. However, putting the responsibility for interference management only on the network entails lots of practical issues and limitations in particular for what concern the backhaul and the feedback overheads.

Although it has been considered an implementation issue and not discussed much in LTE, the UE-side interference management can be a solution to reduce the network-side interference management issue [9, 10]. Recently, it has been pointed out that UE-side interference management can provide significant synergy with the network-side counterpart [11], and, in Release 12, a study on UE-side support was begun

but it is still premature. Based on the learning from recent studies and 4G, advanced interference management (AIM) techniques will be likely the key driver of 5G. Moreover, while the interference management schemes in 4G are quite implementation-specific, the AIM techniques in 5G should be concretely specified and controlled by the standard for fast network deployment and different manufacturers interoperability.

1.3.1 Towards advanced UE receivers

In conventional cellular systems, the receivers mainly presume a noise-limited operational scenario. In this case, the receivers can easily be designed based on either optimal approaches, such as maximum-likelihood (ML) and maximum a posteriori probability (MAP) criteria, or suboptimal approaches, such as zero-forcing (ZF) or minimum mean square error (MMSE) equalization-based architectures. However, most modern wireless cellular systems are often dominated by strong co-channel interference among neighboring cells rather than thermal noise.

The interference is distinguished from the noise in its statistical and physical characteristics; rather than being normally distributed as is thermal noise, the interference have a similar structure to the desired signal because they are signals in the other cells. In the previous cellular systems the interference was treated as part of the thermal noise since there was no practical way to handle the difference.

In the next generation cellular systems, proper treatment of strong interference is required for further performance improvement; thus, a new receiver design featured with AIM is essential. By AIM at the receiver, or simply by an advanced receiver, the receiver is able to take advantage of the structure of the interference signals, including modulation constellation, coding scheme, channel, and resource allocation. In the previous cellular communication standards, receiver technologies have not been touched specifically because they were regarded as an implementation issue concerning only the manufacturer. However, there is huge potential and synergy when the UE-side AIM is considered in conjunction with the network-side AIM.

1.3.2 Practical Challenges

The advanced receiver and joint scheduling techniques bring performance gains over conventional systems, such as reduced data decoding error rates and increased system throughput. Although advanced receivers and joint scheduling schemes promise a huge theoretical gain, there still remain a number of practical issues we need to face toward real implementation.

In a practical cellular deployment, there can be more than one interference signal. Facing all these interference signals is quite challenging to the receiver. However, the performance are usually dominated by a set of few interferers: in fact, the their received power is far higher than the noise level and comparable to the desired signal and it is sufficient to consider only one or two dominant interference signals.

Moreover, a certain piece of information on the interference is required for the AIM. Firstly, the interference channel needs to be estimated reliably for interference detection and decoding. In addition, modulation and coding schemes, and finally resource allocation of the interference signal, can be provided by the network through control signaling. As long as the signaling overhead is a concern, some extra information can be detected blindly at the receiver without explicit signaling. However, this can increase the processing load of the receiver, and worsens the performance when the estimation is not reliable.

Joint scheduling requires the Transmission Point (TP) to be aware of the receiver characteristic as a function of the interference signal rate. Many cellular systems, including LTE, attribute this information to the CSI feedback from the UE. With conventional receivers, a single CSI report per UE was assumed, since the receiver characteristic is not dependent on the interference signal rate. However, with advanced receivers, a single CSI report may be too short for describing the relationship between the receiver characteristic and the interference signal rate. To address this problem, a multiple-CSI feedback framework can be used, as already done for CoMP in LTE Release 11. In this framework, each of the multiple CSI reports is based on different interference hypothe-

ses, which correspond to different points on the receiver characteristic curve.

The role of joint scheduling is to jointly determine serving UEs and transmission schemes for a set of multiple TPs, to which we refer as a cluster, so that the overall utility function of the cluster is optimized. This joint scheduling, depending on the specific scheme, can be implemented in either a centralized or distributed manner.

In the centralized case, all the required information is first sent from the TPs within the cluster to the central controller which determines all the calculation and sends a corresponding scheduling data to each TP. Although centralized schemes often outperform distributed schemes, they suffer from a heavy processing load and proper backhaul.

On the other hand, in the distributed case, each TP does its own calculation and exchanges a small amount of summary information with the others for overall coordination. The distributed schemes are beneficial when the cluster size is very large since generally the amount of this summary information is very small. In many cases, the distributed schemes are iterative and suffer from large delay.

Whether centralized or distributed, message exchange among different TPs, often geographically apart, is inevitable. The message exchange is realized through the backhaul links interconnecting different TPs, which are usually high capacity/reliability and low-latency connections. However, the backhaul links are still non-ideal and will become restrictive as the backhaul requirement grows in the next generation cellular standard.

1.4 Interference management in Heterogeneous Networks

The popularity of wireless networks has lead to the increased capacity demand because ever more users prefer wireless technology as compared to wired services. The wireless access mainly consists of two technologies, the wireless cellular networks, that provide voice services to users

with high mobility, and the wireless local area networks (WLANs), more suitable to provide higher data rates to restricted mobility users [12]. Nowadays, the wireless cellular networks have evolved towards providing high data rate services to their users and thus, striving to replace the WLANs as well [13]. Standards like 3GPPs High Speed Packet Access (HSPA), Long Term Evolution (LTE) and LTE advanced, 3GPP2s Evolution-Data Optimized (EVDO) and Ultra Wide Band (UWB) and Worldwide Interoperability for Microwave Access (WiMAX) have been developed to provide high speed communication to end users [14] and to face up this increasing demand.

High demand for cellular services can originate from indoors and this is the reason that leads cellular networks to provide good quality coverage in these contexts. Due to the penetration losses, the indoor user requires high power from the serving BS, therefore other users would have less power and the overall system throughput may be reduced. Moreover, having a large number of outdoor BSs to meet the needs of a high capacity is also very expensive. The modulation and coding schemes for high data rates used in the standards mentioned above, require good channel conditions, which means that in the case of indoor coverage, QoS cannot be guaranteed due to the variations in channel conditions [15].

This emphasizes the need of having some indoor coverage solutions, for example picocells, Distributed Antenna Systems (DAS) and relays or repeaters. Picocells are very small cells, providing coverage to a limited indoor area [16]. These are located inside large buildings, which are categorized as hotspots (e.g airports, shopping malls, universities). Picocells work the same way as macrocells and are connected to each other and macrocell BSs through cables. The DAS is another good solution for the indoor coverage problem. This system is made up of a number of distributed Antenna Elements (AEs) and a Home BS [17]. The antenna elements are connected to the Home Base Station offline through dedicated lines, usually optic fibre cables or dedicated RF links. This can provide good quality communication to areas where outdoor BSs cannot reach. In addition to good quality indoor coverage, DAS

can also reduce the transmit power which leads to reduced interference and hence high capacity. Although picocells and DAS provide good and cost effective alternatives as compared to the older outdoor macrocell network, these are still too expensive to be deployed for home and small office users. Moreover, the overall network processing load would also increase as the number of picocells increase.

The relaying in LTE advanced for the indoor environment [18] is an interesting hot-topic. As LTE advanced is set to provide high data rates to end users, it would also require an indoor system where it can provide full functionality to the indoor users. In this approach a wireless relay is placed inside a building to compensate the penetration loss caused by the walls of the building.

With the growing demand of innovative 3G services, a significant potential for the access to the network are the so called femtocells [13–15]. Femtocells, also known as Home Base Station are small, low power access points and visually look like an ordinary wireless router. These indoor access points may be installed also by the users, which creates a small wireless coverage area and connect user equipment (UE) to the cellular core network through subscribers broadband internet access [14, 15]. The access point known as Femtocell Access Point (FAP), works as BS, enabling high quality voice, data and multimedia services to be delivered to mobile devices in indoor (or outdoor) settings. The FAP can be connected to the operators core network through users DSL, optical fibre or cable broadband connection. Femtocells would require some portion of spectrum from the operators for its operation. This can be a separate portion of spectrum allocated by the operator or the same portion of spectrum as used by macrocell [19]. In the latter case the issue of interference arises. This interference can be between neighboring femtocells as well as between femtocells and macrocell.

Femtocells are deployed within a macrocell in an ad hoc mode and any user can deploy femtocells in its home and even can move femtocells from one location to another. Therefore, it is a challenging problem for operators to manage radio resources dynamically [20]. It also requires efficient self organizing techniques to make sure it is aware

of its surrounding environment and should have distributed optimizing techniques to mitigate any interference. Furthermore, in case of dense co-channel femtocell deployment where spectrum shortage may occur, it is also desirable for the femtocell to have the functionality of opportunistic spectrum access. This requires that the femtocells should have cognitive functionalities, which makes it more intelligent.

Cognitive femtocells have the capability to sense spectrum in the surrounding environment to locate any vacant spectrum portions. These spectrum holes are then used by the cognitive femtocells to provided connectivity to its users. They can collaborate and cooperate with neighboring cognitive femtocells for more accurate spectrum sensing. The femtocells became main stream technology when the 3GPP release 8 introduced them and it is likely that the future LTE networks would include femtocells for the indoor cellular coverage. Thus, femtocells will be deployed at a large scale in the near future.

1.4.1 Technical and Business Aspects

Femtocells can provide a better solution for the indoor coverage problem. Basically due to small cell radius, the distance between transmitter and receiver is reduced, hence transmitted signal is less attenuated and in turn receiver can receive a good Received Signal Strength (RSS). The penetration losses, due to walls acting as insulation to the femtocells, make the interfering signals weaker: so the femtocells transmit with low power while maintaining good indoor coverage quality.

Furthermore, a femtocell usually serves a very small number of users as compared to a macrocell, due to which, it can devote a large portion of its resources to the available users. This enables femtocells to provide good QoS to its users as compared to macro BS which have to serve many users simultaneously in a large area. Femtocells can solve the spectrum underutilization problem for the regulators. As there are small cells, the channels are re-used more often.

Two main modes of femtocell deployments are common: separate channel and co-channel deployment. In a separate channel deploy-

ment, a specific channel is allocated for the femtocell network, which is not used by the macrocell avoiding interference between femtocell and macrocell users.

In the co-channel deployment, the femtocell uses the same channels as the macrocell [19]. This is much prefered by the operators because dedicating a certain portion of spectrum for femtocells might be expensive. The co-channel deployment also increases the overall system capacity. On the other hand, there is a greater risk that femtocell and macrocell users causing interference to each other [19]. Thus efficient and intelligent interference management is required for a successful co-channel femtocell deployment.

With the benefits of larger capacity, femtocells also provide a viable solution to outdoor coverage problems. The coverage holes in the footprint of a macrocell can be eliminated with femtocells because they can provide coverage to macro-cellular users which are nearby and in their range. This property of femtocells can be of importance at the macrocell edges.

The development of 2G femtocells was not a great success and many manufacturers avoid manufacturing it because of its drawbacks and economic viability. The main disadvantage is that a GSM femtocell, for data service uses General Packet Radio Service (GPRS), which does not provide high data rates. Hence, the use is only limited to good quality voice. 3G femtocells are mainly based on the air interface of Universal Mobile Telecommunication system (UMTS). The UMTS technology has the capability of connecting through IP based networks, which make it more applicable to femtocells. Unlike the GSM based femtocells, the 3G femtocells have better power allocation schemes, which can be used to avoid causing interference to the macrocell users. The UMTS femtocells are also standardized by the 3GPP as HNBs [21] and this is one of the main reasons that encourage manufacturers in the development of such femtocells. OFDM based femtocells provide a variety of high data rate services to the end users [22]. It is also a hot research area nowadays and a lot of research is going on in order to efficiently implement LTE femtocells in the future [23–27].

Femtocells can provide an excellent platform for the operators to maximize their revenue, increase network capacity without any further investment in the old macro cellular network. With the penetration of smart mobile devices, offloading the macro network is an crucial hot topic for mobile operators due to the extensive use of the broadband network. The femtocell faces competition from the already existing and mature Wi-Fi [28]. The femtocell should provide reasonable prices as well as better and versatile services as compared to Wi-Fi, in order to attract more customers.

One of the main drawback is that a user must have a broadband internet connection in order to use femtocells and also the QoS depends on the backhaul connection. The role of user broadband internet connection as backhaul link can also be of benefit to the operators and they can offer two services (broadband internet connection and femtocell) to a user and thus increase the overall revenue.

1.4.2 Access mode, Mobility, Self-Organization and Security Issues

Currently three access modes have been defined for a femtocell [29].

- Open Access mode: Every user can access the femtocell in this mode and benefit from its services.
- Closed Access mode: in this mode, only specific users can access a femtocell. The owner can decide as to which user can access the femtocell.
- Hybrid Access mode: this access mode only allows particular outside users to access a femtocell. The conditions of access to a femtocell by an outside user can be defined by each operator separately and entry to any guest or new user can be requested by the owner.

The open access mode can be used in public areas like airports, shopping malls and universities to provide good coverage to the users in that

area [30]. Home users generally prefer closed access mode, but in this mode, any outside users near the femtocell experiencing high signal levels from the femtocell would not be able to access the femtocell, thus causing interference. Access modes have a direct impact on the interference experienced in the system and therefore, it should be carefully selected after much analysis.

Femtocells are mainly intended for indoor users and thus no specific mobility management is necessary. However, in dense femtocell deployment scenario there may be useful manage some mobility and handover procedures [22]. A femtocell can have a large number of neighbors and these neighbors are created on an ad hoc basis, making it difficult to constantly keep track of neighboring femtocells. Handover in femtocells highly depends upon the access mode being used. In the open access case, the number of handover could be very large, while it is likely reduced in closed and hybrid access modes [31].

Femtocells are deployed by end users and can be turned on and off at any time, hence the deployment is completely random. The number and locations of femtocells continuously change into the macrocell coverage. This makes the classic network planning and design tools unusable. The femtocells need to be intelligent enough to autonomously integrate in the preexisting radio access network [32], and self configure and optimize without causing any impact on the existing cellular system. Two approaches in [27] propose cognitive capabilities for an OFDMA based femtocell. First, the femtocells dynamically senses the air interface and then tunes the sub-channel allocation according to the sensing results.As the number of femtocells increase in an area, the problem of self organization would become more challenging and hence there is a need of more innovative solutions.

Providing efficient security to femtocell networks is one of the other key challenges. In the case of open access mode, security is of much importance as the users private information needs to be protected. The femtocell network is subject to many security risks. The femtocells are also prone to Denial of Service (DoS) attacks. A hacker can overload the link between a FAP and mobile core network. This would prohibit

a subscriber to connect to the core network and the femtocell service would not be available. Security is also required to prevent unwanted users to access a femtocell network and use the resources. This is mainly for the close access mode, where only specific users can access [33].

Due to these threats, operators and manufacturers provide some level of security. Mainly the Internet Protocol Security (IPSec) is used to provide security to the link between FAP and operators core network. There is a security gateway in the operators core network and when the FAP wants to connect to the core network, a secure tunnel is established between them. All the data to and from the femtocell travels through the secure tunnel, hence making the data more secure [34].

1.4.3 Type of Interference and Management Techniques

Due to the deployment of small indoor base stations, the cellular architecture changes and now it consists of two tiers or layers [16,19,26,35,36]. The first tier is the conventional macro-cellular network while the second tier or layer is the femtocell network.

The femtocell layer is unplanned and it is made up of random distribution of femtocells. This has a number of advantages in term of capacity, coverage and quality [20]. However, the new architecture also brings forth new problems and design challenges. Among these challenges the interference management is the most important [37]. The femtocell is preferred to be deployed in co-channel fashion in order to achieve higher capacity. This in return, gives rise to severe interference management challenges [38]. Observing this scenario, the two-tier architecture enables to divide the interference in to two main types.

Co-tier Interference

This type of interference consider the interference caused by network elements that belong to the same tier of network [15]. In the case of femtocells, it is the interference caused to a femtocell by another femtocell. Usually the femtocells causing interference to each other are

immediate neighboring. The small cells deployment is random and they can be palced very close to each other in apartments, where the wall separation might not be enough to avoid causing interference to each other. The access methods used in femtocells have a huge impact on the overall interference. The co-tier interference is more severe in closed access as compared to the open access [39]. The dead zones also depend on the QoS requirement of each service. If a service requires higher SINR, it might not be possible to provide the service near the windows or edges of a femtocell.

The uplink co-tier interference is caused by the femtocell user equipment (UE) that acts as a source of interference to the neighboring small cells. In particular, the 3G system like UMTS and High Speed Uplink Packet Access (HSUPA) applies intelligent power control techniques to limit the uplink interference. In the case of OFDMA femtocells, the FAP should sense the surrounding radio environment for certain sub channels. A UE would require certain number of sub channels depending on the QoS, the FAP should then allocate sub channels that are subject to lower level of interference. As compared to the CDMA, the OFDMA system provides better chances of avoiding interference due to the division of spectrum into small and flat sub channels [25].

The downlink co-tier interference is caused by an FAP. High chance of power leaks through windows, doors and balconies must be considered due to the close deployment of femtocells. To avoid such interference the 3GPP recommends using adaptive power control techniques at FAPs which becomes more important in the case of closed access femtocells since a UE is not served by the strongest FAP but by the one to which it is subscribed.

Cross-tier Interference

This type of interference is caused by network elements that belong to different layer of the network. Small cells would cause large amount of interference to neighbors that are using macrocell services for indoor purpose. This problem becomes more severe in the case of closed access

mode [39]: in fact, a macro UEs would receive strong signals from the neighbor, to which access is denied forming some huge dead zones.

In the case of OFDMA, two types of uplink cross-tier interference can occur. If a femtocell UE is transmitting with high power on certain sub channels near a macrocell BS, these sub channels become unusable for the macrocell BS and hence the overall efficiency is reduced [16]. The downlink cross-tier interference can be caused by an FAP to a close by macrocell UE [15]. The downlink interference management is mostly dependent on the allocation of sub channels. The FAP would not cause any interference to a macrocell UE, if the macrocell UE uses a different set of sub-channels.

The types of interference are perceived differently in different air interface technologies. Each of these technologies uses different techniques to manage the co-tier and cross-tier interference. The research is still going on in this area and many schemes have been proposed.

Interference Cancellation in Femtocells

These are schemes that reduces interference at the receiver end; the interference is cancelled after the signal is received. The interference cancellation is defined by Andrews [40] as the class of techniques that demodulate/decode desired information, and then use this information along with channel estimates to cancel received interference from the received signal.

Two classical ways of interference cancellation used extensively in wireless networks are Successive Interference Cancellation (SIC) and Parallel Interference Cancellation (PIC) [40, 41]. PIC detects all users simultaneously. The initial estimate may be used to cancel interference in near future and, in this way, parallel detection is repeated again over several stages. The PIC is also known as multistage interference cancellation [42]. On the other hand, SIC detects one user per stage. The strongest received signal is detected first, then the next strongest, and so on [43].

PIC has decreased latency but higher overall complexity because N number of users must be detected in parallel and there are P cancellation stages. Latency is proportional to P, which is much smaller than N for cellular systems, but complexity is proportional to PN. SIC have complexity and latency proportional to N, and this latency may be unaffordable if there are many users with real time data [40].

In this context, Multistage SIC represents the smoother trade off between the two techniques [44]. A group of users are detected in parallel, and then has their aggregate interference subtracted from the composite received signal, and then another group is detected in parallel. The main part of interference cancellation techniques require knowledge about the interfering signal characteristics. It also requires antenna arrays at the receiver system to cancel any interference. All make these techniques less suitable for UEs and they are mostly suitable for implementing in base stations and hence mostly used for the uplink interference management [45].

Interference Avoidance in Femtocells

Managing smal-cells from a centralized controller is very hard due to the ad hoc nature of the heterogeneous deployment. It is therefore preferred to induce some intelligence into the small-cells, to enable it to self organize and address interference without any outer controller.

To cope with the cross-tier interference, initially spectrum splitting was suggested [46]. It was recommended that a spectrum band should be divided into two portions. One portion should be allocated for macrocell users and the other portion for femtocell operations. This approach lead to reduced efficiency due to the high cost and scarcity of spectrum. Since femtocells can operate as plug and play devices, it is also hard to know the exact number of femtocells at a given time, thus, this approach seems impractical.

Power control is a key technique in the interference avoidance, especially in dense femtocell deployment. If the transmit power of a femtocell is controlled and optimized, the outdoor macrocell UE can be protected

sufficiently. The drawback of this technique is that it is complex and time consuming and would not be feasible to implement in a small-cell. A simple technique in [47] provides power control to femtocells to avoid interference to nearby macrocell users. In this case the assumption is that the femtocell takes information about macrocell users from the macrocell base station. Once the macrocell user is interfered, the nearby femtocell reduces its power accordingly.

The OFDMA system design provides much flexibility for what concern the interference avoidance schemes [24]. The OFDMA small-cell needs to know about its surrounding environment which enables the FAP to have more detailed measurement reports from the users and hence allocate sub channels more efficiently. The spectrum would be divided in to two main portions. One portion would be dedicated to macrocell operations, while the other one for femtocell. However, there still can be Inter Carrier Interference (ICI) and Multiple Access Interference (MAI) due to lack of synchronization, leading to meager orthogonality. This problem turn even more severly in dense femtocell deployment scenarios.

There is always a trade off between spectrum utilization and co channel interference depending on the type of deployment, i.e. co channel, dedicated channel. In order to keep a balance, in LTE systems, the deployment of femtocells also known as HeNBs can be set to a partial co channel deployment. In this deployment scheme, some channels are reserved for the usage of macrocell, while other channels are shared between macro and femtocells. Several works about eICIC show this technique. Resource allocation is very relevant in OFDMA systems (as in the previous technologies) and various schemes have been proposed, such as the Round Robin (RR) and Proportional Fair (PR) schemes [35]. On the other hand, allocating sub channels that reduce the interference and increase the Area Spectral Efficiency (ASE) is desired for femtocell.

A femtocell having cognitive capabilities can avoid interference by using its spectrum sensing functionality. The femtocell can sense the environment and is able to recognize an interference signature [48]. This interference signature enables a femtocell to select specific channels that

are not subjected to the surrounding interference. The main idea is to reuse any available channel that does not cause interference to the macro or to other small-cells.

In [49] a similar interference avoidance OFDMA scheme for cognitive small-cells is presented: based on the closed access mode, it avoids the cross tier interference between femtocell and macrocell. This would be done by stressing the femtocell to use resource blocks that are used by macro UEs spatially far away from the small-cell.

Distributed Interference Management Schemes

In general, femtocells have limited knowledge about the global femtocell network which makes the centralized techniques very difficult to deploy. Probably, providing sufficient knowledge to the femtocells this approach could be applied, but this would cause much congestion on the backhaul network. Furthermore, as the number of femtocell can be very large, this makes it impractical for the operator to provide large information to the femtocell through the backhaul. In this case, distributed schemes are much more suitable.

Development of distributed coverage optimization algorithm can be challenging due to the lack of global information and central control. The algorithm in [50] runs individually on each FAP in order to achieve user load balancing and minimization of coverage holes.

Game theory has been used in network resource allocations and is also used in femtocells for power allocation scheme. One such scheme is proposed in [51], where a decentralized power control algorithm that considers loads of individual femtocell is proposed for closed access femtocell networks. In this case, the algorithm is based on a non cooperative game model and the properties of a super-modular game are used to implement the decentralized power control algorithm. This shows that the power of femtocells with less user load is reduced more as compared to femtocells with more users.

The problem of co tier interference is also addressed in a distributed algorithm [52] where fractional frequency reuse factor (FFR) is adjusted

according to the environment. This is done with the help of femtocell location and interference information. In fact, it classifies femtocells into different groups, where sub channels are allocated first to avoid interference and then allocation of transmit power takes place according on the received signal strength information (RSSI).

The efficiency of an interference management scheme depends on the specific femtocell scenario. In case of less dense deployment, simple schemes can be helpful and provide sufficient interference management for both the macrocell and femtocell network layers. The main aim is to enable femtocell to be deployed densely and hence, efficient interference management schemes that can cope with the ad hoc nature of femtocells and provide QoS to both macrocell and femtocell users should be developed. It should also be kept in mind that these are small low powered devices and should be able to handle the complexity of these schemes.

Femtocell limitations should be studied and the schemes should be able to overcome them. In the centralized schemes, a central entity which can provide information about the surrounding global scenario is needed. Also communication links between femtocells and the central entity are needed, which can create extra burden and delay. On the other hand, this can also save the femtocell a lot of processing overhead required for sensing the environment and using this information. Moreover, distributed techniques provide much flexibility. The femtocells can take their own decisions based on their local environment and also exchange information with its neighboring femtocells. As compared to the centralized schemes, the distributed schemes are more complex and require self organization and self optimization capabilities.

1.5 Role and impact of MIMO Systems

In recent years, there has been a shift to wireless multimedia applications, which is reflected in the convergence of digital wireless networks and the Internet. In order to guarantee a certain quality of service, high bit rates and good error performance are required. However, the main issues related to the wireless channels, mainly caused by multipath sig-

nal propagation and fading effects, make it challenging to accomplish both of these goals at the same time because, given a fixed bandwidth, there is always a fundamental tradeoff between bandwidth efficiency (high bit rates) and power efficiency (small error rates).

Conventional single-antenna transmission techniques aim to operate in the time and/or in the frequency domain and channel coding is typically used in order to overcome the detrimental effects of multipath fading. However, with regard to the ever-growing demands of wireless services, the time is now ripe for evolving also the antenna part. In fact, when utilizing multiple antennas, the previously unused spatial domain can be exploited. The great potential of using multiple antennas for wireless communications has only become clear during the last years.

In particular, at the end of the 1990s multiple-antenna techniques were shown to provide a novel means to achieve both higher bit rates and smaller error rates. In addition to this, multiple antennas can also be utilized in order to mitigate co-channel interference, which is another major source of disruption in cellular wireless communication systems and therefore multiple-antenna techniques can represent a key technology for modern and future wireless communications [53].

Spatial multiplexing techniques simultaneously transmit independent information sequences or layers, over multiple antennas. Using M transmit antennas, the overall bit rate compared to a single-antenna system is thus enhanced by an M factor without requiring extra bandwidth or extra power. Channel coding is often used, in order to guarantee a certain error performance and to keep layers separated. The achieved gain, in terms of bit rate, is called multiplexing gain.

Multiple antennas can also be used to improve the error rate of a system by transmitting and receiving redundant signals representing the same information sequence. By means of two-dimensional coding in time and space the information sequence is spread out over multiple transmit antennas. Later, at the receiver, an appropriate combining of the redundant signals has to be performed and optionally, multiple receive antennas can be used in order to further improve the performance. The

advantage over conventional channel coding is that redundancy can be accommodated in the spatial domain, rather than in the time domain.

Finally, multiple-antenna techniques can also be utilized to improve the signal-to-noise ratio (SNR) at the receiver and to suppress co-channel interference in a multiuser scenario. This is achieved by means of an adaptive antenna arrays [54], also called smart antennas or software antennas. By using beamforming techniques, the transmit and/or receive beam patterns can be steered in certain desired directions, whereas undesired directions can be suppressed. Beamforming can be interpreted as linear filtering in the spatial domain. The SNR gains, achieved by beamforming, are often called antenna gains or array gains.

Clearly, the various benefits offered by multiple-antenna techniques do not come for free. For example, multiple parallel transmitter/receiver chains are required, leading to increased hardware costs. Moreover, real-time implementations of near-optimum multiple antenna techniques can be challenging. However, some testbed trials have demonstrated that remarkable performance improvements can be achieved in practice, with respect to single-antenna systems, even if low-cost hardware is used [55].

1.5.1 Spatial Multiplexing Techniques

In general, the capacity of a MIMO system with M x N antennas grows linearly with the minimum of M and N [56, 57] is an intriguing result. For single-antenna systems it is well known that given a fixed bandwidth, capacity can only be increased logarithmically with the SNR, by increasing the transmit power.

The basic principle of all spatial multiplexing schemes is as follows: at the transmitter, the information bit sequence is split into M subsequences, that are modulated and transmitted simultaneously over the transmit antennas, over the same frequency band, while the transmitted sequences are separated at the receiver by employing an interference cancellation algorithm.

In frequency-flat fading case, there are several options for the detection algorithm at the receiver, which are characterized by different trade-

offs between performance and complexity. A low-complexity choice is to use a linear receiver, based on the zero-forcing (ZF) or the minimum-mean-squared-error (MMSE) criterion.

The maximum-likelihood (ML) optimum receiver performs a brute-force search over all possible combinations of transmitted sequences and selects the most likely one. Clearly, ML detector is overburdened by its complexity that grows exponentially with the number of transmit antennas and the number of bits per symbol of the modulation scheme. Thus, the ML detector complexity is often prohibitive.

The BLAST detector was originally designed for frequency-flat fading channels and provides a good trade-off between complexity and performance. In contrast to the ML detector, the estimation of the M subsequences, called layers in the BLAST terminology, is not performed jointly, but successively layer by layer.

Starting from the result of the linear ZF or MMSE receiver (nulling step), the BLAST detector selects first the layer with the largest SNR and estimates the transmitted bits of that layer, while treating all other layers as interference. Then, the influence of the detected layer is subtracted from the received signals (canceling step). So, nulling is performed once again on the modified received signals and the layer with the second largest SNR is selected. Afterwards this procedure is repeated, until all M layers are detected. Due to the nulling operations, the number of receive antennas must at least be equal to the number of transmit antennas, otherwise the overall error performance degrades significantly. The BLAST detection algorithm is very similar to successive interference cancellation (SIC), originally proposed for multiuser detection in CDMA systems.

In order to guarantee a certain error performance, channel coding techniques are usually required in conjunction with spatial multiplexing: horizontal coding, vertical coding, or a combination of both. Horizontal coding means that channel encoding is performed after the demultiplexer, separately for each of the M layers. The assignment between the encoded layers and the transmit antennas remains fixed, therefore all code bits associated with a certain information bit are transmitted over

the same antenna. At the receiver, channel decoding can be performed individually for each layer. When vertical coding is used, channel encoding is performed before the demultiplexer and the encoded bits are spread among the individual transmit antennas. Compared to horizontal coding, vertical coding thus offers an additional spatial diversity gain. However, the drawback of vertical coding is an increased detector complexity, because at the receiver all layers have to be decoded jointly.

Depending on the physical channel delay spread, the transmit and receive filter, and the symbol duration, the zero inter-symbols interference assumption might not be valid in a practical system: in fact, ISI can cause relevant performance degradations if no counter measures are applied.

Using a multi-carrier transmission scheme and multiplex data symbols onto parallel narrow sub-bands could be an approach. Transmission schemes developed for frequency-flat fading channels can then be applied within each sub-band. For this reason, combining OFDM with multiple antennas (MIMO-OFDM) is very straightforward [58].

Alternatively, a single-carrier approach and suitable techniques for mitigating ISI can be used. Mainly, there are two main classes of techniques, namely transmitter-sided predistortion and receiver-sided equalization techniques; predistortion techniques require channel knowledge at the transmitter side, based on the receiver feedback information.

More recently, an alternative receiver concept has been proposed for spatial multiplexing systems (without ISI) [59], which is based on the concept of probabilistic data association (PDA). The key idea is to detect iteratively each layer considering the other interfering layers as Gaussian noise. Within each iteration, the mean and the variance of the assumed Gaussian noise are adjusted by exploiting knowledge about already detected bits.

When a sufficiently large number of layers is used the Gaussian assumption fits well, and a near-optimum error performance is achieved. In coclusion, it is important to underline that the same principle of the PDA detector can also be applied to mitigate ISI.

1.5.2 Spatial Diversity Techniques

Spatial diversity techniques predominantly aim at an improved error performance: this can be accomplished on the basis of a diversity gain and a coding gain. There are two types of spatial diversity, referred to as macroscopic (large-scale) and microscopic (small-scale) diversity. Macroscopic diversity is associated with shadowing effects in wireless scenarios, caused by the major obstacles between the two points.

Macroscopic diversity can be gained when there are multiple transmit or receive spatially separated antennas. In this case, the probability that all links are simultaneously obstructed is smaller with respect to a single link. Microscopic diversity is available in rich scattering environments with multipath fading and it can be gained by placing multiple co-located antennas: typically, antenna spacings of less than a wavelength are sufficient. Similarly, the diversity gains are generated by the lower probability that all links being simultaneously in a deep fade.

Diversity reception techniques are applied also in systems with a single transmit antenna and multiple receive antennas. The combining of the individual received signals is done to provide a microscopic diversity gain. In frequency-flat fading case, the optimum combining strategy in terms of SNR maximization is maximum ratio combining (MRC), which requires a perfect channel knowledge at the receiver. In literature several suboptimal combining strategies have been proposed, such as Equal Gain Combining (EGC), where the received signals are (co-phased and) added up, or Selection Diversity (SD), where the received signal with the maximum instantaneous SNR is selected.

The main idea of transmit diversity is to provide a diversity and/or coding gain by sending redundant signals over multiple transmit antennas. An adequate preprocessing of the signals is performed to allow a coherent detection at the receiver, typically without channel knowledge at the transmitter. With transmit diversity, multiple antennas are required only at the transmitter side. In any case, multiple receive antennas are however used to further improve performance.

In 1998 Alamouti proposed a simple technique for two transmit antennas [60] and in the same year, Tarokh, Seshadri, and Calderbank presented their space-time trellis codes (STTCs) [61], which are two-dimensional coding schemes for systems with multiple transmit antennas. While delay diversity and Alamoutis transmit diversity scheme provide solely a diversity gain, STTCs yield both a diversity gain and an additional coding gain. The preprocessing of the redundant transmission signals is performed by the space-time encoder, which depends on the specific scheme under consideration, and the corresponding detection/decoding process is carried out by the space-time decoder.

Alamoutis transmit diversity scheme [60] performs an orthogonal space-time transmission, which allows for ML detection at the receiver by means of simple linear processing. STTCs [61] may be interpreted as a generalization of trellis coded modulation to multiple antennas.

On the basis of simulation results, it was shown in [61] that STTCs offer an excellent performance that is within $2 - 3$ dB of the capacity boundary. However, this performance comes at the expense of a high decoding complexity. Instead, motivated by the simple receiver structure of [60], orthogonal space-time block codes (OSTBCs) were introduced in [62] and they represent a generalization of Alamoutis scheme to more than two antennas. OSTBCs are designed to achieve full diversity with regard to the number of transmit and receive antennas. In contrast to STTCs, it is necessary to underline that OSTBCs do not offer any additional coding gain but in order to further improve the performance of space-time coded MIMO systems, the space-time encoder can be concatenated with an outer channel encoder.

Conventional space-time codes such as STTCs and (O)STBCs offer at most the same data rate as an uncoded single-antenna system, therefore several high-rate space-time transmission schemes with a normalized rate greater than one have been proposed in literature. These represent a bridge between space-time coding and spatial multiplexing techniques. Some of these transmission schemes explicitly combine ideas of certain space-time codes and the BLAST scheme. For example, high-

rate space-time codes that are linear in space and time, so-called linear dispersion codes, were proposed in [63].

All of the space-time coding techniques discussed above require some form of channel knowledge at the receiver side. In contrast to this, so-called differential/non-coherent space-time transmission schemes do not require any channel knowledge and are thus of particular interest for practical MIMO systems.

In practical implementations, various detrimental effects can arise that are often not taken into account in the initial design of space-time transmission schemes, such as ISI effects, wireless channel time-variance, carrier frequency offsets between the two points, inaccurate channel knowledge at the receiver and spatial correlation effects caused in example by an insufficient antenna spacings or a lack of scattering from the physical environment. Another important issue is that the performance gains actually achieved in a practical MIMO system might be smaller than promised in theory, because implementing an optimal transmitter/receiver might be too complex and resorting to suboptimal solutions would be the best choice.

Since cooperative wireless networks have recently gained considerable attention, the concept of multiple-antenna systems can be transferred towards multiple distributed transmitting or receiving nodes. On the one hand, cooperating network nodes build the basis of ad-hoc networks, which are imagined for sensor networks, public safety communication networks, or tactical networks for military applications. On the other hand, cooperating nodes also promise benefits for hierarchical networks, such as cellular networks. In fact, cooperating network nodes are able to share their antennas and thus establish a virtual array.

1.5.3 Smart Antennas and Beamforming Techniques

Besides offering increased data rates and improved error rates, multiple antennas can also be used to improve the SNR at the receiver and to suppress co-channel interference (CCI) in a multiuser scenario. Both goals can be achieved by means of beamforming techniques.

Beamforming can be interpreted as linear filtering in the spatial domain. Considering an antenna array with N antenna elements, which receives a signal from a certain direction, and the geometry of the antenna array, the impinging radio signal reaches the individual antenna elements at different time instants, which causes phase shifts between the different received replicas. However, if the underlying complex baseband signal is assumed to be a narrowband signal, it will not change during these small time differences.

If the direction of arrival of the signal is known, the phase differences of the RF signals can be compensated by means of phase shifters or delay elements. Thus, the overall antenna pattern will have a maximum in that direction: this principle is called conventional beamforming [54].

If only the phases of the received signals are balanced, the shape of the overall antenna pattern remains the same. Hence, conventional beamforming is equivalent to a mechanical rotation of the antenna array. If the amplitudes of the received signals are also scaled before the combining step, it is possible to modify also the antenna pattern shape. In particular, an antenna array with N antenna elements provides $N - 1$ degrees of freedom. If the narrowband assumption for the complex baseband signal is not met, the baseband signal can change during time intervals and the individual antenna elements will observe different samples of the complex baseband signal. In this case, broadband beamforming techniques are required that combine narrowband beamforming with time-domain filtering [54].

In a wireless communication scenario, transmitted signals often arrive to the receiver via just a few distinct paths, a line-of-sight path and other paths associated with significant reflectors and diffractors in the environment. If the directions of these dominant propagation paths are known at the receiver side, beamforming techniques can be applied, in order to adjust the receiver beam pattern such that it has a high directivity towards the dominant angles of reception. By doing this, relevant SNR gains can be obtained in comparison to an omni-directional beam pattern. Such SNR gains due to beamforming techniques are often called antenna gains or array gains in the literature.

Beamforming techniques can also be useful, in order to reduce the delay spread of the physical channel caused by multipath signal propagation. To this purpose, the transmitter or receiver beam pattern model some nulls in the directions of dominant distant reflectors, i.e. echoes with excessively large delays are eliminated from the received signal [54].

In a practical system, the directions of dominant propagation paths must be estimated i.e. by means of the well-known MuSiC or the ESPRIT algorithm. Moreover, when transmitter or receiver are moving, the antenna patterns must be updated on a regular basis its estimations. Such adaptive antenna arrays are often called smart antennas or software antennas in the literature. However, due to the required equipment and processing power the use of smart antenna technologies is currently limited to fixed stations, such as base stations or recent small-cells. In any case, future wireless communication systems it is likely that this technology will also be feasible for hand-held devices by means of microstrip antenna arrays [54].

Smart antennas are also beneficial in multiuser scenarios, in order to suppress co channel interference. Both transmitter and receiver sided beamforming algorithms can be employed for mitigating CCI. When transmitting, each user can adjust his pattern by placing nulls in the directions of other co-channel users and a high directivity towards the desired direction. The use of smart antennas for CCI cancellation offers the opportunity to accommodate multiple co-channel users within the same frequency resource allowing a space-division multiple access (SDMA). This approach can enhance significantly the network capacity in terms of users per cell, as shown in [64].

The concept of antenna arrays with adaptive beam patterns is not new. It has its origins in the field of radar and aerospace technology, especially in applications such as target tracking and high-resolution remote sensing. However, intensive research on smart antenna techniques for wireless communication systems started only in the 1990s [65].

Smart antenna techniques employed for array gains or CCI suppression can easily be combined with spatial multiplexing or spatial diversity even if beamforming scheme should be adapted to the underlying spa-

tial diversity/spatial multiplexing technique in order to achieve a good overall performance. MIMO transmission schemes that combine ideas of beamforming with spatial multiplexing or spatial diversity techniques were considered in [66] and [64], [67–69], respectively.

A particularly simple solution is to build a hybrid system, where a switching between the different techniques is possible. So, the best transmission strategy can be chosen at any time, depending on the current properties of the wireless channel and the requested QoS.

Generalized transmit beamforming techniques use full instantaneous channel knowledge at the transmitter side, but since full channel knowledge might be difficult to acquire in practice at the transmitter, the use of statistical channel knowledge was investigated [68, 69]. This statistical channel knowledge can be gained easily in practical systems, i.e. via offline field measurements, ray-tracing simulations, based on physical channel models or longterm averaging of the channel coefficients.

Alternatively, partial CSI can be fed back from the receiver. Here, the challenge is to choose the CSI feedback such that it can be represented by just a few bits, but can still efficiently be utilized at the transmitter side.

1.6 Beamforming for Heterogeneous Deployments

In recent years, one of the most promising radio access technologies that is evolving in order to increase the spectrum efficiency and satisfy the increasing demand of services is Long Term Evolution-Advanced (LTE-A). By adopting advanced techniques that permit a more efficient usage of the available spectrum, such as Carrier Aggregation, transmission bandwidth beyond 20 MHz and enhancement of multi-antenna techniques, these requirements can be reached. In particular, MIMO systems with up to 8×8 antenna arrays are considered as key elements, supported by a flexible reference signal structures.

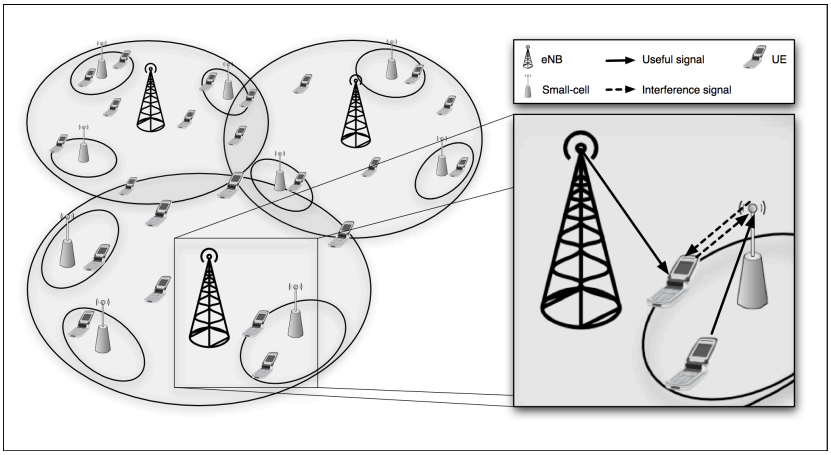

Figure 1-1: Heterogeneous interference scenario with the spectrum sharing approach.

However, these technologies are reaching their theoretical limits and it is commonly agreed that a network composed of only macro-cells will not be able to satisfy the current forecast of the mobile data traffic explosion. 3GPP (3rd Generation Partnership Project) is working toward a further evolution of LTE Release 12 and beyond (also referred as LTE-B) in which the heterogeneous network deployment represents one of the main enhancements [70].

In heterogeneous deployment, the territory coverage and, consequently, the service supply shall be guaranteed not only by the traditional macro-cells, but also by small-cells, especially in areas requiring high peaks of data transfer or in particular environments, where coverage shall be improved or a reserved access shall be guaranteed. It is attractive for operators to offer extended services and represents new market opportunities. It offers many other advantages such as high-data rate, reduced network cost and energy saving.

Two different approaches have been proposed for the deployment of small-cells in future LTE networks: *sharing the same frequency* band with the macro-cell or using *separated higher frequency* bands [71].

Starting from LTE-Release 10, the concept of small-cells has been introduced, referring to a low power, short range wireless access point that coexists in the same geographical area of the macro-cell, sharing the same spectrum. With the promising advantages, this type of small-cells deployment also causes several practical issues, especially in terms of inter-cell interference. Indeed, an inefficient deployment of the small-cells may degrade the performance of the whole system. A possible alternative for future LTE standard evolutions is to seek new spectrum resources in higher bands, e.g., beyond 10 GHz, which have not been exploited in cellular systems. This will lead to separated frequency band deployment of macro-cells and small-cells, which may simplify the network operation.

In both deployment scenarios, multi-antenna techniques and processing in the spatial domain will be key enabling factors. This section presents some candidate beamforming techniques that can be adopted to overcome the impairments arising from a heterogeneous network deployment. By considering a *spectrum sharing* deployment, beamforming techniques can be used to reduce intra-cell and inter-cell interference, while in *separated high frequency* deployment they are useful to compensate the increased path loss. In particular, the high beamforming gain offered by the emerging Massive MIMO can be an essential improvement for the small-cells. Using higher frequency bands, a common ground between typical millimeter techniques and Massive MIMO antenna patterns can be reached thanks to the reduced dimension of the antenna elements.

1.6.1 Spectrum sharing deployments

In this section, we will consider the spectrum sharing deployment, where inter-cell interference is the main bottleneck. However, beamforming techniques can be used to efficiently exploit the spatial domain to separate small and macro-cells. In the following subsections, we will first distinguish between two typical deployment scenarios and then the role of beamforming will be discussed.

Deployment scenarios

Low-power base stations can be either user deployed or operator deployed. If the low power nodes are installed in an ad-hoc manner, directly by the end users, and can be moved, activated/deactivated at any moment (Unplanned Deployment), the traditional network planning and optimization becomes inefficient, since the operator cannot control such nodes. Therefore, new decentralized interference reduction schemes shall be introduced, which operate independently in each cell and with only local information. Low power nodes shall have *cognitive* capabilities, i.e., shall be able to monitor the network status and optimize their transmissions/receptions to improve coverage and reduce interference. This kind of deployment foresees an efficient and opportunistic usage of the spectrum that is one of the key elements to be included in future LTE-B standards. On the contrary, when small-cells are installed by the operator, the transmission is coordinated by the network (Coordinated Deployment) and interference management schemes can be adopted by the network. In particular, two solutions have been proposed to be included in the current LTE-A standard and enhanced in the future releases:

- **CoMP (Coordinated MultiPoint)**. It introduces the possibility of transmitting in a coordinated way from different network points toward users that are on the cell edge and more vulnerable to interferences. Different operation modes have been supposed, from the easiest selection of the best transmission point, to the joint transmission from different network points or coordinated scheduling and beamforming schemes.

- **eICIC (enhanced InterCell Interference Coordination)**. Macro and small-cells use the same frequency channels, but they adopt a joint optimal resource allocation with the goal of using orthogonal portions of the resources to prevent co-channel interference.

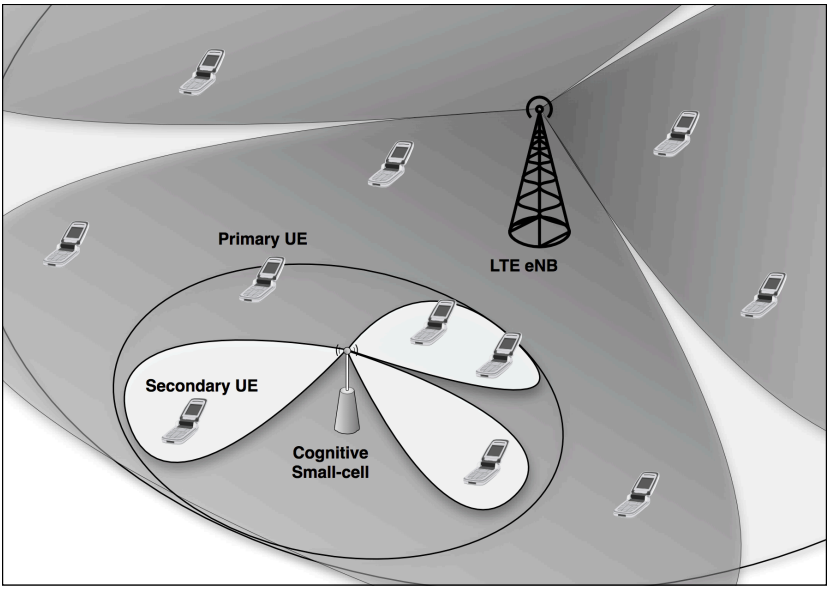

Figure 1-2: Cognitive small-cell beamforming

Finally there are two different operating modes for small-cells, which bring different interference scenarios.

- The small-cell can be operated in the *closed access* mode and consequently some macro-cell users may be in its coverage range, but not allowed to connect. The small-cell may cause a high interference to nearby macro-cell users in DownLink (DL) transmission; on the contrary, the macro-cell user may interfere on UpLink (UL) data received at the small-cell.

- The small-cell can also be *open access*, where all users are free to connect with the small-cell. However, this will generate a load balancing problem, if each user is associated to the small-cell only based on the received signal power almost all users would connect to the macro-cell with the consequent reduction of advantages derived from a heterogeneous development of the network.

Consequently, small-cell Range Extension solutions are suggested, which, on their turn, generate interference problems.

A general representation of a heterogeneous deployment scenario using the spectrum sharing approach is given in Fig.1-1.

Beamforming in Cognitive Small-Cells

Interference management in heterogeneous networks can be achieved with a careful cell planning. However, in some cases, it can be very expensive and it is not even possible in an Unplanned Deployment scenario. In this case, interference management can be considered from a Cognitive Network point of view where the macro-cell is the primary system that has higher priority on the resource usage and the small-cell represents the secondary system that has lower priority.

Cognitive capabilities permit the system to autonomously identify the presence of other systems through a periodic sensing that is essential to identify the unoccupied portions of spectrum. The knowledge about the surrounding environment is used to adapt the transmission by means of power control algorithms and/or suitable resource allocation schemes in order to limit the mutual interference. The simplest way to perform a proper transmission is to use blanking techniques to avoid transmitting in regions occupied by the primary system, in this case the macro-cell. Power management algorithms can then be applied and solved by means of game theory. This technique allows to obtain orthogonal signals but reduces the spectral efficiency. In the following, we will present some more promising approaches for decentralized interference management via beamforming.

Beamforming: With the recent advances in multi-antenna technologies, beamforming can be exploited to allow co-channel frequency allocation with a spatial separation of the interfering signals. In Beyond LTE-A networks also the 3D Beamforming concept will be exploited allowing to steer the beam in both azimuth and elevation so that spatial reuse is fully exploited. Small-cell is equipped with an antenna system made up of correlated elements, by means of the radiated beam can

be modeled. Steering accuracy and null beams selectivity grow linearly with the number of elements composing the antenna system.

The use of beamforming at the secondary transmitter would allow to maximize its performance while the interference to the primary receiver would be minimized. This operation, also known as Cognitive Beamforming (CB), requires solving optimization problems to find optimal precoding vectors and power allocation strategies with complex numerical solutions. CB is based on the knowledge of all the propagation channels over which the secondary transmitter interferes with the primary receiver. This is impracticable in actual scenarios as the two systems operate in an independent manner and the primary system ignores the presence of the secondary one. In [72], a CB scheme working under non-perfect channel knowledge was proposed, which would be a more practical approach. Other works, e.g., [73], focused on the optimization of the total capacity depending on the choice of the preset antenna patterns. This solution presents high complexity due to the best pattern selection search process.

Multi-antenna systems introduce also another resource dimension, namely, the direction of arrival (DOA). In particular, the small-cell beam can be steered toward a direction that maximize the information signal while nulls can be placed in the DOA of the primary system signals as depicted in Fig.1-2. This scheme requires knowledge of the DOA of the multiple signals received from the Macro-cell User Equipments (MUEs), and the performance is strongly dependent on the propagation channel and on the number of antenna elements (i.e., the number of nulls which can be realized is limited by the number of elements of the multi-antenna system). An interesting method is proposed in [74] for small-cell interference suppression focusing on problems that arise for practical system. In particular, using a periodic sensing phase the directions of arrival of MUE signals are estimated by means of a suitable DOA Estimation algorithm. The method to calculate DOA is based on the eigenvector decomposition of the autocorrelation matrix of the received signal. This kind of method is widely explained in literature, and

its high accuracy and simplicity compared to other approaches are often underlined.

The described approaches can be further improved if integrated with a resource allocation algorithm [75], so that the interference reduction will be more effective, as each user of the secondary service will be allocated in correspondence of the resources of its best primary user.

Sensing: Cognitive approaches can be very effective only if the knowledge of the environment is reliable. The amount of resources dedicated to sensing is an interesting trade-off and it requires to be carefully evaluated according to the operating scenario where small-cells are placed. The computational complexity depends on the sensing period and the complexity of the sensing algorithm. In addition, the sensing accuracy depends on many factors, such as the propagation channel, the angle dispersion of the multipath components and the number of samples collected during the sensing period. This last point is very important. In LTE, the smallest physical resource unit that can be allocated is a Physical Resource Blocks (PRB) that consists of 12 contiguous subcarriers. Using a single PRB to acquire knowledge about a MUE can be insufficient, leading to inaccurate estimates. The possibility of gathering together all the PRBs allocated to a given user shall represent a significant improvement. As an example, Fig. 2-13 shows how the DOA estimation performance increases when the number of PRBs used for sensing increases. In these results, it has been assumed that an antenna system with $L = 4$ elements and the propagation channel introduces 4 different paths with different DOAs.

In an Unplanned Deployment, the small-cell has no knowledge about the resource allocation performed by the macro-cell. Some works assumed that the small-cell is able to decode the control channel sent by the macro-cell, but it is not always possible. Another possibility is to apply suitable algorithms that estimate which PRBs belong to the same MUE, for example, exploiting the mutual projection of the eigenvectors obtained from each PRB [76]. With these methodologies, the cognitive approach of beamforming will be an efficient and practical way to suppress interference in the Unplanned Deployment scenario.

Table 1.1: Spectrum sharing techniques comparison

	Cognitive Systems	**Coordinated Systems**
Deployer	User/Operator	Operator
Network signaling overhead	Low	High
Capacity loss	During sensing step	No
Environmental information amount	Low	Up to high
Environmental information accuracy	Low-medium	High
Hardware requirement	Sensing equipment	High data rate back-haul

1.6.2 Beamforming with CoMP

The small-cells may also be deployed by the same operator. In this way, different tiers of access nodes need to be interconnected through an interface, as the X2 interface in LTE-A provided for the information interchange between TPs (Transmission Points). Such coordinated deployment is radically different from the cognitive-based schemes explained previously. With efficient coordination, the signal received from other cells can be used constructively and it can be an information resource rather than an interference source. This is the basic idea behind the Coordinated Multi-Point. However, the need of information exchange between the nodes introduces some problems concerning the capacity of the backhaul links and, consequently, the high cost of deployment of the network. Hence, key issues in Beyond LTE-A networks are represented by the reduction of the signaling exchanged by the TPs and the availability of cost-efficient backhaul links.

The CoMP schemes can be considered as an evolution of the ICIC, that is a technique, included in the LTE standard, to reduce the interference through a coordination between neighboring cells. So far, ICIC algorithms proposed in the literature are based on two approaches:

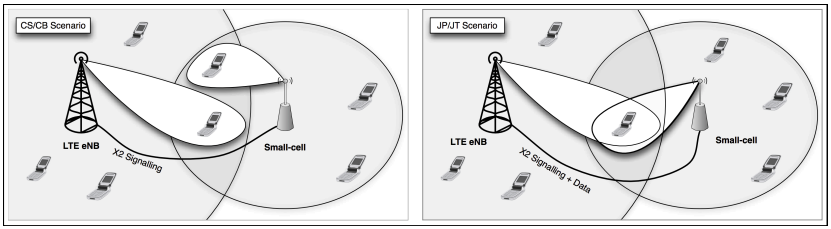

Figure 1-3: CS/CB and JP/JT approaches for CoMP.

Frequency Reuse Partitioning and Power Control. The CoMP evolution brings higher flexibility of the exchanged information, ranging from a static or semi-static approach to dynamic joint decision about the scheduling. It allows to take full advantage of the increased capacity offered by heterogeneous systems especially by means of beamforming algorithms, which allow the spatial reuse of the resources by avoiding mutual interference and efficiency loss. LTE-B system will introduce further enhancements to the CoMP approach, by means advanced receivers able to manage efficiently the interference.

In general, joint resource allocation can be managed with:

- *hierarchical* schemes, where an eNB set elects a master (usually one eNB or the Mobility Management Entity-MME) to be in charge of coordinating some operations and the decision-making on behalf of the group.

- *horizontal* schemes, where the same algorithm runs at each CoMP node and it will return the same resource allocation pattern.

3GPP LTE-A standard highlights two approaches for CoMP that mainly differ on the required network signaling overhead. These are shown in Fig.1-3 and described in what follows.

The former LTE CoMP scheme is named **Coordinated Scheduling/Coordinated Beamforming (CS/CB)**. It is based mostly on the sharing of information provided by each terminal to its TPs, as well as other information exchanged among TPs to contribute to a joint

decision. In this context, the data addressed to a specific UE is transmitted by a single TP, while other TPs can use the same radio resources (i.e., the same PRBs) to transmit to angularly separated UEs using beamforming. There have been a number of proposals aiming to reduce the coordination complexity and the required side information, e.g., it was proposed in [77] that interference can be suppressed through spatial cancellation with multiple antennas at the base station, which would require only local side information. For the CS/CB approach, the signaling increase is limited and the X2 interface provides adequate capacity. This scheme also allows to borrow some techniques devised for cognitive small-cells, as both the schemes are based on the use of spatial diversity. On the other hand, the key role of beamforming in CS/CB will be much more effective than in cognitive beamforming, since more accurate side information is available.

The latter CoMP scheme proposed by the 3GPP is named **Joint Processing/Joint Transmission (JP/JT)**. When a higher signaling overhead is supported, more sophisticated cooperation can be applied. In JP/JT, data transmission for each UE is done simultaneously by multiple TPs. Hence, the UE can combine multiple copies of the signal to improve the received signal quality. The waste of resources due to multiple transmissions is compensated by beamforming that allows to spatially reuse the same resources to transmit toward angularly separated UEs.

This scheme requires that the user data is available at all TPs, so the main challenge is represented by the high capacity requirement of the *backhaul links*, which represents a bottleneck for this solution. One efficient approach to reduce the signaling overhead and the backhaul requirement of JP/JT is clustered cooperation [78], where TPs within the same cluster will coordinately serve users in this cluster and some form of inter-cluster interference management may also be performed. For the further evolution along this path, as the operators are starting to upgrade their backhaul links, a more radical approach for coordination has been recently proposed, which is the cloud radio access network (C-RAN) [79]. In this new architecture, all the baseband signal processing

Table 1.2: Different frequency techniques comparison

	Conventional Bands	**High frequency Bands**
Carrier frequency	< 10 GHz	> 10 GHz
Available spectrum	Low	High
Supported antennas	$\leq$10	$\approx$100
Beamforming performance	Low-medium	High
Channel conditions	-	High atmospheric absorption Low penetration depth

is shifted to a single baseband unit pool, thanks to the high-capacity backhaul links which will normally be supported by optic fibres. Such a network architecture will enable efficient centralized resource allocation and interference management, which can then greatly improve both the network capacity and energy efficiency.

In conclusion, in many emerging scenarios, where the high density of heterogeneous systems will stress the problems due to the interference, the benefits offered by CoMP are very attractive. However, it is challenging to implement in practical systems. In particular, two main issues should be addressed. One is the dynamic settlement of the CoMP areas and the topology updating algorithms for the TPs involved in a joint process; the other is the signaling overhead as well as the impairment in the available side information, e.g., imperfect channel state information. Lots of efforts have been put on these aspects, and there is no doubt that CoMP will be an essential part in future communication networks.

1.6.3 High frequency deployment

One of the most discussed proposals for systems Beyond LTE-A to overcome inter-cell interference is to deploy small-cells in a separated higher

frequency band. Indeed, the limited available spectrum makes dedicated deployment of small-cells in the current cellular band very unlikely. On the other hand, large bandwidths at higher frequencies ($f_c > 10$ GHz) are still unexplored, primarily due to the harsh propagation conditions of the radio channel. The main challenge is represented by the path loss, which is proportional to a power (usually greater than 2) of the carrier frequency and, hence, any signal in high frequency band would suffer a deep attenuation. For example, assuming the system is moved from 2 to 20 GHz, the received signal would suffer an attenuation penalty of at least 20 dB[1], which will reduce in turn the system coverage. Hence, it becomes of cardinal relevance for future deployments to find transmission techniques aiming to improve the quality of the link in order to counteract this drawback.

In particular, Massive MIMO represents a particular interesting technology. It consists of using a very large number of antennas to fully exploit the spatial diversity among the users. A possible application is to form very narrow beams to provide a significant gain that can partially counteract the increased path loss. One of the major problems of Massive MIMO in conventional operating bands is the dimension of the antenna system, which may be acceptable for large installation like the LTE eNB, but is completely inappropriate for domestic use. On the other hand, in a high operating frequency range, the antenna element dimension becomes smaller and then this technology will be more applicable.

From the above discussion, high frequency deployment and Massive MIMO are closely related. Massive MIMO can be seen as an enabling technology for communications in high frequencies, and, at the same time, the small antenna size at high frequency makes Massive MIMO practical.

In the following section, the main feature of Massive MIMO will be illustrated.

[1] considering an attenuation exponent equal to 2 in the path loss formula

Massive MIMO

Massive MIMO represents a new research field that spans communication theory, propagation characterization and the associated electronic component design. Recently, this topic has attracted great attention from both academic and industry, thanks to its great potential in improving communication performance [80]. Massive MIMO systems consist of equipping base stations with antenna arrays composed of a large number (i.e., a hundred or more) of small antennas plugged together. Ideally, with a widely separated antenna array, each additional element adds a degree of freedom that can be exploited, which introduces very attractive advantages. In [81], it is demonstrated that if the number of base station antennas M is much larger than the number of antennas per terminal K, such that $M/K \gg 1$, then deploying more and more antennas is always beneficial, i.e., the effects of fast fading and correlated noise decreases toward zero, even in low SNR (Signal to Noise Ratio) environments. By relying on very simple signal processing, Massive MIMO can increase the link capacity and at the same time improve the radiated energy-efficiency [82,83]. This is achieved by focusing signal strength in a specific direction and creating very narrow radiated beams. Hence, it is possible to efficiently transmit independent data flows to different user terminals during the same time-frequency block, thus exploiting spatial separation of the users (*multi-user* beamforming). It is straightforward to note that strategy can be used symmetrically in the uplink, by using the high beam resolution to split in the angular domain different signals arriving in the same time/frequency slot.

The creation of very narrow beams also permits to reduce the inter-symbol interference thus decreasing the spectrum inefficiencies of the cyclic prefix in OFDM (Orthogonal Frequency Division Multiplexing) symbols. In addition, the total available transmission power is spread among the M antennas, allowing the reduction of per-antenna power consumption. In [83], it has been showed that for an eNB equipped with a linear detector, Massive MIMO can decrease the amount of per-user transmission power. The amount of saved power is inversely propor-

tional to the size of the antenna array in the case of perfect Channel State Information (CSI), while to the square-root of the number of antennas for imperfect CSI. This leads to the general complexity reduction of radio frequency front-end of the eNBs and also allows to apply inexpensive low-power components. The usage of Massive MIMO also leads to a significant reduction of latency on the air interface, since it dramatically reduces the probability of having fading dips affecting received signals. Finally, robustness regarding intentional and unintentional jamming is increased thanks to the presence of many excess degrees of freedom that can be used to eliminate signals coming from jammers.

We conclude that by implementing small-cells equipped with Massive MIMO is possible to efficiently use the available frequency resource, reduce the interference and assure improved transmission capabilities. However there are some main challenges that need to be addressed.

Challenges in Massive MIMO

In theory, Massive MIMO systems can achieve all the performance improvements as stated above. In practice, the design of very large array systems suffer from several implementation issues that need to be resolved.

Antenna dimension: The realization of Massive MIMO systems requires that more than hundred small antennas are placed at the eNB front-end [84]. This leads to the implementation of 2-D or 3-D antenna arrays where the coupling effects among antenna elements are more evident, thus reducing the system capacity. In addition, there is a need of a significant physical space to accommodate the antennas. The deployment in higher radio spectrum for small-cells means that the base station antennas can be designed without the need of large spaces, easing the placement problem.

Channel State Information: To correctly operate massive MIMO systems need to acquire CSI. Traditionally, in multi-antenna systems, pilots are sent by each antenna element in the DL. This is not possible

when the number of antenna elements is very high, as the number of pilot symbols would become too high, especially in mobility scenarios with short channel coherence time. As a consequence, massive MIMO systems shall operate in the TDD (Time Division Duplexing) mode, where channel reciprocity can be exploited and CSI will be estimated at the eNB. However, when the number of user equipments is high, acquiring reliable and updated CSI will still be challenging and represent an interesting research topic. In particular, in mobility conditions the support of control signaling and connectivity when operating with high directive links is not trivial.

Signal Processing: When the number of antenna elements increases, the complexity of the algorithms used to determine suitable precoding vectors or decoding processes also increases. This requires suitable optimizations especially for small-cells deployment, since in this case the transmission points have less computational resources. To provide very accurate narrow beams that can follow UEs represents an important issue to be investigated, especially in the mobility environment. A possible solution is the use of low complexity algorithms which can be implemented directly in hardware. The loss of performance due to the simplicity of the algorithm would be compensated by effects of the high antenna number.

Chapter 2

Cognitive Systems

2.1 Introduction

The large diffusion of new web-based services and mobile applications requiring high data-rate is leading to a mobile data traffic explosion. Therefore, it is increasing the need of an efficient exploitation of the available radio resources, in order to offer a satisfying connection to the users. This increasing demand for higher data rate and quality of mobile communications leads to an evolution of mobile communication systems. One of the most promising radio access technologies is the Long Term Evolution (LTE) defined by the Third Generation Partnership Project (3GPP). It is able to satisfy new communication requirements, thanks to its low latency, high spectral efficiency that guarantee high data rate and real time services and a new all-IP system architecture [85].

In particular LTE is designed to meet high-speed data and media transport as well as high-capacity voice support thanks to key technologies such as MIMO (multiple input, multiple output), OFDM (orthogonal frequency division multiplexing) and SC-FDMA (single carrier FDMA). OFDM is a multicarrier technique that permits to face with severe multipath fading and allows an efficient use of the spectrum thanks to suitable resource allocation schemes [86], [75]. Many recent commu-

nication standards such as Long Term Evolution (LTE), LTE-Advanced (LTE-A) and WiMAX, are based on OFDMA. In addition, MIMO permits to exploit spatial dimension to improve the system performance. LTE uses Orthogonal Frequency Multiple Access on the Down Link (DL) and Single Carrier Frequency Division Multiplexing in the Up Link (UL) to allow data to be directed to multiple users simultaneously on a subcarrier basis for a specified number of symbols. SC-FDMA is introduced in the UL in order to reduce the PAPR (Peak to Average Power Ratio) thus reducing the power consumption of the mobile terminals. However, LTE technology is continuously evolving to meet future requirements. In particular, LTE Release 10 (LTE-Advanced) includes all features of Release 8/9 and adds several innovations to increase the system capacity and the spectrum efficiency.

One of the promising solution to improve the radio resource reuse efficiency in next-generation wireless systems is the heterogeneous network deployment [70]: it makes possible to increase the system capacity by integrating basic macro-cell (eNB) coverage with femtocells. In general, a femtocell is a low power, short range wireless access point that operates in licensed frequency bands and it is connected to broadband Internet backhaul. It is attractive for operators to offer extended services on their licensed spectrum and represents new market opportunities. Femtocell is especially developed for indoor coverage where access would otherwise be limited or unavailable and, hence, also called Home eNodeB (HeNB) [87]. In indoor environments, femtocells can reach the expected data rate and satisfy the increasing users bandwidth request. Indeed, it has been estimated that in future about 60% of voice and 90% of data traffic will originate from indoor environments (i.e., home, office, airports, schools) [88].

In particular three types of femtocells can be deployed depending on the access mode:

- *closed access mode*: the access is restricted to a limited set of user equipments (UEs). Femtocell is user-deployed;

- *open access mode*: the access is open and femtocell is deployed directly by an operator to eliminate coverage holes;

- *hybrid access mode*: femtocell is usually user-deployed and, hence, some users have the priority.

In all the cases the femtocell has to use the same spectrum of the macro-cell without interfering with it. An inefficient deployment of the femto-cell network may degrade the performance of the wireless system. For this reason access methods and resource allocation strategies require further investigations before femtocells will be widely adopted. In general, high spectral efficiency is obtained with a co-channel frequency allocation at the expense of quality of service (QoS), while orthogonal channel allocation leads to a high QoS at the expense of poor spectral efficiency. In [89, 90], well-known frequency reuse allocation schemes are proposed for a joint femto/macro cell allocation. The goal is to use orthogonal portions of the spectrum to prevent co-channel interference. These schemes require a prior cell planning and assume static network characteristics. However, in general, performing careful cell planning can be very expensive and is not possible when the femtocell is user-deployed (i.e., closed or hybrid access modes). In this case there is not any coordination with the operator: the mutual interference cannot be managed efficiently by means of conventional network planning methods, requiring a suitable interference management.

In particular, this problem can be considered from a Cognitive Network point of view. The macro-cell represents the primary system that has higher priority on the resource usage, and the femtocell acts as a secondary system that has lower priority. Recently, cognitive femtocells received great attention as a possible solution to provide high capacity and coverage with guaranteed QoS for future indoor services [91]. Cognitive capabilities of the HeNB are used to acquire knowledge about the surrounding environment and to adapt its transmission by means of power control algorithms and/or suitable resource allocation schemes. In particular, a high flexibility in the resource assignment can be exploited in OFDMA systems. It is obtained with a dynamic allocation of

the PRBs that represent the smallest resource unit that can be allocated to a user. In [92, 93] HeNB looks for PRBs not used by the macro-cell UEs (MUEs) thus avoiding mutual interference using idle PRBs. The femtocell allocates the PRBs on the basis of the estimated interference levels forwarded by the femtocell UEs (FUEs). In [94] the cognitive network is able to decode the mapping information sent by the primary eNB. Alternatively, the HeNB can perform co-channel transmission by estimating its interference on a given MUE and adapting its transmission power on a PRB basis [95]. This is done by estimating the channels linking the HeNB to the MUE.

Traditionally spectrum sensing is considered as measure of the spectrum energy in order to detect if a frequency band is occupied or not by the primary user in a certain geographical area on a given time. However, with the recent advances in multi-antenna technologies, also space and angle dimensions can be exploited to allow co-channel frequency allocation. In [72, 96] cognitive beamforming schemes are used at the secondary system transmitter (i.e., HeNB) in order to maximize its performance and minimize at the same time the interference on the primary system receiver. This scheme requires the knowledge of all propagation channels. Another resource dimension that can be exploited is the direction of arrival (DOA): if a primary user is transmitting, the secondary user can transmit in the other directions avoiding interference on the primary user [74, 97, 98].

All the above cited methods are effective only if the knowledge of the environment acquired during the first sensing interval is reliable. This may depend on many factors, but, in particular, in a mobile communication channel the multipath fading and the AWGN noise fluctuations reduce the sensing accuracy. In addition, DOA estimation capabilities are affected by angle dispersion of the multipath components: even when only one primary UE is located within the femtocell coverage area, each propagation path entails a different DOA of the signal, making the accuracy of the estimation critical. Furthermore, the quality of the estimation is strongly conditioned by the number of samples col-

lected during the sensing period: in particular, if only few samples are available, the acquired knowledge can be not accurate.

In [97] the estimation of the Direction of Arrival (DOA) of primary system is introduced as new opportunity but how the DOA information can be used it is not considered in the paper. [98] assumes a perfect knowledge of primary signal DOA in order to insert a null in the direction of the primary system. DOA estimation and actual multipath indoor channel propagation conditions have not been considered.

In Sec. 2.2 a system to reduce the interference due to a femtocell on a primary system downlink is proposed: the femtocell is equipped with a multiple antenna system and it is able to estimate the DOA of the different signal replicas received from the User Equipment (UE) connected with the macro-cell by using suitable sensing intervals in the uplink frame. Then the femtocell transmits using a null steering algorithm in order to reduce the interference toward the primary system UE. The analysis considers actual propagation conditions. In particular different propagation paths with different DOAs varying during the time are taken into account. Hence, the effects of not ideal conditions due to a number of signal higher than the number of antennas and due to DOA variations are considered.

However, if the HeNB does not know which PRBs compose the subchannel allocated to a given MUE, the estimate takes place only on the smallest resource portion (i.e., the PRB). In order to have an accurate knowledge of the surrounding environment and, hence, to perform a suitable resource allocation, the HeNB should know which PRBs belong to a specific subchannel. However, in closed access mode, this knowledge is not provided *a priori*. Sec. 2.3 investigates a method to gather together the PRBs belonging to the same user (i.e., to the same subchannel) exploiting the similarity of signals DOA for grouping. We suggest to apply a modified K-means [99] clustering algorithm to a particular data set, represented by mutual projections of the eigenvectors of each PRB autocorrelation matrix. In particular, a new method to determine the inputs needed by the K-means algorithm is proposed. The results show how this method allows the detection of the PRBs

allocation with great accuracy by means of the proposed initialization procedure that provides the number of clusters and accurate cluster centers. The performance of the method is compared with that of a hierarchical approach for which inputs are not needed a priori and with that of a K-means algorithm that receives its inputs from a first hierarchical stage. Finally, we show the benefits of PRBs clustering in the DOA estimation performance, especially when the number of paths increases making difficult the DOA estimation.

Sec. 2.4 describes an extension of [74], where a single MUE was assumed to transmit on all the available frequency resources. Here, DOA estimates are performed using few samples (on a single PRB), and hence can be inaccurate thus limiting the performance of the interference reduction scheme. For this reason this section shows how the proposed solution accuracy can be improved by collecting together the PRBs belonging to the same MUE. This information is not known a priori by the femtocell but can be achieved by using suitable methods to aggregate the PRBs and, hence, to increase the snapshot for estimates [76]. This leads to improved performance and reduces the complexity, because the same beamforming weights are applied to all the PRBs belonging to the same MUE. This scheme represents a very simple transmitting strategy that can be easily implemented in practice and easily integrated with adaptive allocation strategies.

Towards this end, Sec. 2.5 proposes a joint beamforming and resource allocation scheme for a LTE-A system which utilizes the angular information (i.e., AoA) of the primary and secondary User Equipments (UEs) instead of the channel state information of the interference links. In particular, the femto-cell acquires information about the geographical position of the Macro-cell UEs (MUEs) and femto-cell UEs (FUEs) without making use of any form of coordination with the macro-cell. The surrounding environment is heard by means of a periodic sensing phase and the AoAs are estimated thanks to the presence of a multiple antenna system [74]. AoA information is exploited to allocate the time-frequency resources to the FUEs that minimize the interference toward the primary MUEs and maximize the femto-cell capacity. In

particular, two methods are proposed here. The first represents the optimal solution, it determines the achievable gain for each FUE in each resource unit and performs an optimal allocation that maximizes the capacity of the FUE with the constraint of avoiding the transmission in the MUE directions. The second is a faster heuristic method, based only on the information obtained from the sensing step (i.e., AoA), thus reducing the computation complexity. Both methods represent a very simple transmit strategy that can be easily implemented in practice.

2.2 Interference mitigation with MuSiC direction of arrival estimation and Null Steering

In an indoor environment, where the LTE macro-cell (eNodeB) cannot guarantee complete coverage and/or satisfy high data rate demand, a small cell is added in order to offer enhanced performance. The femtocell uses LTE technology, but it is an user-deployed Home eNodeB (HeNodeB) with close or hybrid access mode, exploiting private access network: there is no coordination between the two LTE entities and the eNodeB is not aware of the HeNodeB presence. In addition, in order to carry out a worst case analysis, both systems (i.e., eNodeB and HeNodeB) use the same uplink and downlink frequencies and the same bandwidth. In this scenario severe interference can arise from the femtocell transmission. In particular the signal received by an UE, near to the femtocell but connected with the macro-cell, can be strongly degraded. Hence, this work is focused on the downlink of the LTE macro-cell. Different bandwidths ($1.25 - 20$ MHz) and number of subcarriers are considered according to the LTE standard. The frequency of carriers have been selected equal to 2 GHz because in this spectrum all bandwidths provided by LTE can be used [100]. These frequencies are used in many regions such as Canada, US and Latin America and similar frequencies are are also provided for deployment in UE. LTE radio frames are organized according to the FDD mode of 3GPP stan-

dard. The HeNodeB is equipped with an antenna array used to perform DOA estimation and beamforming. It is considered an horizontal Uniform Linear Array (ULA) with $L = 4$ elements[1], spaced of $d = \lambda/2$, where λ is the wavelength. Generally speaking, the number of antennas is related to implemented algorithms and it is a compromise between commercial size issues of the device and the required performance. The signal transmitted by the UE (directed to the eNodeB) is received by the HeNodeB through different propagation paths due to multiple scatters and obstacles. In particular, assuming an indoor environment, the different paths can have very different DOAs [101]. We assume that each path has a DOA that is uniformly distributed in an angle of 360 degrees.

In this scenario, the received signal arrives to the antennas through a series of rays arranged in clusters. The power distribution of rays that form the cluster is the Power Azimuth Spectrum (PAS) and it is usually modeled with a Gaussian distribution in outdoor environments and with a Laplace distribution in indoor scenarios [101]. This distribution has strong angular concentration of rays, therefore the average value is the best candidate to feature the angle of arrival of the whole cluster [102]. The number of resolvable paths, or clusters, changes with the selected bandwidth according to the channel model that refers to Recommendation ITU-R M.1225 [103]. The channel impulse response for macrocell downlink follows the tapped-delay-line "A-Channel" outdoor model, whereas the UE-HeNodeB link uses the indoor case parameters. Focusing on the indoor environment, it is usually characterized by multipath propagation with M replicas and $\mathbf{h}$ vector contains channel coefficients of each replica, i.e.,

$$\mathbf{h} = [\alpha_1 e^{j\phi_1}, \quad \alpha_2 e^{j\phi_2}, \quad \cdots \quad , \alpha_M e^{j\phi_M}]^T \tag{2.1}$$

where α_i and ϕ_i are two independent random variables following Rayleigh and uniform distribution for $i = 1, 2, \cdots, M$. Assuming a symmetric channel, the HeNodeB steers a null lobe toward each DOA or at least

[1]Two or four antenna array systems are provided by LTE standard in TX

toward those carrying the most of energy, in order not to interfere with primary UE. The i-th signal replica arrives on the antennas forming the angle θ_i , $i = 1, 2, \cdots, M$, with array perpendicular. The delay of the i-th signal between two consecutive antennas is:

$$\tau = \frac{d \sin(\theta_i)}{c} = \frac{\sin(\theta_i)}{2f_0} \tag{2.2}$$

where c is the light speed and f_0 is the operational frequency. Considering $\tau \ll T_s$, where T_s is the sampling period, the arriving signal phase is rotated by $2\pi f_0 \tau$. Hence, the n-th sample received by l-th antenna can be expressed as

$$r_l[n] = \sum_{i=1}^{M} x[n - t_i]\alpha_i e^{j[\phi_i + (l-1)\pi \sin(\theta_i)]} + v_l[n] \tag{2.3}$$

where $x[n]$ is the n-th sample of the signal transmitted by the primary UE (QPSK modulated), t_i is the delay due to scattered propagation of the i-th replica and $v_l \sim \mathcal{N}(0, \sigma_v^2)$ is the AWGN noise. The noise is independent among the antennas and the paths are independent each other. Let us denote the $\mathbf{s}(\theta)$ vector containing the $s_l(\theta) = e^{j\pi(l-1)\sin(\theta)}$ elements, with $l = 1, 2, \cdots, L$, usually referred in literature as steering vector, since it can be used to steer the antenna pattern on the direction θ. Denoting with $\mathbf{S} = [\mathbf{s}(\theta_1), \quad \mathbf{s}(\theta_2), \quad \cdots, \quad \mathbf{s}(\theta_M)]$ the matrix containing the steering vectors of the incoming signals DOAs, the arriving signals model can be expressed in matrix form by

$$\mathbf{r} = \mathbf{S} \cdot \mathrm{diag}(\mathbf{h}) \cdot \mathbf{x} + \mathbf{v} \tag{2.4}$$

as $\mathbf{x} = \big[x[n - t_i]\big]^T$ and diag$(\cdot)$ denotes the diagonal matrix.

2.2.1 Proposed System

The aim of the proposed system is to allow the coexistence between two LTE cells operating on the same frequencies minimizing the interference of the HeNodeB on the primary macrocell UE through null

steering beamforming. The femtocell HeNodeB must be able to sense the presence of the UE and, then, to estimate the DOAs of the signals by means the use of a multiple antennas system. We assume that a first phase of sensing is performed in order to detect the presence of a macrocell UE[2]. If the UE presence is detected, the femtocell schedules one OFDM symbol in each-sub frame in the uplink transmission to estimate the DOA and tracking the UE mobility. In particular the LTE uplink frame supplies one OFDM symbol in each slot as reserved for the transmission of special Reference Signal (RS), named Sounding Reference Signals (SRSs) usually allocated to the UEs to provide channel state information (CQI) to the eNodeB. The sensing procedure can take place in one of these OFDM symbols: in particular, once each subframe (one subframe lasts two slot, so it contains two SRSs). The SRS is used by the HeNodeB in order to detect the DOA of a UE. This operation can be done during one OFDM symbol in the uplink band, once each sub-frame of the LTE frame tracking of the possible changes due to UE mobility. The number of antennas in a MIMO system is a trade off among required performance, complexity and overall device dimension: it is well-known in literature that as the number of antennas increases, the precision and the capacity of the communication system get an improvement. Furthermore, the directivity of the antenna system and the number of detectable signals grows linearly with the number of antennas.

DOA Estimation

There are several algorithms in the literature dealing with DOA estimation [54,104]. One of the most discussed methods is the Multiple Signal Classification (MuSiC), based on the eigenvalue decomposition, which is characterized by high accuracy and resolution [105]. When the number of available antennas is low, as in practical applications, FFT-based methods (e.g., the periodogram) are outperformed by eigen-structure

[2]This phase is out of the scope of the proposed technique, but this can be done through using spectrum sensing techniques.

algorithms, which exploit the received signal autocorrelation matrix. In particular, we resorted to the MuSiC method for its reliability, high resolution and accuracy.

The received signal autocorrelation matrix is defined as

$$\begin{aligned}\mathbf{R_r} &\triangleq E\big[\mathbf{r}\mathbf{r}^H\big] \\ &= E\big[\mathbf{S}\,\mathrm{diag}(\mathbf{h})\,\mathbf{x}\mathbf{x}^H\mathrm{diag}(\mathbf{h})^H\mathbf{S}^H\big] + E\big[\mathbf{v}\mathbf{v}^H\big] \\ &= \mathbf{SPS}^H + \sigma_v^2\mathbf{Id}_L \end{aligned} \tag{2.5}$$

where $\mathbf{Id}_L$ is the identity matrix with dimension $L \times L$, $[\cdot]^H$ represents the hermitian transformation and $\mathbf{P}$ is defined as

$$\mathbf{P} = E\big[\mathrm{diag}(\mathbf{h})\,\mathbf{x}\mathbf{x}^H\mathrm{diag}(\mathbf{h})^H\big]. \tag{2.6}$$

The DOA estimation algorithm needs to know the number of signals to be estimated, K, that must be lower than L. Calculating the eigenvalues of $\mathbf{R_r}$ two disjoint eigenspaces can be identified: the former consists of the signal eigenvectors on which noise is overlapped and it is named *signal subspace*, the latter is composed by eigenvectors only due to noise and it is called *noise subspace*. Signal eigenvectors correspond to the K (with $K \leq L-1$) greatest eigenvalues and the other $L-K$ are noise eigenvectors. Among all the possible steering vectors, the MuSiC algorithm searches for those that are orthogonal to noise subspace. In particular looks for steering vectors that maximize the function

$$P_{SM}(\theta) = \frac{1}{\|\mathbf{s}^H(\theta)\mathbf{U}_N\|} \tag{2.7}$$

where $\mathbf{U}_N$ is the noise subspace matrix with $L \times (L-K)$ dimensions and $\|\cdot\|$ is the norm of the vector. The codomain of function in (2.7) is very large and direct detection of maxima is difficult. Therefore, logarithm of function is introduced to lead to a shape compression and an easier identification of local maxima related to real DOAs. The next two derivatives highlight the concavities and allow to obtain a series of

much more narrow maxima, concentrated around the DOAs:

$$P_{SM_{MOD}}(\theta) = \frac{d^2(\log_{10} P_{SK}(\theta))}{d\theta^2} \tag{2.8}$$

then the local maxima of (2.8) that are greater than an empirically set threshold are searched. In this way the angular tracking is more precise and stable.

The performance of the Spectral MuSiC is related to noise level overlapped to signal and to the number of paths through which the signal is received by the femtocell. Let us provide some intuitive examples: assuming the bandwidth equal to 5 MHz and high SNR value, all the arrival directions are identified because even the weakest replicas can not be confused with noise, because it has low power and it is uncorrelated among the antennas. When the AWGN noise increases, the receiving array it is still able to identify the direction of main signal and also of the secondary paths with most power. However in this condition the last paths with signal power close to that of noise are neglected by DOA algorithm and it is not able to identify their direction of arrival. In addition the number of antennas limits the algorithm capabilities because the maximum number of overlapping signals that can be identified is $L - 1$. With a greater number of signals, it is not possible to separate the noise subspace correctly because it is interfered by less powerful signals eigenvectors and hypothesis of disjoint subspaces is weakened. However, in actual scenarios the number of antennas is limited by device dimension and complexity constraints. In addition in an indoor environment the multipath components must be considered as separate signals because they arrive with a very wide angle dispersion and it is not possible to know how many resolvable paths will be received. The proposed system takes into account these actual hypothesis. The MuSiC algorithm assumes that the number of signals to be detected is always equal to $K = L - 1$ and looks for $L - 1$ DOAs. It means that:

- if $M < L - 1$ only M estimated DOAs correspond to actually received signals,

- if $M = L$ all M estimated DOAs correspond to all the received signals,

- if $M > L - 1$ only $L - 1$ estimated DOAs are detected.

The DOA estimation is updated every sub-frame to take into account time variation of the DOA due to UE mobility.

Null Steering

The information about the DOAs provided by MuSiC algorithm is then used to limit the interference in the following OFDM symbols through a pre-processing of the transmitted signal, which allows to perform null beams in the selected transmission directions.

Null steering algorithm is based on the same theoretical construct used by classical beamformer generating the weights that regulate amplitude and phase of the output signal from each antenna of the array. It is noticed that the null steering algorithm is constrained by the same limitations of MuSiC: it can generate K null beams up to $L - 1$ [106]. Furthermore, the design of the pattern requires to set a main steering direction, denoted by φ. This pointing direction is used by the HeNodeB to convey to its indoor users. In this scenario null steering algorithm presented in [54] and derived from classical beamforming algorithms is used.

The weights $\mathbf{w}$ are obtained by imposing the steering vector $\mathbf{s}(\varphi)$ equal to 1 while the steering vectors $\mathbf{s}(\theta_1), \cdots, \mathbf{s}(\theta_k)$, where null beams are required, equal to 0. Denoting with

$$\mathbf{A} = \left[\mathbf{s}(\varphi), \mathbf{s}(\theta_1), \mathbf{s}(\theta_2), \cdots, \mathbf{s}(\theta_K)\right]$$

the matrix containing the steering vectors of interest, while the vector $\mathbf{c} = [1, 0, \cdots, 0]^T$, which contains $K + 1$ elements. The above mentioned system can perform a smaller number of nulls than maximum, depending on the number of estimated paths by DOA algorithm in a TTI (Transmission Time Interval). For this reason, $\mathbf{A}$ can be not a

Table 2.1: Number of replicas in indoor ITU-R M.1225 channel

B (MHz)	1.25	2.50	5.0	10.0	15.0	20.0
$\mathbf{F_s}$ (MHz)	1.92	3.84	7.68	15.36	23.04	30.72
Paths	1	2	3	4	6	6

square matrix and the estimated weights can be obtained by

$$\mathbf{w}^H = \mathbf{c}^H \mathbf{A}^H (\mathbf{A}\mathbf{A}^H)^{-1}. \tag{2.9}$$

The obtained pattern has very selective null beams with a shape very similar to notch filter, that allow a good system operation and high values of interference reduction. The number of nulls which can be achieved is related to number of available antennas, as explained in [54, 106, 107]. It is possible that the number of signal's replicas between the femtocell and the UE is higher than $L - 1$. In this case the null steering algorithm is able to direct nulls only toward some directions thus reducing the interference of the most powerful paths.

Despite this non ideal working conditions, the numerical results in Sec. 2.4.2 show that the proposed system is able to efficiently counteract the femtocell interference. The joint implementation of the MuSiC and null steering highlights that interference is greatly mitigated if angles evaluation is very good due to deep angular selectivity of nulls. Conversely, a small inaccuracy by Spectral MuSiC leads to a degradation of the performance.

2.2.2 Performance Analysis

The performance of proposed system, obtained by means computer simulations, are presented here. A different bandwidth **B** leads to a different sampling frequency $\mathbf{F_s}$ and, hence, to a different number of paths following ITU-R M.1225 Reccomendation [103] as reported in Table 2.1. Our analysis starts with the DOA estimation capabilities. In a mobility context the channel impulse response and also the DOAs of the multipath components vary in time depending on the UE mobility. The DOA

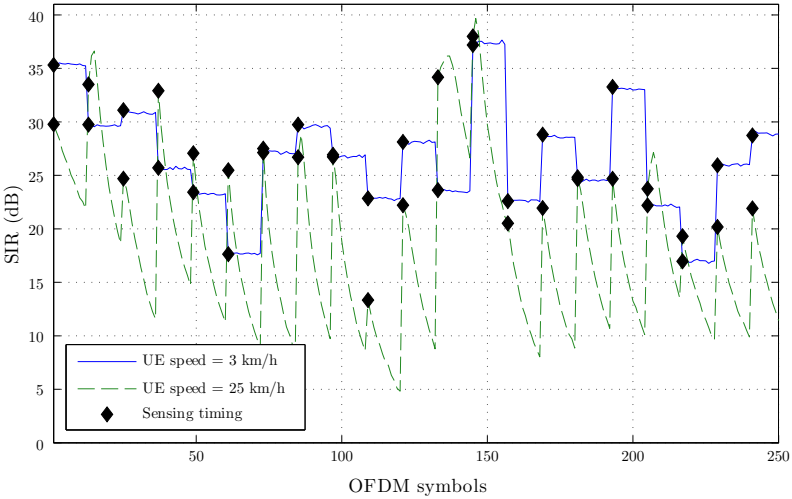

Figure 2-1: Received SIR at UE side assuming a mobility of 3 $\mathrm{km\,h^{-1}}$ and 25 $\mathrm{km\,h^{-1}}$, with active DOA estimation and Null-Steering (5 MHz bandwidth)

estimation and interference mitigation algorithms must be able to follow the DOA variations. For all proposed results, modulation is QPSK and the choice length of the CP (Cyclic Prefix) is "long". Figure 2-1 shows an example of the received Signal to Interference Ratio (SIR) obtained by means the proposed mitigation system for different speeds of the UE during a single run. The results have been derived assuming that without interference mitigation UE experiences a $SIR = 0$ dB. The DOA estimation is updated every sub-frame in our scheme. With pedestrian mobility (3 $\mathrm{km\,h^{-1}}$) the tracking algorithm is able to follow the DOA variations among to successive sensing intervals and the interference power level variation, due to an imperfect positioning of the null beams, is limited. Increasing the UE speed there is a growth of interference between two sensing intervals due to the rapid variability of the channel. However, a significant SIR improvement is obtained even in this case. This is clearly shown in Figure 2-2 where BER is

derived for different UE speeds as a function of the signal to noise ratio (E_b/N_0) received at the HeNodeB (referred to the macro-cell downlink). It is possible to see that there is only a slight increase of the BER with the speed for high E_b/N_0. Figure 2-3 shows the euclidean distance between the estimated and real known DOA values for different operational bandwidth as a function of the E_b/N_0. Finally Figure 2-5 shows the performance of the proposed system for different bandwidths when $SIR = 0$ dB. The DOA estimation accuracy worsens when the number of resolvable paths (i.e., bandwidth) increases. Up to 5 MHz all the resolvable paths can be detected but the noise on the weaker replicas increases the estimation errors. For bandwidth higher than 5 MHz the intrinsic limit of DOA estimation algorithm is overcame (i.e., more than $L - 1 = 3$ replicas are received) and the curves behaviour is not more regular. Higher is the number of the signals weaker is the separation between signal and noise subspaces. For low E_b/N_0 values a higher bandwidth leads to a better DOA estimation thanks to higher snapshot [54, 104] (with the same number of resolvable paths 20 MHz curve is lower than the 15 MHz one). However, when E_b/N_0 increases the eigenspaces interference disallows a decreasing of the estimation errors as in the $B \leq 5$ MHz cases. The interference reduction leads to a more accurate reception of primary service downlink signal at UE side. Figures 2-4 and 2-5 show the BER of the macro-cell downlink at the UE side as a function of the E_b/N_0 for different SIR values[3]. In deriving these results we assume: 3 $\mathrm{km\,h^{-1}}$ UE speed and UE signal energy received at the HeNodeB with a ratio $E_b/N_0 = 10$ dB. In Figure 2-4 the BER curves of the proposed methods for different SIR are compared with those obtained for the system without interference mitigation and for the ideal case of perfect mitigation (i.e., perfect DOA estimation) that coincides with the case without interference. When the proposed scheme is activated at the HeNodeB the interference is very well mitigate for an UE with E_b/N_0 less than about 15 dB. For higher E_b/N_0 there is a level of residual interference, due to a not perfect steering of nulls, which increases for the different simulated levels of SIR.

[3]The SIR value refers to the case without interference mitigation.

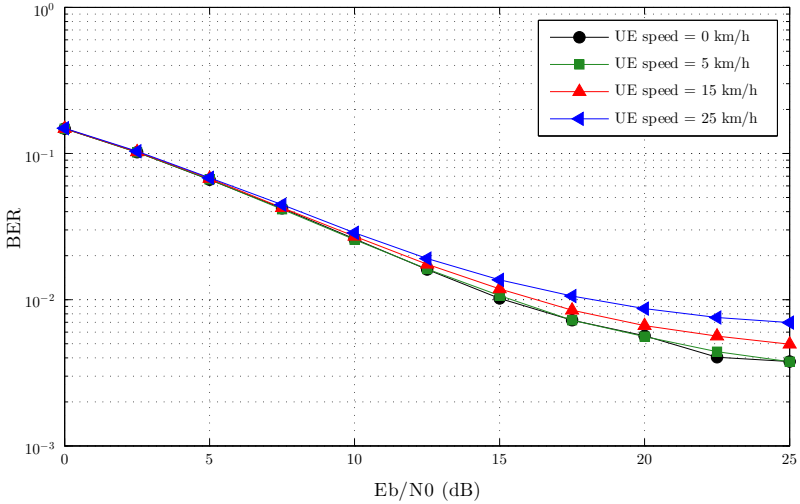

Figure 2-2: BER perfromance for different UE speeds $0 - 25$ km h^{-1}, with the proposed algorithm (5 MHz bandwidth, $SIR = 0$ dB)

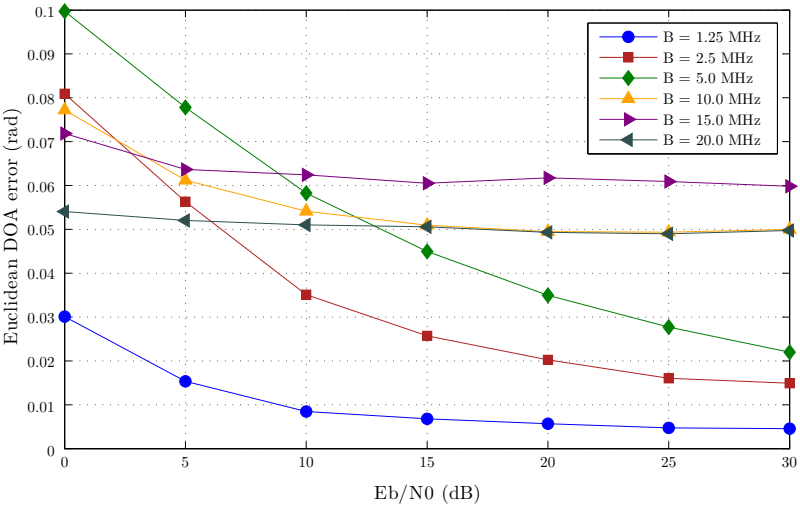

Figure 2-3: DOA estimation error for different bandwidths

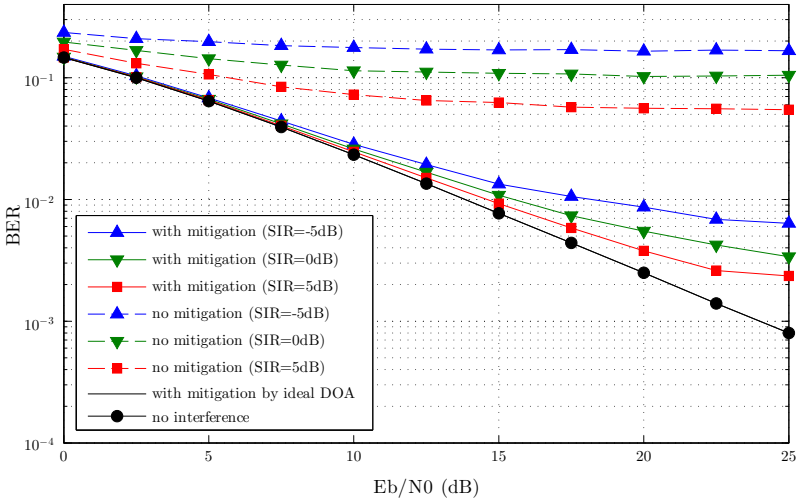

Figure 2-4: Macro-cell downlink BER vs E_b/N_0 with or without proposed interference mitigation scheme (5 MHz bandwidth)

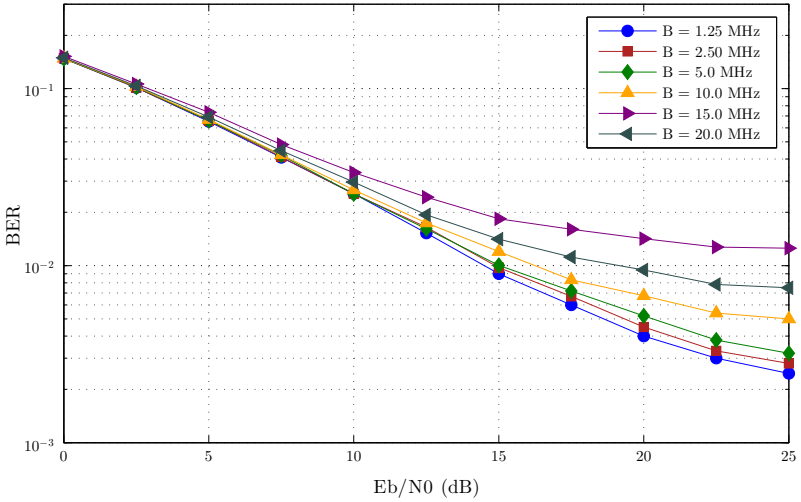

Figure 2-5: Evaluation of primary UE BER with femtocell mitigation routine varying bandwidth

BER curves follows the DOA estimation performance behavior. It shows that even when the number of resolvable path is higher than the estimated DOAs and the generated nulls, the benefits of the proposed system are significant: directing nulls toward the strongest paths is sufficient to increase the received SIR.

2.3 Resource clustering method for uplink estimation

An LTE-A network is considered where an user-deployed HeNB is placed in an indoor area to improve the coverage offered by a macro-cell eNB representing the primary signal. The scenario where the proposed technique takes place is the same of that in Sec. 2.2. Therefore, both systems are modeled according to the 3GPP LTE-Advanced standard [108,109], considering FDD (Frequency Division Duplexing) mode. In order to take into account the worst interference condition, we suppose the two systems operate with the same carrier frequency, f_0, and bandwidth. In particular, the frequency carrier has been assumed equal to 2 GHz.

In this scenario, the macro-cell UEs (MUEs), that are located within the femtocell coverage area, receive the downlink signal of the eNB with partial or complete overlap of the HeNB downlink, with a consequent performance degradation. For this reason, the HeNB has cognitive capabilities to acquire the knowledge of the surrounding environment and then to activate the selected interference mitigation strategies [74, 92, 93, 95, 97, 98] for its downlink transmissions. In particular, the proposed techniques focus on the first phase, the acquisition of the knowledge of the environment within the HeNB coverage area.

The scenario is based on an OFDMA system where the time-frequency resources are divided into units called PRBs that represent the smallest elements that can be allocated. In particular, LTE PRB is made up of $S = 12$ subcarriers over 6 or 7[4] consecutive OFDM symbols. The time-frequency resources are then organized in frames, that are divided

[4]Depending on the cyclic prefix length.

in subframes, each one made up of 2 time slots. The number of PRBs per slot, P, depends on the system bandwidth (i.e., $6 \leq P \leq 100$).

During a slot, the eNB allocates to each active MUE a subchannel made up of a disjoint set of PRBs. PRBs in each subchannel may be not contiguous and the number of PRBs allocated to a MUE depends on many factors (e.g., number of active UEs, system bandwidth, type of data flow) and on the scheduling algorithm adopted by the eNB in each frame. Therefore, there is a wide variability in the allocation of PRBs to the subchannels.

If K_M is the number of active MUEs during a slot period, the k-th MUE (MUE_k) with $k = 1, \ldots, K_M$, can communicate using the subchannel S_k that is made up of P_k PRBs so that:

- $\sum_{k=1}^{K_M} P_k \leq P$
- if $PRB_j \in S_k \Rightarrow PRB_j \notin S_q \quad with \quad \begin{cases} q \neq k; \quad q, k = 1, \cdots, K_M \\ j = 1, \cdots, P \end{cases}$.

Introducing the matrix T of dimension $K_M \times P$, whose element $t_{k,j}$ is one if PRB_j has been assigned to user k and zero otherwise, we can write the n-th sample of the signal transmitted by MUE_k as

$$s_k[n] = \sum_{j=1}^{P} t_{k,j} \sum_{s=1}^{S} \chi_k(j,s) e^{j\frac{2\pi}{N}[((j-1)S+s]n} \tag{2.10}$$

where $\chi_k(j,s)$ represents the symbol sent on the s-th subcarrier of the j-th PRB by the k-th MUE, and N is the total number of the OFDM subcarriers.

The Cognitive HeNB has to estimate information regarding the K ($K \leq K_M$) MUEs located in its coverage area so that it can adopt a suitable interference mitigation scheme. To achieve this goal, the femtocell schedules one OFDM symbol in each subframe in the uplink transmission as sensing period. In particular, the LTE uplink frame supplies one OFDM symbol in each subframe as reserved for the transmission of Sounding Reference Signals (SRSs) usually allocated to the UEs to provide channel state information (CQI) to the eNB. The sensing procedure

of the HeNB can take place in these OFDM symbols. In addition, we assume the HeNB is equipped with a linear array of antennas consisting of L equally spaced elements.

The number of antennas considered here has been selected in order to have a good trade off between performance and limited device dimension, as already described in Sec. 2.2, and the distance between two consecutive antenna elements is $d = \lambda/2$. The signal transmitted by the k-th MUE is received by the HeNB through different propagation paths due to multiple scatterers and obstacles. In particular, the multipath propagation effects are modeled using the tapped-delay-line model defined in ITU-R M.1225 Recommendation for indoor communications (Indoor-A model) [103] and the propagation channel is the same defined in (2.1). The received signal replicas arrive at the antennas through a series of rays arranged in clusters, each one from a different direction, depending on the position of the scatterers accountable for multipath. The power distribution of rays that form the cluster has strong angular concentration, therefore the average value is the best candidate to feature the angle of arrival of the whole cluster. The DOAs of different clusters received by the indoor HeNB vary depending on the environment and the scatterers position, thus an uniform angular distribution of clusters in $[0, 2\pi]$ is the more realistic choice [101].

The m-th signal replica of the k-th MUE signal arrives at the antennas forming the angle $\theta_{m,k}$, $m = 1, 2, \cdots, M$, with the array axis. The propagation delay of the m-th signal between two consecutive antenna elements is $\delta_{m,k}$, defined in (2.2). Considering $\tau \ll T_s$, where T_s is the sampling period, the arriving signal phase is rotated by $2\pi f_0 \delta_{m,k}$. Hence, the n-th sample of the signal received by l-th antenna element of the HeNB can be expressed by $x_l[n]$, similarly defined in (2.3) with different notation:

$$x_l[n] = \sum_{k=1}^{K_M} c_k \sum_{m=1}^{M} s_k[n - \tau_{m,k}] h_{m,k} e^{j[\pi(l-1)\sin(\theta_{m,k})]} + v_l[n] \qquad (2.11)$$

The term c_k is equal to one if the MUE_k is located in the HeNB coverage area, or zero otherwise. To simplify the notation and without loss of generality, in what follows we consider $K = K_M$, and hence we omit term c_k (i.e., $c_k = 1 \quad \forall k = 1; \cdots, K_M$). The samples of the received signal are used to estimate the autocorrelation matrix needed by the PRBs clustering method proposed below.

2.3.1 Proposed PRBs clustering methods

A cognitive HeNB needs to acquire the knowledge of the surrounding environment and, in particular, information regarding the MUEs that are in its coverage area. With this information it is possible to carry out some countermeasures to limit its interference on the primary system. The accuracy of the environment knowledge depends on the portion of signal that can be used to perform the estimate of the intended parameter (e.g., DOA, Signal to Interference plus Noise Ratio, Interference Level), but if the PRBs allocation in the macro-cell is not known at the HeNB, the measures can be done only on a single PRB. This section proposes a method to gather together the PRBs belonging to the same MUE, in order to extend the snapshot (i.e., the available samples) that can be used for the measurements. In particular, we propose a modified version of K-means clustering algorithm. Hence, in this section we first briefly introduce the main concepts of clustering with particular reference to the K-means algorithm. Then, the proposed approach is detailed. Hierarchical clustering is introduced as a comparison method.

Basics on clustering algorithms

Clustering algorithms are used to group the elements of a data set in K groups, on the basis of suitable attributes/features [110]. They perform better when elements belonging to the same cluster are similar each other and different from the elements of other clusters. Clustering algorithms can be classified in two main classes:

- Partitional

- Hierarchical

Partitional methods start from an initial partition of data and move elements of the data set iteratively from one group to another until a stabilization is reached. The K-means is the most known and used partitional cluster analysis method thanks to its simplicity and fast execution speed [99, 111]. It has been used in a variety of domains for different applications such as for distribution systems, data mining, computing networks. The procedure can be easily described as follows:

- *initialization*: the number of clusters, K, is known; K initial cluster centers are chosen randomly;

- *iterations*: each data element is assigned to the nearest center; then the centers are recomputed as the center of mass of all points assigned to it; the iterations are repeated until the process stabilizes or a maximum number is reached.

Hierarchical approaches proceed through a series of steps that build a tree structure (called dendrogram) by either merging or splitting elements so as to optimize some criterion. Each step corresponds to a different number of clusters. The most common procedure is agglomerative (i.e., merging), it means that groups are merged until the number of clusters reaches the expected one [112].

K-means algorithm has two main drawbacks: the number of clusters K must be known and the performance strongly depends on the choice of the cluster centers. Indeed, it has been demonstrated that K-means algorithm gives different results selecting different initial cluster centers and the better results are obtained when the initial partition is close to the final solution [113]. For this reason many papers in the literature presented methods to improve the selection of cluster centers supposing the number of clusters known *a priori*. The determination of the number of clusters is considered a more challenging issue [111]. A typical but not very efficient approach is to run K-means independently for different values of K choosing the best value of K based on a predefined criteria. Another viable solution is to combine the strength of both approaches

(i.e., hierarchical and iterative) trying to discard their disadvantages by using a two-stage procedure where a hierarchical algorithm is used to define the number of clusters and cluster centers, then these results are used as starting points for subsequent partitional clustering (i.e., K-means) [114].

Indeed, in hierarchical methods the number of clusters can be derived examining the incremental changes in the observed metrics (the euclidean distance in our case). A large increase implies that dissimilar clusters have been merged; thus, the number of clusters prior to the merger is most appropriate [112].

In this section the performance of the proposed method is compared with that of a hierarchical agglomerative single-link[5] clustering method [110] and with that of a two-stage K-means clustering algorithm where the number of clusters K is provided by the hierarchical agglomerative algorithm and the cluster centers are selected randomly. Hierarchical methods have good performance in terms of time efficiency but it requires a memory usage that is proportional to the square number of the groups in the initial partition. In addition usually these algorithms make only one pass through the data set thus poor cluster assignments cannot be modified.

Proposed clustering method

As stated before, in traditional K-Means algorithm, the parameter value K is given in advance and randomly initial cluster centers are selected. We propose here an improved K-means algorithm based on a two stage procedure. During the first stage, newly proposed here, the number of clusters K and the initial cluster centers are determined. During second stage the K-means algorithm is used to refine clustering using the inputs provided by first stage. In particular, in the case considered here, we are interested in identifying the resource assignment in an OFDMA system.

[5]the distance between two clusters is the minimum of the distances between all pairs of patterns drawn from the two clusters

To this goal, we consider a new application of the clustering algorithm where:

- the data set is represented by the eigenvectors of the autocorrelation matrix of the signal received by each PRB
- the number of cluster, K, represents the number of MUEs in the HeNB coverage area
- each cluster represents a subchannel S_k

Data set

The clustering algorithm must be applied using suitable attributes to identify which time-frequency resources (i.e., PRBs) have been assigned to the same user by the eNB. Indeed, the selection of the attributes used to group the elements is one of the fundamental step in cluster analysis. In the considered case the attribute must be characterized by an information that is specific of a given user. To this goal we propose to use the information regarding the DoA of the incoming signals. We assume that two signals arriving from the same direction belong to the same user[6].

Let us consider the autocorrelation matrix of the signals received on PRB_j,

$$\mathbf{C}_{\tilde{x}\tilde{x}}^{(j)}[s] = E\left[\tilde{\mathbf{x}}^{(j)}[s]\left(\tilde{\mathbf{x}}^{(j)}[s]\right)^H\right] \tag{2.12}$$

with $j = 1, \cdots, P$, where $(\cdot)^H$ denote the Hermitian operator and the l-th element of the vector $\tilde{\mathbf{x}}^{(j)}[s]$ represents the s-th sample received on PRB_j on the l-th antenna in the time domain. It can be expressed as

$$\tilde{x}_l^{(j)}[s] = \sum_{k=1}^{S} w_k^{(j)} \sum_{n=1}^{N} x_l[n] e^{-j2\pi \frac{nk}{N}} e^{j2\pi \frac{ks}{S}} \tag{2.13}$$

[6]The probability that two users have the same DoA is low.

with $s = 1, \cdots, S$, where $w_k^{(i)}$ is a weight which filters the subcarriers belonging to the j-th PRB defined as

$$w_k^{(j)} = \begin{cases} 1 & \text{if} \quad (j-1)S + 1 \leq k \leq jS \\ 0 & \text{otherwise} \end{cases} . \tag{2.14}$$

Hence, the autocorrelation matrix of the signal received on PRB_j can be estimated as[7]

$$\widehat{\mathbf{C}}_{\tilde{x}\tilde{x}}^{(j)} = \frac{1}{S} \sum_{s=1}^{S} \tilde{\mathbf{x}}^{(j)}[s] \tilde{\mathbf{x}}^{(j)^H}[s] \tag{2.15}$$

In order to obtain a comparison metric between two PRBs, the autocorrelation matrix of the signals received on each PRB is decomposed through the Singular Value Decomposition, i.e.,

$$\widehat{\mathbf{C}}_{\tilde{x}\tilde{x}}^{(j)} = \mathbf{U}_j \mathbf{\Lambda}_j \mathbf{U}_j^H \tag{2.16}$$

where each column of $\mathbf{U}_j$, $\mathbf{u}_l^{(j)}$ with $l = 1, \cdots, L$, represents an eigenvector of $\widehat{\mathbf{C}}_{\tilde{x}\tilde{x}}^{(j)}$ and $\mathbf{\Lambda}_j$ is a diagonal matrix which contains the relative eigenvalues $\lambda_{l,j}$. For each PRB_j, $j = 1, \cdots, P$, the eigenvector relative to the greatest eigenvalue, $\mathbf{u}_{\tilde{l}_j}^{(j)}$ with $\tilde{l}_j = \arg\max_l \lambda_{l,j}$, contains most of the information regarding the DOAs of the signals received in the considered PRB_j. Hence, these eigenvectors can be suitable attributes to aggregate PRBs: signals coming from same direction will have similar eigenvectors while signals coming from different directions will have different eigenvectors. We define the matrix $\mathbf{U}$ as $\mathbf{U} = [\mathbf{u}_{\tilde{l}_j}^{(1)}, \cdots, \mathbf{u}_{\tilde{l}_j}^{(P)}]$, whose dimensions are $L \times P$.

In order to evaluate similarity among the elements of the data set we build the matrix $\mathbf{R}$, whose dimension are $P \times P$, defined as $\mathbf{R} = |\mathbf{U}^H \mathbf{U}|$. The element $r_{i,j}$ of the matrix $\mathbf{R}$ is the magnitude of the projection of the first eigenvector of the i-th PRB on the first eigenvector of the j-th

[7] $\tilde{\mathbf{x}}^{(j)}[s]$ with $s = 1, \cdots, S$ are independent and identically distributed random variables.

PRB, i.e.,

$$r_{i,j} = \left| \left(\mathbf{u}_{l_j}^{(i)} \right)^H \mathbf{u}_{l_j}^{(j)} \right|. \tag{2.17}$$

The element $r_{i,j}$ expresses how the PRB_i is correlated to PRB_j, hence it expresses the similarity between the DOAs of the signal received by PRB_i and PRB_j. Note that the elements of the matrix may assume values in the interval $[0; 1]$, where 1 denotes perfect match between two PRBs, while 0 means that they are orthogonal and hence completely uncorrelated. Fig. 2-6 represents an example of $\mathbf{R}$ in the case of $K = 3$ users when $P = 6$ and with contiguous PRBs frequency allocation (i.e., the subchannel of k-th user is defined by $S_k = \{PRB_{(k-1)K+1}, \cdots, PRB_{kK}\}$, with $k = 1, 2, 3$).

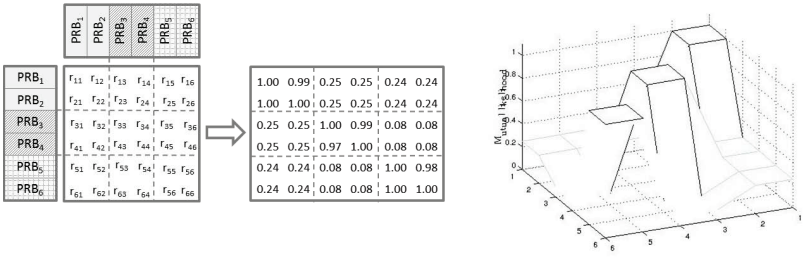

Figure 2-6: Example of matrix $\mathbf{R}$ with 3 users and contiguous frequency allocation.

In this example, we see that 3 clusters can be clearly identified, they represent the subchannels allocated to the users. We want to stress that this is a simple case that is used for a clear explanation. In general, when the number of clusters grows, the clusters discrimination is more complicated due to the multipath channel propagation and different directions of arrival of the incoming signals.

Stage 1: Number of clusters and cluster centers

This subsection describes the first stage of the clustering algorithm that is newly proposed here. It is used to determine the number of clusters (i.e., the number of MUEs in the HeNB area) and suitable

initial cluster centers. The algorithm is made up of two thresholding and row deletion operations that are detailed in Procedure 1.

In the first operation, at the t-th iteration (with $t = 1, \cdots, P$) the thresholding is operated on matrix $\tilde{\mathbf{R}}^{(t)}$ where $\tilde{\mathbf{R}}^{(1)} = \mathbf{R}$. A row of $\tilde{\mathbf{R}}^{(t)}$ is selected: rows are selected successively, while the first row (i.e., $t = 1$) is randomly chosen. If the j-th element of the selected i-th row is over the threshold Γ, all the elements of the j-th row (with $i \neq j$) of $\tilde{\mathbf{R}}^{(t)}$, are put to zero (all the corresponding PRBs are assumed to belong to the same cluster). This thresholding operation is used to know which PRBs are strongly similar, for this reason Γ should assume high values. Fig. 2-7 shows the results of this first step when the second row is selected as starting point. $\tilde{\mathbf{R}}^{(6)}$ represents the result of the first stage. The number of rows of $\tilde{\mathbf{R}}^{(P)}$ different from zero represents a

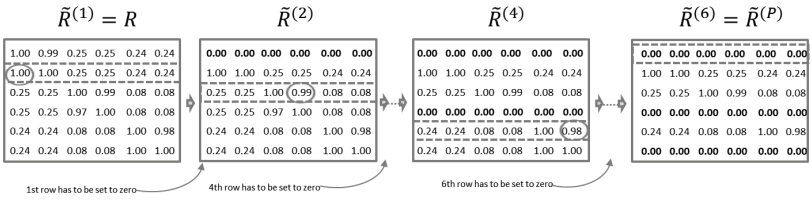

Figure 2-7: First thresholding and rows deletion operation.

rough estimation of the number of clusters, K'.

The second operation is used to refine this result by exploiting the whole information contained in each row of $\tilde{\mathbf{R}}^{(P)}$. The idea is that the similarity between PRB_i and PRB_j depends not only on the correlation between them, but also on the correlation of each one with all the other PRBs (i.e., if two PRBs are both similar to a third PRB maybe there is a correlation also among them).

Let $\mathbf{q}' = [q'_1, \cdots, q'_{K'}]$ be a vector of length K' that contains the indexes of the rows of $\tilde{\mathbf{R}}^{(P)}$ that are different from zero. We can define the upper triangular matrix $\mathbf{Z}$, whose dimensions are $K' \times K'$, so that its (i, j) element is defined as the correlations between the non-zero rows

Procedure 1 Proposed algorithm - first stage

• First Iterative thresholding and row deletion
$\mathbf{T} \leftarrow$ random_permutation($[1, \cdots, P]$)
$K' \leftarrow 0$
for $t \leftarrow 1$ to P **do**
  $f = T + t$
  $j = 1$
  while $j < P$ **do**
    if $\tilde{r}_{f,j}^{(t)} > \Gamma \quad \& \quad f \neq j$ **then**
      $K' \leftarrow K' + 1$
      $\mathbf{q}' \leftarrow f$
      $\tilde{\mathbf{r}}_{\mathbf{j}}^{(\mathbf{t})} \leftarrow [0, \cdots, 0]$
      $j = P$
    else
      $j = j + 1$
    end if
  end while
end for
• Matrix Z
for $i \leftarrow 1$ to K' **do**
  for $j \leftarrow 1$ to K' **do**
    $z_{i,j} = \mathbf{r}_{q_i'} \mathbf{r}_{q_j'}$
  end for
end for
• Second Iterative thresholding and row deletion
$K \leftarrow K'$
$\mathbf{q} = \mathbf{q}'$
$\tilde{\mathbf{R}}^{final} = \tilde{\mathbf{R}}^{(P)}$
for $i \leftarrow 1$ to K' **do**
  for $j \leftarrow 1$ to K' **do**
    if $i > j \quad \& \quad z_{i,j} > \Gamma$ **then**
      $K \leftarrow K - 1$
      $\mathbf{q} \leftarrow \mathbf{q} - q_j$
      $\tilde{\mathbf{r}}_{\mathbf{j}}^{\mathbf{final}} \leftarrow [0, \cdots, 0]$
    end if
  end for
end for

of $\tilde{\mathbf{R}}^{(P)}$, $\tilde{\mathbf{r}}_i^{(P)}$,

$$z_{i,j} = \begin{cases} \frac{\tilde{\mathbf{r}}_{q_i'}^{(P)} \left[\tilde{\mathbf{r}}_{q_j'}^{(P)}\right]^T}{\sqrt{\|\tilde{\mathbf{r}}_{q_i'}^{(P)} \tilde{\mathbf{r}}_{q_j'}^{(P)}\|}} & \text{if} \quad i < j \\ 0 & \text{i} \geq j \end{cases} \tag{2.18}$$

A second thresholding operation[8] is performed on $\mathbf{Z}$. The proposed procedure looks for elements that are higher than the selected threshold. If G is the number of elements of $\mathbf{Z}$ that are higher than Γ, it means that too many centers at the first step have been found:

- the final number of cluster centers is $K = K' - G$;
- if element $z_{i,j}$ of $\mathbf{Z}$, is over the threshold, the q_j'-th row of matrix $\tilde{\mathbf{R}}^{(P)}$ is put to zero resulting in matrix $\tilde{\mathbf{R}}^{final}$;
- a new vector $\mathbf{q} = [q_1, \cdots, q_K]$ of length K is defined as the vector that contains the indexes of the rows of $\tilde{\mathbf{R}}^{final}$ that are different from zero.

If $G = 0$ we have: $K' = K$, $\mathbf{q} = \mathbf{q}'$ and $\tilde{\mathbf{R}}^{(P)} = \tilde{\mathbf{R}}^{final}$ as in the example reported in Fig. 2-8.

The final results of the first stage of the proposed algorithm are:

- the number of cluster K,
- the initial cluster centers; these are the rows of $\mathbf{R}$ whose indexes are included in $\mathbf{q}$. In particular the set of initial cluster centers $\mathbf{C}^{(0)}$ is $\mathbf{C}^{(0)} = [\mathbf{c}_1^{(0)}, \cdots, \mathbf{c}_K^{(0)}]$ with $\mathbf{c}_i^{(0)} = \mathbf{r}_{q_i}, \quad i = 1, \cdots, K$.

The performance of the proposed method is dependent on the threshold Γ, but an accurate optimization is not needed. Threshold Γ is used to determine which elements are strongly correlated and, hence, a high value of Γ must be selected. We have verified that a value of $\Gamma = 0.95$ is always correct. Indeed, even if the algorithm can find too many clusters (i.e., $K' > K$) during the first step, the second step reduces this selection.

[8]The threshold value here is the same of the first step.

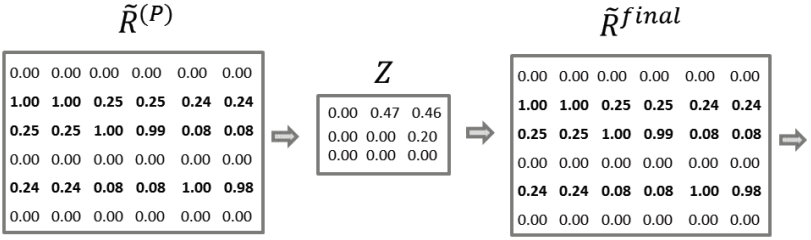

Figure 2-8: Second thresholding and rows deletion operation.

STAGE 2: K-means Clustering

In the second stage the classical K-means algorithm is applied using the inputs provided by the first stage. In particular, the data set is represented by the rows of matrix $\mathbf{R}$ and the set of initial cluster centers is $\mathbf{C}^{(0)}$. Each cluster corresponds to a subchannel S_k with $k = 1, ..., K$. The algorithm works iteratively. At iteration t we have:

- the euclidean distance among all the cluster centers, derived at previous iteration, $c_i^{(t-1)}$ $(i = 1, \cdots, K)$ and all the rows of $\mathbf{R}$, $\mathbf{r_j}$ $(j = 1, \cdots, P)$ is calculated as:

$$d_j(\mathbf{c}_i^{(t-1)}) = \|\mathbf{r}_j - \mathbf{c}_i^{(t-1)}\| \tag{2.19}$$

- each PRB_j, with $j = 1, \cdots, P$, is assigned to the subchannel S_k with $k = 1, \cdots, K$, if $d_j(\mathbf{c}_k^{(t-1)})$ is lower than $d_j(\mathbf{c}_i^{(t-1)})$ for all $i \neq k$

- a new set of cluster centers, $\mathbf{C}^{(t)}$, is calculated, whose elements are

$$\mathbf{c_k^{(t)}} = \sum_{j:\ PRB_j \in S_k} \frac{\mathbf{r}_j}{P_k^{(t)}} \quad k = 1, \cdots, K \tag{2.20}$$

where $P_k^{(t)}$ is the number of elements belonging to cluster k-th at iteration t. The iterations stop when the algorithm converges or when the maximum number of iterations is reached. The algorithm is quite

simple but if the amount of data is high, time and complexity result to be high. Moreover, if the clusters centers are not suitably chosen, the algorithm requires a high number of iterations and, in some cases, it cannot converge.

2.3.2 Performance Analysis

This section presents the numerical results obtained by means of computer simulations in order to validate the scheme proposed in the previous section. We assume the HeNB equipped with a linear array of L antennas and the presence of a variable number of MUEs in its coverage area. The number of PRBs allocated to each MUEs varies and the allocation can be either contiguous or interleaved. The propagation channel between the MUEs and the HeNB is characterized as a multipath indoor channel with 4 paths, where each path has a DOA that is uniformly distributed over 360 degrees. The number of PRBs is assume equal to $P = 100$.

First we want to verify the choice of the attributes of the data set used for clustering (i.e., DOA information). We focus on a scenario with two MUEs (i.e., $K = 2$) and analyze the PRBs clustering performance in terms of mean percentage error in the PRBs allocation as a function of the angle separation between the users. In particular, the received signal is obtained as the sum of different multipath components received with different DOAs, hence, we refer here to the angle separation between the DOAs of the main signal component of the users (i.e., the main path). In order to evaluate the effect of secondary multipath components, Fig. 2-9 shows the results for different number of multipath components when the Signal to Noise Ratio (SNR) at the HeNB receiver is equal to 15 dB and $L = 4$. We can see that the proposed method (Cluster Centers - Proposed Approach, CC-PA) has good performance only when the separation between the users is beyond a critical angle. As expected, when the users are too close, the proposed algorithm is not able to separate the two clusters. This is due the choice of the clustering data set whose attributes are based on the similarity of the DOA

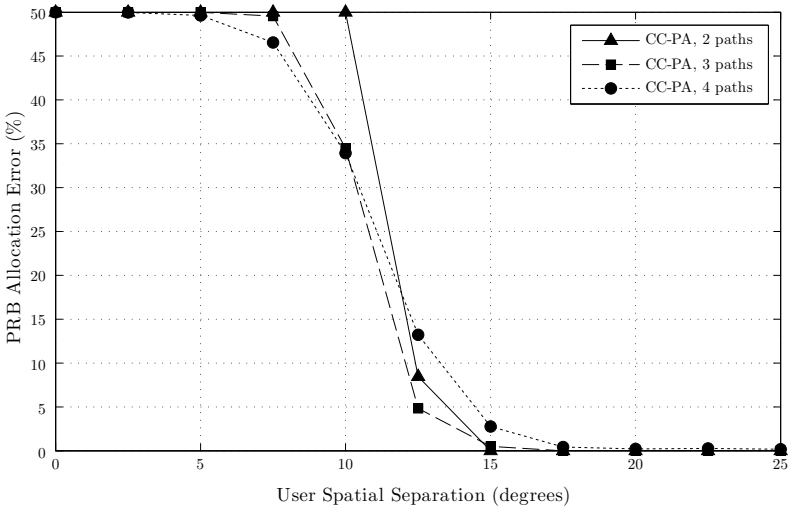

Figure 2-9: Mean percentage error for different number of multipath components when the angle separation between two users varies.

of the incoming signals. Therefore, if the signals of two users arrives at the antennas from the same direction, they cannot be distinguished. However, the probability that the main propagation path of two different MUEs comes from the identical direction can be considered very low. In addition we can see that the performance are almost the same changing the number of multipath components. It depends on the fact that the contribution of the main path is always dominant. However, we can observe that until the first paths of the two users are not sufficiently separated, having a higher number of paths is better because it implies higher diversity among users. Conversely, increasing the separation angle there are crossing points among the curves because the main paths separation becomes dominant.

The effectiveness of the proposed clustering method compared with other alternatives is shown in Fig. 2-10. This figure represents the performance of the K-means with the proposed algorithm as a function of the number of MUEs in the coverage area of the femtocell assuming

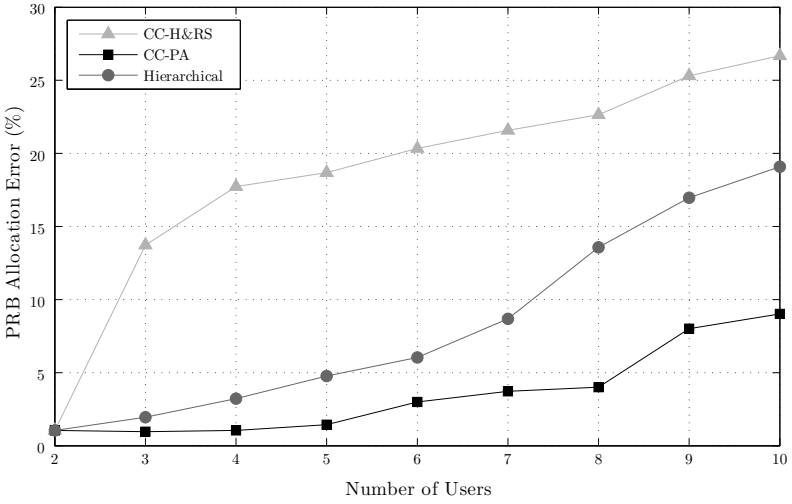

Figure 2-10: Mean percentage error when the number of users varies.

$L = 4$. The performance of a agglomerative single-link hierarchical clustering (Hierarchical) algorithm and a K-means algorithm that uses as inputs the number of clusters estimated by the hierarchical procedure and random cluster centers (Cluster Centers - Hierarchical & Random Selection, CC-H& RS), are reported as comparison. The figure shows that when the number of clusters and the cluster centers are calculated with the proposed method, the percentage of PRBs allocation errors is lower compared to the other methods, especially for a high number of clusters. In particular, as demonstrated in the literature, K-means suffers for an inaccurate selection of the clusters centers that leads to high errors because in some cases the algorithm is not able to converge. Hierarchical clustering has better performance than the K-means with random initial centers, but it is outperformed by the proposed method since it suffers for higher inaccuracy in the estimation of the number of clusters, as evident in Fig. 2-12.

The performance of the clustering methods is shown as a function of the SNR value in Fig. 2-11 for different numbers of clusters (i.e.,

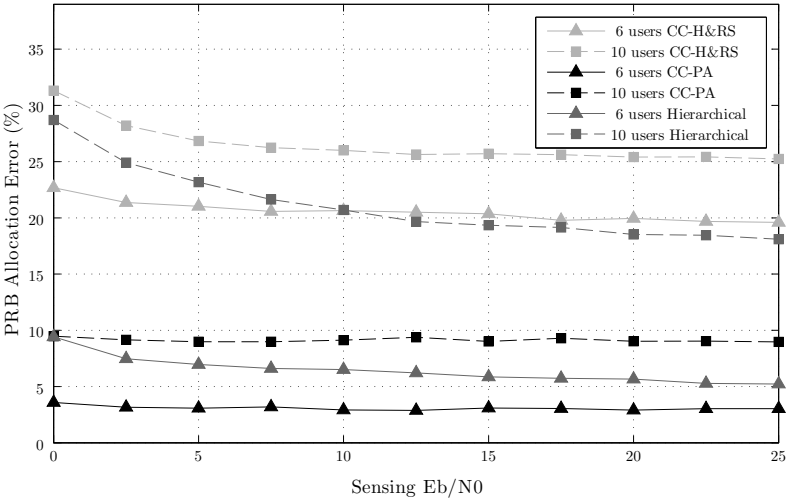

Figure 2-11: Mean percentage error as a function of the SNR value, for different numbers of clusters.

MUEs). It is possible to note that the SNR effect on the proposed method is negligible, while the other two methods for an inaccurate estimates of K at low SNR values (i.e., both methods uses the parameter K estimated by the hierarchical approach). This results depends on the particular data set that has bee selected, indeed the effect of the noise is negligible because it is reduced by the mutual projection of the PRB correlation matrix eigenvectors. This operation is repeated two times in the proposed method (calculating the matrix $\mathbf{Z}$), and hence it is more robust at low SNR values.

The performance comparison between CC-PA and the CC-H& RS allows the evaluation of the benefits of our method in terms of the selection of the cluster centers. However, the proposed method is used also to determine the number of clusters K that is a parameter needed by any clustering algorithm. Fig. 2-12 shows the mean percentage error on the determination of the number of clusters of the proposed K-means method and the value K calculated by means of a hierarchical approach

for different number of antennas, $L = 4, 6, 8$. It is possible to see that our methods achieves better performance and there is a significant improvement by increasing the number of antenna elements. The proposed PRBs clustering method effectiveness is then tested by considering a DOA estimation algorithm. For this purpose we consider the known Root MuSiC (Multiple Signal Classification) algorithm that is based on the decomposition of the autocorrelation matrix of the received signal [105]. The effect of snapshot size in DOA estimation algorithms is widely addressed in the literature [115], and it is shown how this heavily affects the performance of the estimate. Usually MuSiC algorithms works optimally for over-sized snapshot which often are not available at the receiver in certain contexts. The snapshot dimension can be increased in the frequency domain by means of PRBs grouping. Fig. 2-13 consider $L = 4$ antennas and shows the DOA estimation capabilities in terms of mean square error of the Root MUSIC estimation when it works on a different number of PRBs. It is possible to note that the performance is poor with a single PRB, while it is possible to get a remarkable improvement even with a few of aggregated PRBs. From this figure it is evident the need to know which PRBs belong to the same user, in order to perform the DOA estimates on an extended snapshot.

Finally, we can do some considerations on complexity. K-means algorithm has been selected for its simplicity and execution speed, that are the main reasons for its wide applicability. Its complexity is O(PKI) where I is the number of iterations while the hierarchical agglomerative requires a time complexity that is $O(P^3)$[9] and requires higher storage memory [110]. In all the simulations the number of iterations is limited to $I = 5$. The only additional complexity of our proposed method to determine the initial values is due to the calculation of matrix $\mathbf{Z}$ (matrix $\mathbf{R}$ represents the data set and hence it is needed for every clustering algorithm). It requires $(K')^2$ correlations. The other operations are simply thresholding and row cancellations.

[9]There are some variants that reduce the complexity to $P^2 \log P$.

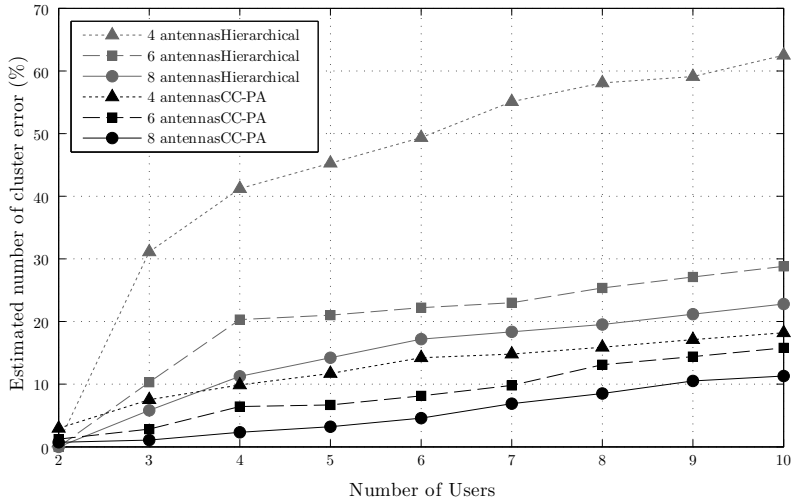

Figure 2-12: Mean percentage error on number of clusters for different number of antennas.

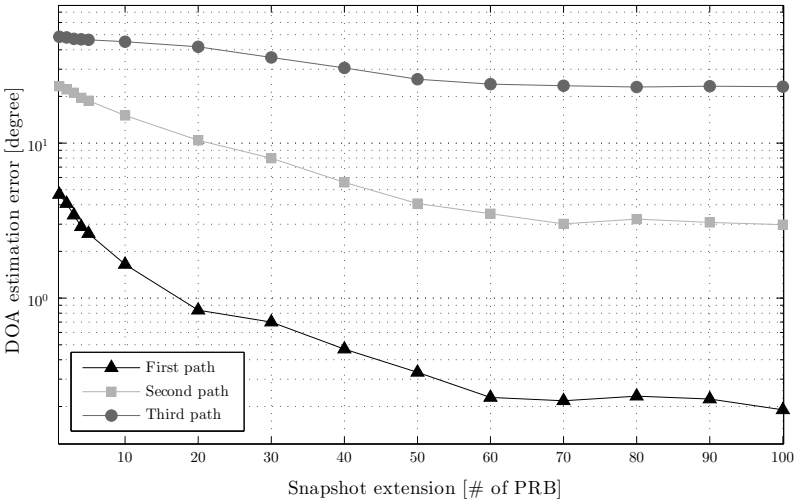

Figure 2-13: Performance for each resolvable path of root MuSiC algorithm when the numbers of sensed PRBs varies.

2.4 PRB-wise angular interference suppression method for cognitive small-cell

With reference to the operating scenario considered in Sec. 2.2, the secondary system is represented by a user-deployed small-cell, also called Home eNB and the primary system is the macrocell base station. Thus, the UEs of the primary service located within the femtocell coverage receive the DL signal of the eNB with partial or complete overlap of the HeNB downlink, with a consequent performance degradation, as shown in Fig. 2-20. Both systems are modeled according to the 3GPP LTE-A standard [108] by considering FDD (Frequency Division Duplexing). In order to take into account the worst interference conditions, the two systems operate with the same carrier frequency, $f_0 = 2$ GHz, and bandwidth. The HeNB exploits its cognitive capabilities to adapt its transmissions. The only information that the macro-cell BS (eNB) shares with the HeNB using backhaul link is the scheduled information of the macro-cell [116]. The HeNB is equipped with a linear array of antennas consisting of L equally spaced elements. The number of antennas has been selected in order to take into account the device dimension. Using uniformly spaced array elements with $d = \lambda/2$ and $f_0 = 2$ GHz, $L = 4$ antennas can be considered suitable to perform accurate beamforming operations maintaining the device dimension similar to other household devices.

The proposed system takes into account multipath propagation effects using the tapped-delay-line model defined in the ITU-R M.1225 Recommendation [103]. Two different Power Delay Profiles (PDPs) are considered:

- Outdoor-A for the eNB and the MUEs links;
- Indoor-A for the HeNB and the MUEs links.

Assuming a propagation channel characterized by M multipath components, the n-th sample of the signal received by l-th antenna element

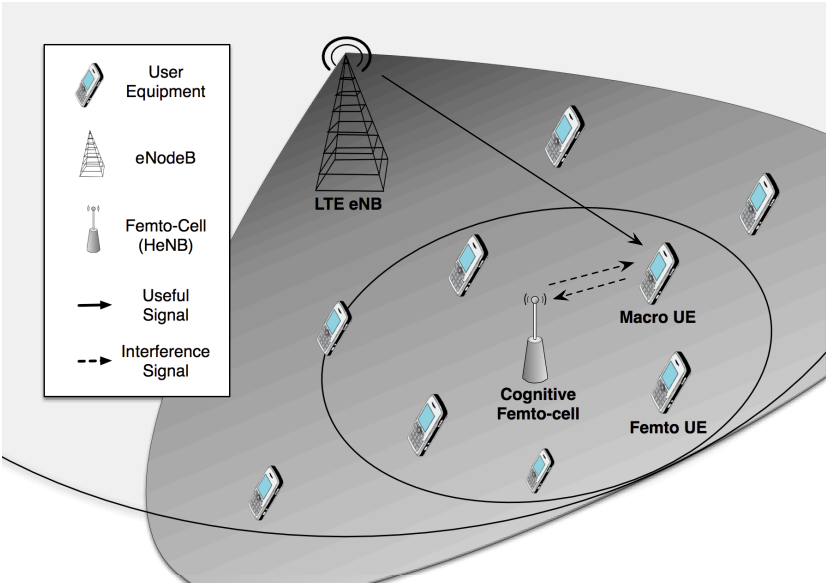

Figure 2-14: Considered scenario set up by a macrocell, some MUEs, a femtocell and its FUEs.

of the HeNB on the i-the PRB can be expressed as

$$r_{l,i}[n] = \sum_{m=1}^{M} x_i[n - \tau_m] h_m e^{j[2\pi f_0 (l-1)\delta_m]} + v_l[n] \tag{2.21}$$

where $x_i[n]$ is the signal on the i-th PRB by a MUE or a Femtocell UE (FUE) and the other terms are defined in the same way that in (2.3). The propagation delay of the m-th signal between two consecutive antenna elements is a function of the DOA as in (2.2). Defining the steering vector towards the direction θ_m, $\mathbf{s}(\theta_m)$, which contains the elements $s_l(\theta_m) = e^{j\pi(l-1)\sin(\theta_m)}$ with $l = 1, 2, \cdots, L$, the received signal on the i-th PRB can be expressed by

$$\mathbf{r}_i = \mathbf{S} \cdot \mathrm{diag}(\mathbf{h}) \cdot \mathbf{x}_i + \mathbf{v} \tag{2.22}$$

where $\mathbf{x}_i = \left[x_i[n-\tau_1], \cdots, x_i[n-\tau_M]\right]^T$ and $\mathbf{S}$ and $\mathbf{h}$ are specified in (2.4).

For what concerns the DOAs, the signals replica received by the indoor HeNB vary depending on the environment and the scatters position and thus an uniform angular distribution of clusters in $[0, 2\pi]$ is the more realistic choice.

2.4.1 Interference Suppression Method

The interference suppression method, proposed here, is made up of two following steps and works taking into account the multiple access scheme used by LTE-A system. The first step is represented by the sensing, used to estimate the directions of arrivals of the primary users signals. In the second step, the proposed method calculates suitable weights to steer the DL radiation pattern in order to place zeros in correspondence with the estimated MUE directions.

However, any DOA estimation algorithm can detect up to $L-1$ directions of arrival and the Null Steerer algorithm can place up to $L-1$ nulls. On the other side, in an actual scenario several MUEs can be present in the femtocell area, each one characterized by multiple propagation paths with different DOAs. This means that it is very likely that the number of signal received by the HeNB is higher than $L-1$. To overcome this problem, the proposed method works on a PRB-wise way. As stated before, in LTE-A the PRB is the smallest resource unit allocated to a single user. According to the proposed scheme, DOA estimation and null steering are performed on each PRB separately. This allows an estimate of $L-1$ DOAs for each PRB and, hence, the separation of the MUEs signals. In that sense, the method proposed in this section is an extension of [74], where an interference reduction scheme for an OFDM (Orthogonal Frequency Division Multiplexing) rather than an OFDMA system is proposed. Indeed, the main assumption in [74] was that all the subcarriers were allocated to a single user, and thus the number of received signals depended only on the number of multipath components of the channel.

The drawback of working on a PRB basis is that the snapshot (i.e., the available samples) used to estimate the DOA is limited to 12 subcarriers. Indeed, the quality of the estimation is strongly conditioned by the number of samples collected during the sensing period. When only few samples are available, the acquired knowledge can be not accurate. However, in general, the eNB uses more than one PRB to communicate with a MUE (i.e., a subchannel is usually made of several PRBs). Therefore, the idea is to gather together all the PRBs assigned to the same MUE, and to perform the DOAs estimates on the resulting samples. This can be done if the HeNB knows which PRBs have been assigned to a MUEs. This information is not known a priori, but it can be derived, as explained in Sec. 2.3, exploiting the same information used by the interference suppression method [76].

DOA Estimation and Zero Forcing Beamforming on PRBs

The Cognitive femtocell has to estimate the DOA of the signals coming from all the UEs (both FUEs and MUEs) in its coverage area. To this goal, we assume that the femtocell reserves an OFDM symbol in each subframe in uplink as sensing period for the MUEs.

The DOA estimation is performed using the well known Multiple Signal Classification (MuSiC) algorithm [105]. It is based on the eigenvalue decomposition of the received signal autocorrelation matrix, $\mathbf{R}$, that is defined in (2.5). During the sensing interval, the DOA is estimated in each PRB for the MUEs, while the FUEs' DOA can be evaluated in other intervals with a longer duration, since the femtocell can decide the FUEs resource allocation. The eigenvalues of the autocorrelation matrix identify a signal subspace and a noise subspace [105]. To estimate the signals DOA, θ_m with $m = 1, \cdots, K$, the MuSiC algorithm searches the K that maximize the function in (2.7).

At a later stage, the DOA information is used to limit the interference towards the MUEs through a pre-processing of the signal transmitted by the HeNB. It allows to perform null beams in the selected transmission directions. As demonstrated in [117] UL and DL

spatial information are strongly correlated and it is reasonable to use UL estimation in DL transmission. Let $\theta_m^{\mathcal{M}}$ be the DOA of the m-the replica of the signal transmitted by the MUE and $\theta^{\mathcal{F}}$ the main DOA (i.e., direction of the strongest signal replica) of the FUE. The beamforming weights $\mathbf{w}_i = \left[w_{1,i}, \cdots, w_{L,i}\right]^T$ for the transmission on i-th PRB are obtained by imposing the projection on $\mathbf{s}(\theta^{\mathcal{F}})$ equal to 1 and the projection on $\mathbf{s}(\theta_1^{\mathcal{M}}), \cdots, \mathbf{s}(\theta_K^{\mathcal{M}})$ equal to 0 [54]. Denoting with $\mathbf{A_i} = \left[\mathbf{s}(\theta^{\mathcal{F}}), \quad \mathbf{s}(\theta_1^{\mathcal{M}}), \quad \mathbf{s}(\theta_2^{\mathcal{M}}), \quad \cdots, \mathbf{s}(\theta_K^{\mathcal{M}})\right]$ the matrix containing the steering vectors of interest for the i-th PRB is possible to use the same formula in (2.9) to calculate the i-th beamforming weights.

Proposed PRBs aggregation

The interference mitigation scheme described above is mainly subject to DOAs estimation errors. This subsection analyses a potential enhancement that could be considered. Fig. 2-15 shows the Bit Error Rate (BER) experienced by the MUEs in the DL communication when the proposed interference mitigation system is applied and the DOAs of the received signal replicas are perfectly known at the HeNB. The BER performance is expressed as a function of the ratio between the received energy per bit, E_b, and the noise spectral density, N_0, for different number of resolvable multipath components. It is possible to notice that, if the number of multipath components introduced by the propagation channel is lower than L, the system is able to completely eliminate the femtocell interference. The performance worsen when the number of resolvable paths is higher than $L-1$ and there is a residual interference.

In general, the failure in the DOA estimation depends mainly on three factors: the number of antenna elements, the SNR value of the received signal during sensing step and the snapshot size. As stated in the first part of Section 2.4, the number of antenna elements is one of the main operational constraints we have considered. In addition, we selected a DOA estimation algorithm able to provide a high accuracy even when the received signal is degraded (i.e., low SNR values).

The third factor, the snapshot size, is widely addressed in the literature [115]. Usually, MuSiC algorithms optimally work with oversized snapshots, which are not available at the receiver in certain contexts. The main proposed solution is to rely on a high number of antennas, even doubly the number of the signals to be detected. This solution is not applicable in this scenario because the overall size of the HeNB structure is one of the main operational constraints we have considered. Alternatively, the data received during the different sensing stages, performed every 1 ms, could be temporarily collected averaging the values of the autocorrelation matrix in order to obtain better estimates of the autocorrelation matrix. However, the resource allocation of the MUEs should remain unchanged in this time and it cannot be guaranteed. The solution discussed in this section is to increase the snapshot dimension in the frequency domain, by gathering together PRBs belonging to the same user. Indeed, in general each MUE has assigned more than one PRB to communicate with the eNB. Moreover, this would lead to a reduced computational complexity, because MuSiC and Null Steering algorithms would be carried out fewer times, i.e., once for MUE. This problem can be addressed by introducing algorithms able to group the PRBs belonging to the same users.

In particular, the method proposed in Sec. 2.3 exploits the eigenvectors of each PRB autocorrelation matrix $\mathbf{R_i}$ [76]. The idea is to exploit the similarity of eigenspaces signal belonging to the same user, calculating the projection of the informative eigenvector of each PRB on the space represented by the main eigenvector of the other PRBs.

It is important to stress that this PRBs clustering method uses the matrix $\mathbf{R_i}$ used also for the DOA estimation, hence it introduces only a limited complexity increase.

As shown in the next section, the efficiency of the DOA estimation algorithm depends on the number of used PRBs. Hence, it varies between a lower and an upper bound. The worst case occurs when the PRBs allocation is not available or each PRB is allocated to a different user, thus, the size of the DOA estimation snapshot is equal to the number of resource elements in a PRB and some inaccuracies are intro-

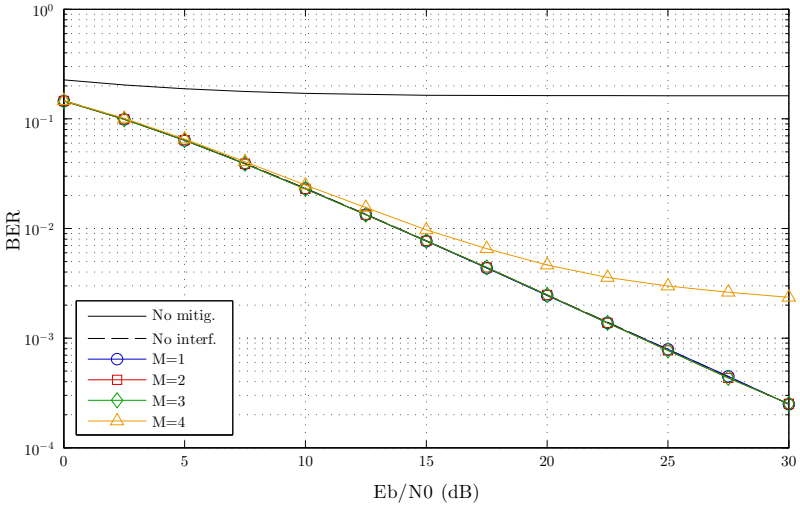

Figure 2-15: Macrocell DL BER performance of the proposed system when ideal DOA estimates are available at HeNB.

duced when the number of incident signals is high. Instead, the upper bound is reached when all PRBs are assigned to a single user: in this case the snapshot is made up of all the subcarriers. This particular case coincides with considering an OFDM system like in [74].

2.4.2 Performance Analysis

This section presents some numerical results obtained through computer simulations in order to validate the system. In order to facilitate the description of the results, we shall use the following notations as:

- $link_1$ the link between MUE and HeNB, that is used for DOA estimation;
- $link_2$ the macrocell DL connecting eNB and MUE.

Firstly, the BER of the macrocell downlink communications is evaluated when the proposed interference mitigation scheme is applied at

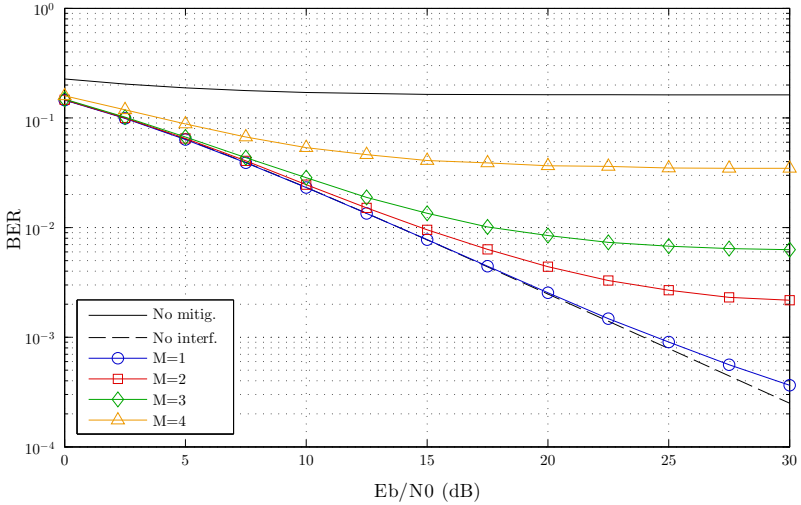

Figure 2-16: Macrocell DL BER performance of the proposed system. E_b/N_0 of $link_1 = 10$ dB

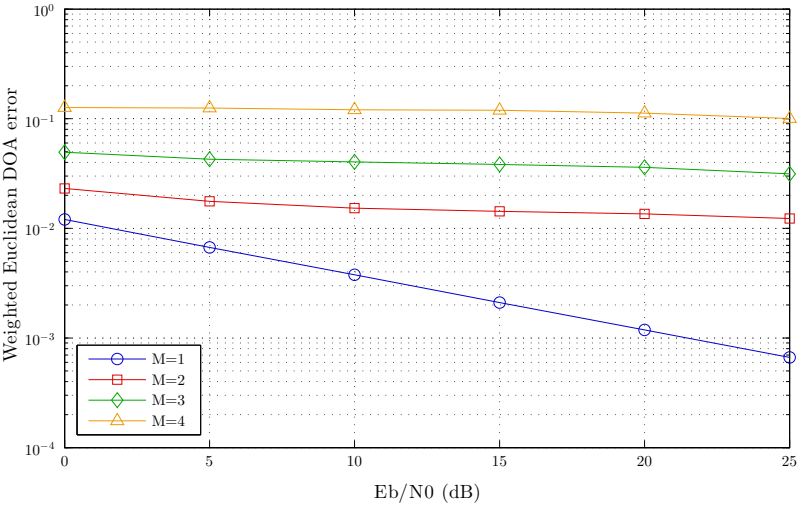

Figure 2-17: DOA estimation errors.

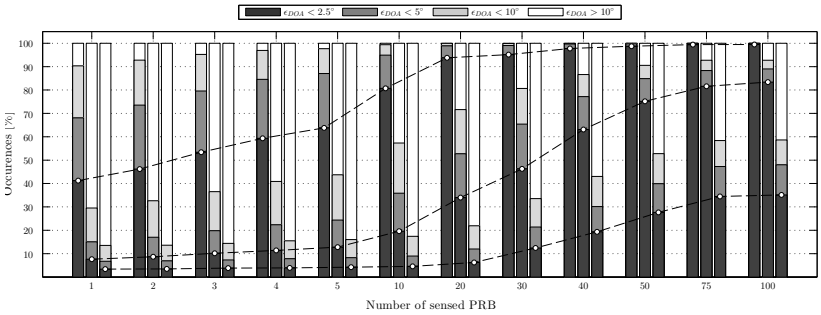

Figure 2-18: DOA estimation precision as a function of the PRBs in the snapshot used for sensing.

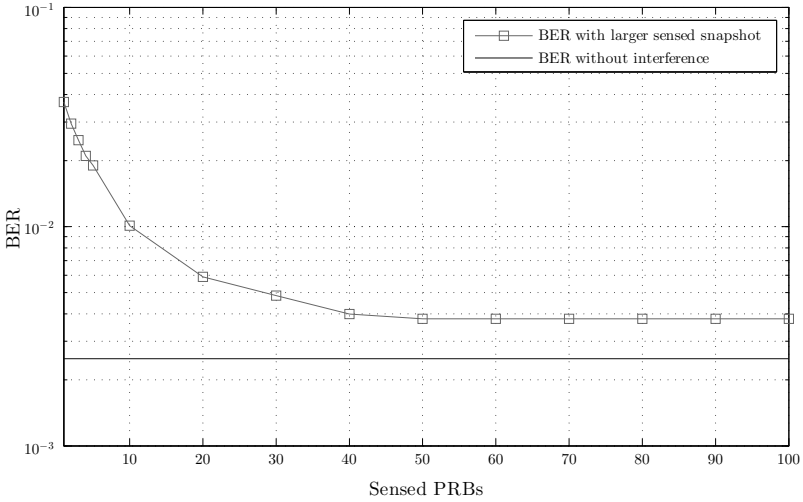

Figure 2-19: Macrocell DL BER performance of the proposed system as a function of the PRBs in the snapshot used for sensing. $M = 4$, $E_b/N_0 = 10$ dB on $link_1$, $E_b/N_0 = 20$ dB on $link_2$

the HeNB. The values are derived as a function of the $link_2$ E_b/N_0, when the E_b/N_0 of $link_1$ is equal to 10 dB. Increasing the number of signal replicas generated by the propagation channel, performance worsen, as shown in Fig. 2-16. when the proposed mitigation is not active, the number of paths does not affects the performance because the whole interfering power arrives to the receiver. When $M > L - 1$, the MUE receives interference from some propagation paths that cannot be detected and cancelled, leading to a performance floor. However, a significant improvement is evident respect to the case without mitigation. It is important to underline that in actual scenarios, where the number of the more powerful paths is low, the proposed system achieves very good performance.

As stated before, the performance of the proposed algorithm strongly depends on the precision of the DOA estimation. For this reason Fig. 2-17 presents the DOA estimation error of the MuSiC as a function of the E_b/N_0 received on $link_1$. The value of the *Weighted Euclidean DOA error* is computed weighting the error with g_m, proportional to the magnitude of each replica, i.e., $g_m = E\left[{\alpha_m}^2\right]$. When $M = 1$ the error curve decreases linearly with the E_b/N_0 and DOA estimates are very accurate. As M increases, the DOA estimation error also increases due to the contribute of the weakest signal replicas. It can be noticed that there is not a significant performance improvement neither for high E_b/N_0 values. However, DOA estimation capabilities can be improved by increasing the snapshot used by the MuSiC algorithm, as explained in Section 2.4.1.

Fig. 2-18 shows the precision of the DOA estimates as a function of the number of PRBs that compose the snapshot when $M = 4$. For each abscissa value there are three bars representing the DOAs estimation error occurrences of the $L - 1$ detectable paths. Different shades of gray are used to distinguish the interval of errors: $[0; 2.5°]$, $(2.5°; 5°]$, $(5°; 10°]$, $(10°; 360°)$. It can be seen that the first path is always detected with high accuracy, even with a limited number of PRBs. Conversely, the second and third paths present a good precision only increasing the number of sensed PRBs.

Clearly, by gathering together PRBs belonging to the same user it is possible to improve significantly the performance of the proposed interference suppression method even with many received paths. This is shown in Fig. 2-19. The BER of the proposed system is reported as a function of the PRBs composing the snapshot when $M = 4$. The performance floor is eliminated and the obtained BER values are very close to the case without interference. In particular, a significant performance improvement is achieved increasing the PRBs up to 20, then a saturation is reached.

2.5 Resource allocation schemes by using Zero-Forcing Beamforming and User Selection

We consider a cognitive user-deployed femto-cell (Home eNB, HeNB) that shares the spectrum resource with a primary macro-cell in a LTE-A heterogeneous network, as illustrated in Fig. 2-20 and already explained in Sec. 2.4. Both systems are modeled according to the 3GPP LTE-Advanced standard [108], considering FDD (Frequency Division Duplexing) mode. In order to take into account the worst interference condition, we suppose the two systems operate with the same carrier frequency, f_0, and bandwidth. The femto-cell base station is equipped with L antennas spaced of $d = \lambda/2$, and it serves $I_{\mathcal{F}}$ secondary users. In this scenario there is not any coordination with the macro-cell base station (eNB) and the downlink (DL) signal, received by the MUEs that are located in the HeNB coverage area, is interfered by the signal transmitted by the HeNB. In order to allow the femto-cell to share the spectrum with the macro cell, suitable beamforming weights are used to eliminate the interference toward the MUEs. The knowledge of the signals AoAs is acquired by means of a first phase of sensing. Hence the HeNB exploits its cognitive capabilities to adapt its transmissions. The only information that the macro-cell BS (eNB) shares with the HeNB

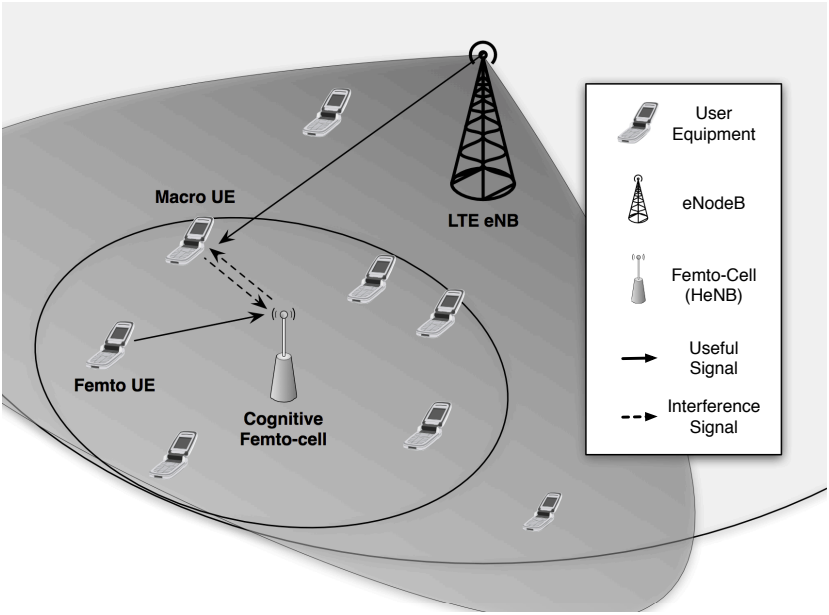

Figure 2-20: Considered scenario set up by a macro-cell, some MUEs, a femto-cell and its FUEs.

using backhaul links is the scheduled information of the macro-cell [116].

The cognitive femto-cell has to estimate the AoA of the signals coming from all the UEs (both FUEs and MUEs) in its coverage area. Considering the FUEs, the AoA estimation can be performed by using the reference signals sent in the UL. The estimation of the AoAs of the MUE is more challenging. We assume that the femto-cell reserves an OFDM symbol in each subframe in uplink as sensing period for the MUEs[10]. About the estimation, the well known Multiple Signal Classification (MuSiC) algorithm [105] is considered. It is based on the eigenvalue decomposition of the received signal autocorrelation matrix,

[10]It can be one of the symbols used for the transmission of Sounding Reference Symbols

R. The performance of this algorithm improves with the number of antenna elements, L, and up to $L-1$ AoAs can be estimated. However, in general number of MUEs in the femto-cell area, and hence the number of AoAs to be estimated, is higher than $L-1$. In this section we propose to work on a PRB basis, hence the estimation is not performed on the whole OFDM symbol, but each PRB separately by using the method described in Sec. 2.4. In this way it is possible to estimate up to $L-1$ for each PRB. As drawback this method reduces the snapshot used for estimation, thus reducing the accuracy of the estimates. However numerical results will show (in Sec. 2.5.2) that estimation errors does not affect notably the performance of the proposed resource allocation methods. In addition, in Sec. 2.3 is shown how aggregating all PRBs belonging to the same could be possible in order to increase the snapshot, by exploiting macro-cell scheduling information that can be available at the HeNB or estimated by using suitable methods as in [76]. In what follows we consider the worst case, in which the AoA estimates are performed on a single PRB. Focusing on the MUEs AoAs estimation, and assuming a propagation channel characterized by M multipath components [103], the n-th sample of the signal in the time domain received by the l-th antenna element of the HeNB on the p-th PRB can be expressed by $r_{l,p}[n]$, already defined in (2.21).

Due to the AoA of the signals, the propagation delay of the m-th signal between two consecutive antenna elements is $\delta_{m,p} = d\sin(\theta_{m,p})/c \ll T_s$, where T_s is the sampling period. Defining $\mathbf{s}(\theta_{m,p})$ the steering vector toward the direction $\theta_{m,p}$, the received signal on the p-th PRB can be expressed by $\mathbf{r}_p$ (defined in (2.4)). The eigenvalues of the received signal autocorrelation matrix $\mathbf{R}_p$ (2.5) identify a signal subspace and a noise subspace [105]. To estimate the AoA, $\theta_{m,p}$, the MuSiC algorithm searches the K angles that maximize the function (2.7).

The AoA information acquired during sensing phase[11] is used to limit the interference towards the MUEs through a pre-processing of the signal transmitted by the HeNB. It focuses the transmission power

[11] As demonstrated in [117] UL and DL spatial information are strongly correlated and it is reasonable to use UL estimation in DL transmission.

on some target directions while forces null beams in other specified directions. In particular, let $\theta_{m,p}^{\mathcal{M}}$ be the AoA of the m-the replica of the signal transmitted by the MUE on the p-th PRB, and $\theta^{\mathcal{F}}$ the AoA of the main replica of the signal transmitted by the FUE. As explained in details in Sec. 2.2.1, beamforming weights $\mathbf{w}_p = \left[w_{1,p}, \cdots, w_{L,p}\right]^T$ for the transmission on the p-th PRB , are obtained by imposing $\mathbf{w}_p$ parallel to $\mathbf{s}(\theta^{\mathcal{F}})$ and orthogonal to each $\mathbf{s}(\theta_{m,p}^{\mathcal{M}})$, [54]. Value $w_{l,p}$ is used to weight the signal transmitted on the p-th PRB by the l-th antenna.

2.5.1 Proposed Resource Allocation Schemes

In this section the proposed resource allocation schemes are presented. The idea is to make use of the angular information about the users (either FUEs or MUEs) to improve the capacity of the femto-cell and to eliminate the interference effect on the primary users (i.e., MUEs). In particular, the proposed methods integrate a ZFBF scheme with a suitable policy for resource allocation. Differently from previous works [118, 119], the proposed method does not use channel state information (CSI) to detect quasi-orthogonal user, but only the estimates of the AoA of the signals arrived to the HeNB. The advantage is that AoA can be estimated directly on the MUE data signal, while the CSI requires specific reference signals that cannot be available for the links connecting HeNB and MUEs. In addition, the proposed schemes work on a PRB basis. Indeed, each PRB can be used by a MUE to communicate, and this MUE is characterized by its own AoAs. The HeNB selects the FUE that has less effect on this primary user (i.e, MUE) and, at the same time, that achieves the highest capacity Let assume that the p-th PRB is used by the macro-cell to communicate with a MUE that is in the coverage area of the femto-cell. The signal transmitted by this MUE is received by the HeNB antennas with a set of AoAs, $(\theta_1^{\mathcal{M}}, \theta_2^{\mathcal{M}}, \cdots, \theta_M^{\mathcal{M}})$. The HeNB is able to detect $K \leq L-1$ AoAs related to the most powerful multipath components. For simplicity, in what follows we assume that $M = K \leq L-1$ [12]. The FUE i-th, is characterized by a set of M

[12] The effects of $M > L-1$ on ZFBF have been considered in [74]

Procedure 2 - Proposed MBG Algorithm

Beamforming weights and gain computation
for $p \leftarrow 1$ to P **do**
  for $i \leftarrow 1$ to $I_{\mathcal{F}}$ **do**
    $\mathbf{A}_{i,p} = \left[\mathbf{s}(\theta_i^{\mathcal{F}}), \quad \mathbf{s}(\theta_{1,p}^{\mathcal{M}}), \mathbf{s}(\theta_{2,p}^{\mathcal{M}}), \cdots, \mathbf{s}(\theta_{K,p}{}^{\mathcal{M}})\right]$
    $\mathbf{w}_{i,p}^H = \mathbf{s}^H(\theta_p^{\mathcal{F}})(\mathbf{A}_{i,p}\mathbf{A}_{i,p}^H)^{-1}$.
    $G_p(\theta_p^{\mathcal{F}}) = \left|\mathbf{s}^T(\theta_p^{\mathcal{F}})(\mathbf{A}_{i,p}\mathbf{A}_{i,p}^H)^{-1}s(\theta_p^{\mathcal{F}})\right|^2$
  end for
end for
PRB allocation
for $p \leftarrow 1$ to P **do**
  for $i \leftarrow 1$ to $I_{\mathcal{F}}$ **do**
    if $\arg\max_t\{G(\theta_t^{\mathcal{F}})\} = i$ **then**
      $\Omega[i,p] = 1$
    else
      $\Omega[i,p] = 0$
    end if
  end for
end for

AoAs, $(\theta_{1,i}^{\mathcal{F}}, \theta_{2,i}^{\mathcal{F}}, \cdots, \theta_{M,i}^{\mathcal{F}})$, with $i = 1, \cdots, I_{\mathcal{F}}$, however, the femto-cell exploits only the most powerful, $\theta_i^{\mathcal{F}}$.

In particular, we propose two resource allocation schemes, described in Procedure 2 and 3, where $\mathbf{\Omega}$ is the scheduling matrix. The $\mathbf{\Omega}$ matrix has dimensions $I_{\mathcal{F}} \times P$, and the element $\Omega[i,p]$ is defined as

$$\Omega[i,p] = \begin{cases} 1 & \text{if PRB } p \text{ is assigned to user } i \\ 0 & \text{otherwise} \end{cases} \tag{2.23}$$

The first scheme allocates the p-th PRB to the FUE that presents the Maximum Beamforming Gain (MBG). The second is a Location Aware (LA) resource allocation scheme: it allocates the PRB to the FUE that has the highest angle separation from the MUE. It is a very simple heuristic that achieves performance close to the MBG solution, but with very reduced complexity.

Procedure 3 - Proposed LA Algorithm

PRB allocation
for $p \leftarrow 1$ to P **do**
  for $i \leftarrow 1$ to $I_{\mathcal{F}}$ **do**
    if $\arg\max_t \left\{ \min_m \{\theta_t^{\mathcal{F}} - \theta_{m,p}^{\mathcal{M}}\} \right\} = i$ **then**
      $\Omega[i,p] \; = \; 1$
    else
      $\Omega[i,p] \; = \; 0$
    end if
  end for
end for

Maximum Beamforming Gain resource allocation

As stated before, this method selects the FUE that achieves the maximum beamforming gain in each PRB with the constraint to avoid transmission towards corresponding MUE. For the p-th PRB and the i-th FUE the matrix containing the steering vectors is

$$\mathbf{A}_{i,p} = \left[\mathbf{s}(\theta_i^{\mathcal{F}}), \mathbf{s}(\theta_{1,p}^{\mathcal{M}}), \mathbf{s}(\theta_{2,p}^{\mathcal{M}}), \cdots, \mathbf{s}(\theta_{K,p}^{\mathcal{M}})\right] \tag{2.24}$$

and the beamforming weights are calculated as in (2.9), substituting $\mathbf{A}$ with $\mathbf{A}_{i,p}$. Finally, the beamforming gain of the i-th FUE in the direction of its main propagation path can be expressed as

$$G_p(\theta_i^{\mathcal{F}}) = |\mathbf{w}_{i,p}^H \mathbf{s}(\theta_i^{\mathcal{F}})|^2 = |\mathbf{s}^H(\theta_i^{\mathcal{F}})(\mathbf{A}_{i,p}\mathbf{A}_{i,p}^H)^{-1}\mathbf{s}(\theta_i^{\mathcal{F}})|^2. \tag{2.25}$$

The resource allocation scheme looks for the FUE $\hat{i}_p$ that maximizes the beamforming gain on the p-th PRB, i.e.,

$$\hat{i}_p = \arg\max_i \{G_p(\theta_i^{\mathcal{F}})\}. \tag{2.26}$$

Location Aware resource allocation

This resource allocation scheme is suboptimal compared to the previous one but presents lower computational complexity. The assumption is that the beamforming gain increases as much as the FUE to MUE angle separation increases.

In particular, we refer to the angle separation between the main propagation paths of the two users. When the FUE is near to the MUE, the null beam is close to the direction of transmission and this can affect the performance of the FUE. For this reason, the proposed Location Aware (LA) resource allocation scheme selects, for each PRB, the FUE that presents the highest angular distance with the MUE. This scheme is very simple because it does not require additional computation, the only needed information is the AoA calculated during the sensing phase. The procedure is described in Procedure 3, which maintain the notation of Procedure 2. Then the beamforming weights are calculated only for the selected FUE as in (2.9).

2.5.2 Performance Analysis

This section presents the numerical results obtained by means of computer simulations. The performance of the two proposed methods is compared with that of a conventional beamforming scheme, that maximizes the capacity of the femto-cell without taking into account the presence of the MUE ("Conventional BF"), and with that of a ZFBF that performs a random allocation of the PRBs without taking into account the beamforming gain ("ZFBF - random allocation"). These two curves represent the upper and lower bounds of the proposed methods capacity, computed as

$$C_k = \frac{1}{P} \sum_{p=1}^{P} \sum_{i=1}^{I_{\mathcal{F}}} \Omega_k[i,p] \log_2 \left(1 + \gamma G_{k,p}\left(\theta_i^{\mathcal{F}}\right)\right). \tag{2.27}$$

where γ is the signal-to-noise ratio and k depends on the resource allocation and beamforming method (conventional - ZF). In particular, the

highest femto-cell capacity is achieved with conventional BF that maximizes the beamforming gain of each FUE, regardless of the presence of the Macro-cell UEs. In this case the beamforming gain toward the main propagation path is equal to $G(\theta_{1,i}^{\mathcal{F}}) = L$. Conversely, with conventional ZFBF the beamforming gain is calculated as in (2.9) when the FUE (and hence its AoA) is randomly chosen. We consider the worst case, where all the PRBs are used for communication with a MUE in the HeNB coverage area. In deriving the results we assume the following working hypothesis

- bandwidth $B = 3$ MHz
- multipath indoor propagation channel in accordance with [103]
- number of FUE $I_{\mathcal{F}} = 3$
- number of antennas $L = 4$
- number of PRB, $P = 12$.

Fig. 2-21 presents the average capacity of the femto-cell as a function of the ratio between the Energy per bit and N_0 (E_b/N_0). As expected the highest capacity is obtained with conventional BF while the ZFBF with random PRB allocation represents the worst case. The proposed methods present intermediate results. We can note that the sub-optimal LA resource allocations scheme has performance very close to the optimal MBG, saving significant computational complexity.

The benefits of the proposed resource allocation methods must be evaluated taking into account also the error probability either of the femto-cell or the macro-cell UEs. Indeed the goal of our schemes is to obtain a good trade-off between increasing the femto-cell capacity and reducing the interference toward the MUEs. Figs. 2-22 and 2-23 represent the bit error probability, P_e, of the femto-cell and the macro-cell, respectively, using an uncoded QPSK modulation. The curves are derived as a function of the E_b/N_0 of the relative links (i.e., E_b/N_0 of the femto-cell DL in Fig. 2-22 and E_b/N_0 of the macro-cell DL in Fig. 2-23) using uncoded QPSK modulation. The behavior of the curves

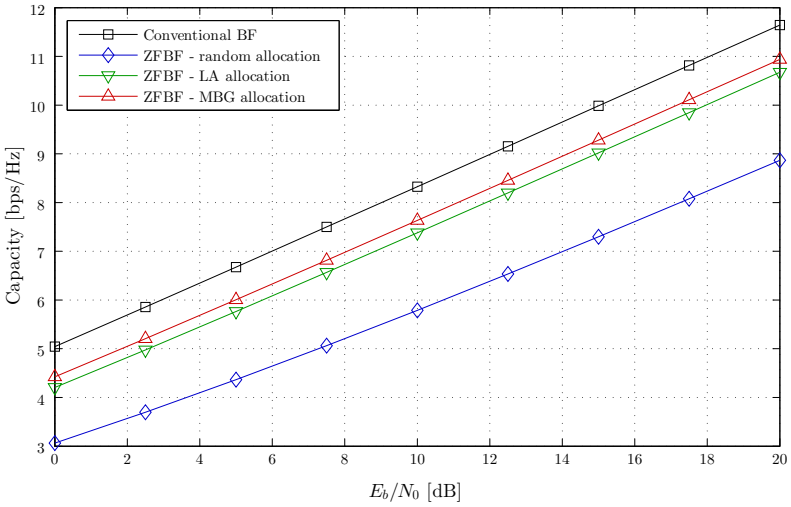

Figure 2-21: Femto-cell average capacity when the proposed resource allocation schemes are used.

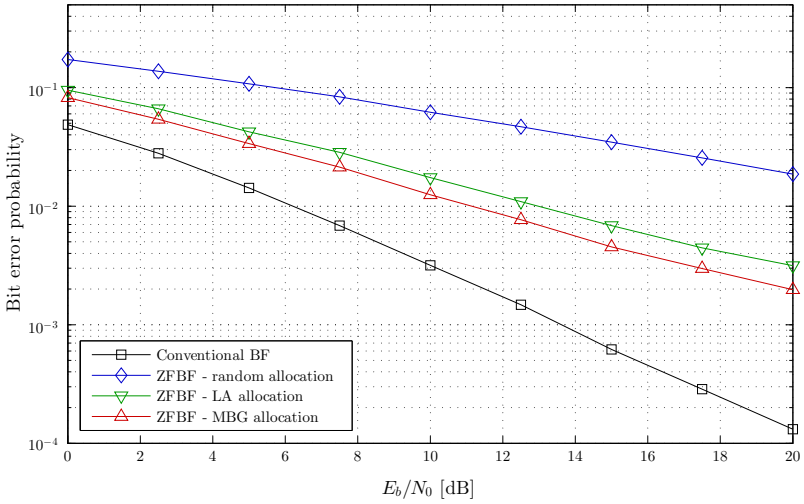

Figure 2-22: Bit error probability of the femto-cell DL.

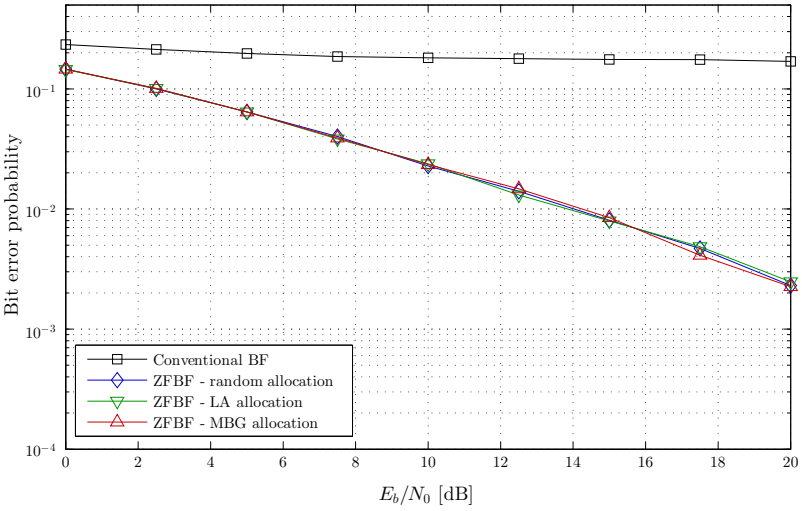

Figure 2-23: Bit error probability of the macro-cell DL.

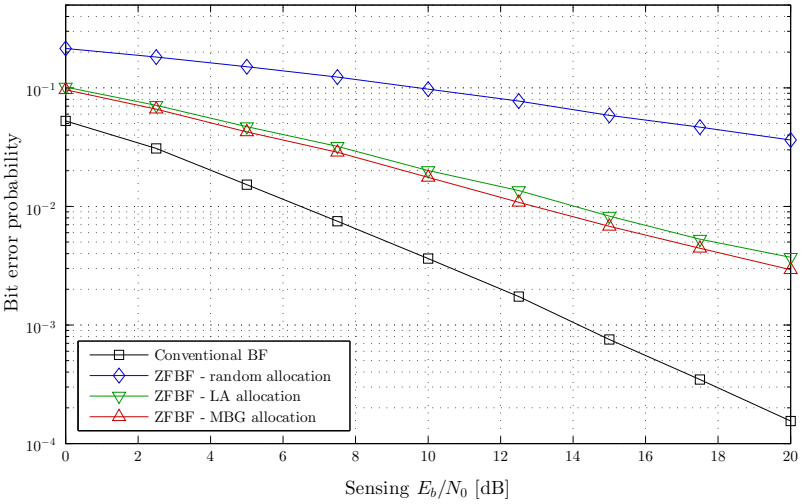

Figure 2-24: Bit error probability of the femto-cell DL in presence of AoA estimation errors.

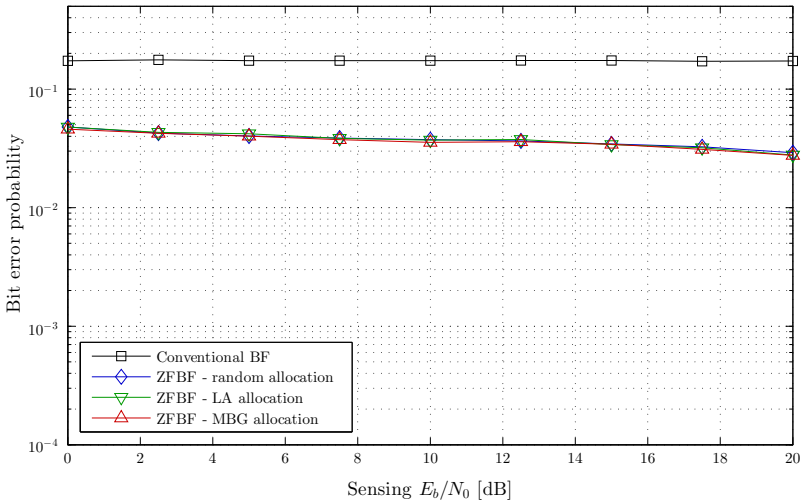

Figure 2-25: Bit error probability of the macro-cell DL in presence of AoA estimation errors. The Macro-cell DL link has $E_b/N_0 = 12$ dB.

in Fig. 2-22 follows that of the capacity and the same considerations can be drown. For what concerns the MUEs P_e, we can notice that the proposed methods and the ZFBF achieve the same results, because the interference is completely removed in both cases. Conversely, the Conventional BF presents very high P_e.

The proposed methods are based on the knowledge of the AoA. Hence, the performance can be affected by errors in the AoA estimation. Figs. 2-24 and 2-25 show the P_e of the two cells, when the AoA is estimated by means the MuSiC algorithm, as a function of the sensing E_b/N_0. In particular considering the femto-cell (Fig. 2-24) the sensing E_b/N_0 corresponds to the DL E_b/N_0. Therefore we can note that the performance follows the ideal AoA case with an obvious performance worsening that affects mainly the conventional BF scheme. In addition in presence of AoA estimation errors the differences among the two proposed methods, MBG and LA, tends to reduce. Hence, we can state that the AoA estimation errors mainly affect the determination of the

maximum BF gain. Differently, in Fig.2-25 the sensing E_b/N_0 is that of the link between the MUE and the HeNB while the E_b/N_0 of the DL MUE is fixed at 12 dB. It is possible to see that the performance has only a little improvement when the sensing E_b/N_0 increases, because the MuSiC is able to provide good estimates even for low values. The P_e worsening achieved by the macro-cell UE (if compared with the results in Fig. 2-23 at 12 dB) is comparable with that of the femto-cell.

Chapter 3

Coordinated Systems

3.1 Introduction

Mobile data volume is expected to grow exponentially in the next years with a massive diffusion of wireless devices and applications. Future mobile communication systems are challenged to guarantee high quality and high data rate services to an increasing number of users and to face with limited resources availability. One of the main enhancements that can be introduced to boost capacity and coverage is the increasing of cell density by resorting to an efficient deployment of Heterogeneous Networks (HetNets) [120, 121]. The idea is to improve spectral efficiency by reducing the cells size and exploiting an overlaid structure: traditional macrocell base stations (BSs) are overlaid with small cells characterized by low power and low coverage, creating multiple coverage layers.

HetNets offer many advantages such as high data rate, reduced network cost and energy saving. However, the coexistence of overlay wide area and local BSs leads to specific HetNet topologies and, hence, to new interference environments that cannot be solved by adopting directly strategies used for traditional macrocell networks. The power unbalancing among macro and small BSs (MBSs and SBSs) can limit

significantly the capacity of the small cells (*inter-layer interference*) that are also subject to the interference of the others small cells (*intra-layer interference*). In addition, to ensure that a sufficient number of User Equipments (UEs) get associated with the small cells, a mechanism called Cell Range Extension (CRE) is generally used [122]. A suitable margin called Range Extension Bias (REB) is added to the measure of the signal strength received from the small cell, so that a UE may be assigned to the small cell even if it receives a higher signal from the macrocell. This cause strong interference from the MBSs. For these reasons, the benefits of HetNets strongly depend on an efficient resource management between high-power macro and low-power small cells. The natural enabler of offloading is the CRE technique jointly used with resource partitioning. In reference to this, the cell association problem has been studied in [122], where the authors have demonstrated that the CRE is a simple approach that permits to achieve results very close to those obtained by using a load-aware utility maximization function. Many works on CRE and eICIC in the literature focus on fixed parameters [123–125], however the optimal selection of the REB value and the ABS pattern strongly affect the performance of the HetNet, so that

- a low REB value leads to a small number of UEs connected to the small cell with a consequent load unbalancing and an inefficient use of the small cell resources;

- a high REB value leads to an high extension of the small cell coverage that could be congested by UEs with poor Signal to Interference-plus-Noise ratio (SINR) values.

In addition, the value of the ABS pattern impacts the average data rates of the offloaded UEs and depends on how many users have been offloaded. Furthermore, the ABS pattern selection should take into account either the benefit of the offloaded UEs or the throughput reduction of the macrocell due to resources loss.

When the different layers of access nodes are interconnected, it is possible to have an efficient coordination among the network layers and

to take dynamic joint decisions about the scheduling. Two main approaches are expected as possible solutions in future networks:

- *Enhanced inter-cell interference coordination (eICIC)*: a joint time resource allocation among macro and small cells is used. Some subframes are partially muted by the macrocell thus to lower the interference on most vulnerable small cell UEs [125–127]. These special subframes are called Almost Blank Subframes (ABSs).

- *Coordinated Multi-Point (CoMP)*: different access nodes transmit simultaneously in a coordinated way towards users that are more vulnerable to interferences. In this way the signal received from other cells can be used constructively, and it can be considered as an information resource rather than an interference source [128];

CoMP provides high flexibility and performance improvement, but requires a high amount of signaling and, hence, very efficient backhaul links, that can be unavailable. On the other hand, the deployment of eICIC is simpler but less flexible.

Although the Cell Range Extension (CRE) mechanism ensures that a sufficient number of UEs get associated with the femto-cell how to set the ABS period and the RE bias is not specified in the standard even though it is an aspect that strongly affects the eICIC performance. Hence, the use of eICIC approach needs the definition of algorithms able to determine the amount of resources that the macro-cell should leave to femto communications (i.e., ABS period) and the UEs association rules (i.e., RE Bias - REB). The optimal solutions of this optimization task have high complexity and are actually infeasible. Therefore, there is the need of finding low complexity sub-optimal solutions.

A performance evaluation of eICIC as a function of the ABS period were derived in [129]. [130] proposed a dynamic way to calculate the ABS period and the RE bias depending on the traffic load of the network was proposed. Similarly, [131] presented an approach deriving a possible allocation of the femto-cell resources together with the ABS period and the RE bias. However, [130, 131] were based on the solution of an optimization problem requiring the knowledge of many information

and, hence, a lot of signaling among the cells. In [132], a proportional fair allocation is performed independently in each cell for different values of the ABS period when the RE bias is fixed. Each configuration gives an utility function. Then, the number of ABS of the network is assumed as the value maximizing the sum of all the utility functions among all the possible values of the ABS period. Also this approach requires a lot of elaborations and signaling. In other works, i.e. in [133], the number of factors that affects an optimum resource allocation when eICIC is considered is high and very often not deterministic. Hence, actual solutions need to impose simplifications and/or fix some parameters. [134] proposes a simple method to calculate the ABS period proportionally to the number of users that are in the Range Extended area, taking into account the number of femto-cells, their position and traffic load, but not the macro-cell load. Conversely, [135] proposed an ABS period that depends only on the macro-cell load where this value is calculated for each femto-cell independently and then averaged because the macro-cell has to set the same pattern for all the femto-cells.

Concerning this, in Sec. 3.2 a simple method to choose adaptively the ABS period that needs only the knowledge of the load required by the users in the Range Extended area of each cell. The idea is to derive suitable threshold values on the network traffic load, that allow the selection of the ABS period among a finite set of values. First, an analytical expression of these thresholds is provided. The exact solution however requires the knowledge of many information. Hence, we propose also an empirical approach based on averaged results obtained through simulations. This is a sub-optimal solution but reduces significantly the signaling and the complexity. The goal of the adaptive scheme is to guarantee the maximum throughput of the overall network. Indeed, eICIC leads to a technical trade-off, because benefit of increased spectral efficiency for the femto-cell UEs (FUEs) comes at the cost of the macro-cell UEs (MUEs) who have access to fewer resources due to the ABSs. After a brief introduction to the eICIC concepts, the considered scenario is presented in Sec. 3.2.1, while different eICIC configurations are evaluated in Sec. 3.2.2. Finally Sec. 3.2.3 presents the simulation

results and the empirical threshold values that can be used to change adaptively the ABS period.

When it is possible to increase the degree of coordination among the nodes, one of the most attractive approaches to reduce inter-cell interference and to increase the cell-edge user throughput is Coordinated Multi-Point (CoMP) transmission [128, 136]. It is an effective way for managing inter-cell interference and is considered a key technology of LTE-Advanced systems. The basic idea behind CoMP is that exploiting backhaul links, multiple Base Stations (eNB in LTE) can cooperate so as to act as a single multiple antenna system with distributed antenna elements. This eliminates the interference and enhances the signal received by the cell-edge users. In particular two different CoMP modes can be used [121]:

- *Coordinated Scheduling and Coordinated Beamforming (CS/CB)*: each TP is equipped with a multi-antenna system and communicates with its user forming a transmission beam that increases the received signal power while reduces the interference coming from other TPs.

- *Joint Transmission (JT)*: multiple transmission points (TPs) simultaneously transmit data towards the same user equipment (UE). In this way the interference is turned into a useful signal.

JT can introduce a high throughput gain for the served UEs, but requires a high backhaul capacity, due to the need of sharing channel state information (CSI) and data among the TPs. Conversely, CS/CB only requires to share CSI and scheduling information. Hence, it is more suitable when the backhaul link is not ideal as in many practical networks. In addition, CS/CB can mitigate the inter-cell interference without sacrificing the throughput of the users served by the macro cell layer. The beamforming techniques that can be adopted are those widely used for multi-user MIMO transmissions. However, in CS/CB schemes it is needed to design suitable UEs selection criteria and CS algorithms that represent a hot research topic. In [137], a zero forcing beamforming is used to derive the signal-to-noise-plus-interference ratio

(SINR) of each user in the CoMP area, then the resources are allocated following a Proportional Fair scheduling policy. In [138], the authors propose an adaptive and distributed CS algorithm, that can operate in either JT or CS/CB mode. The algorithm is divided in two phases: the intra-eNB phase includes CoMP mode selection per each UE and candidate UE selection per each sub-band, while the inter-eNB phase includes the final UE selection per each sub-band through a message exchange. An interference reduction technique based on a user selection algorithm for CoMP CS/CB is proposed in [139]. Each TP determines the beamforming weights for its users and then the effects of interference towards users located at adjacent cells are taken into account.

Differently from previous approaches, the Sec. 3.3 first proposes a criterion to select the CB scheme that is most suitable for a randomly chosen pair of UEs that share the same resource. Then a CS method that permits to create the most suitable UEs pairs is proposed. The goal of the procedure is to maximize the cells throughput but guaranteeing fairness among the cells. Either the CB or the CS schemes are based on the knowledge of the Direction of Arrival (DoA) of the UEs signals.

The section 3.3 is organized as follows. Initially, the system model is described while in Sec. 3.3.1 the CS/CB problem is formulated. Then, Sec. 3.3.2 illustrates the proposed schemes and the numerical results are provided in Sec. 3.3.3.

As stated before, the CoMP technique presents high flexibility and is able to follow rapid topology and traffic load changes. In addition, it is very effective to increase the performance of the cell-edge UEs. On the other side, the CoMP is strongly limited by CSI feedback overhead and backhaul requirements, and it suggests an adaptive or an ad-hoc use of the CoMP. In Sec. 3.4 we are interested in the advantages of integrating CoMP and eICIC that introduce a two-scale interference coordination approach. Only few papers in the literature focus on the joint use of eICIC and CoMP [140–142]. In [140], a Proportional Fair metric scheduling is used to select among different transmission strategies (single-user and multi-user MIMO, with and without CoMP). The scheduler uses ABSs to serve the CRE UEs. These UEs can benefit

from cooperation with the other small cells but not with the macrocell. Conversely, for all the transmissions in the noABSs (i.e., subframes with nominal macrocell transmission power), the CoMP with the macrocell is used. The attention is mainly devoted to the selection of the transmission strategy, while the use of the CoMP and the eICIC is not optimized. In addition, the section assumes a preconfigured scenario (i.e., fixed number of UEs and cells) and does not consider backhauling problems and macrocell load, indeed for all the UEs allocated in the noABSs the macrocell acts as TP.

Differently, the works presented in [141, 142] consider a basic eICIC approach where the use of CoMP is limited to the UEs that are in the CRE area and suffer of high interference, in order to reduce the signaling overhead introduced by the CoMP. In particular, in [142] all the UEs that are in the CRE area are served with a CS/CB CoMP approach. The macrocell is not muted, but it can serve macrocell UEs using beamforming to reduce the interference during ABS. Conversely, in [141] JT-CoMP approach is considered as in this section. [141] proposed an algorithm that fixes two REB values and divides the UEs belonging to the consequent two CRE regions. Only the most vulnerable UEs in the external CRE area are served with a JT from macro or small cells. The section consider a fixed scenario and the algorithm is not optimized, in particular the use of CoMP is not flexible, it does not take into account the resource availability of the neighbor cells, the UEs data request and the UEs served with JTs are predetermined based on their position.

In Sec. 3.4 the joint use of the eICIC is investigated with an adaptive JT-CoMP in an actual scenario trying to limit the signaling overhead. The use of CoMP is optimized and dynamic, it takes into account either the serving cell loads or the UEs serving outage. The idea here is to adopt a basic eICIC approach and add the CoMP functionality in an ad-hoc manner, i.e., only when needed. In this way, the system is able to answer dynamically to the UEs requests, but at the same time the signaling load is maintained low. The system is based on a distributed CoMP approach that can involve all the cells, hence the signaling load

is distributed among several cells (i.e., different backhaul links) and is not concentrated mainly on the macrocell.

The section 3.4 starts introducing the system model and the benchmark solutions, while Section 3.4.1 presents the proposed method. In particular, first the optimization problem is formulated and then an heuristic is proposed to solve the problem. Finally, performance results are reported in Section 3.4.2.

3.2 Adaptive muting radio in eICIC

Femto-cells are nodes characterized by low transmission power and, hence, low coverage area. In addition, the coverage area is limited by the interference of the macro-cell eNB that has a significant higher transmission power. Indeed, the UE usually selects the serving cell on the basis of the signal-to-noise-plus-interference ratio (SINR) measured on specific reference symbols, and only the UEs in close proximity will select the femto-cell. In order to increase the number of users connected with the femto-cell, thus to reduce the load of the macro-cell, the service area of the femto-cell can be increased by means of the Cell Range Extension (CRE). It is based on the use of a Range Extension Bias (REB) that is added to the UE measurements of the signal received by the femto to support the connection with it. The Bias can varies from few dB up to values higher than 10 dB and, in coordinated networks, it is possible to vary the REB dynamically depending on the variability of the scenario.

In LTE, the trigger condition activated by UE reports and determining the UE association with a cell i-th, is

$$\gamma_{i_{dB}} + \lambda_{i_{dB}} > \gamma_{s_{dB}} + \lambda_{s_{dB}} + \Delta \tag{3.1}$$

with $s = 1, \cdots, C$, where C is the number of cells that the UE can select, s is the serving cell and i is the candidate neighboring cell detected as

$$i = \arg \max_{l=1,\cdots,C} \{\gamma_{l_{dB}} + \lambda_{l_{dB}}\} \tag{3.2}$$

In addition, γ_{idB} represents the measure of the SINR, Δ is the handover margin to avoid the ping-pong effect and, finally, λ_{idB} is the REB defined as

$$\begin{cases} \lambda_{idB} = 0, & \text{if } i \text{ is a macro-cell} \\ \lambda_{idB} > 0, & \text{if } i \text{ is a femto-cell} \end{cases} \tag{3.3}$$

However, without any interference management scheme, only small values of REB can be used, otherwise FUE will experience a high interference from the macro-cell. This problem is addressed by the eICIC.

The eICIC concept relies on a time division of the resources among macro and femto-cells. In particular the macro-cell eNB can reduce the interference towards the femto-cell UEs by using the Almost Blank Subframes (ABSs). An ABS is a subframe in which the eNB sends only essential signaling information, thus resulting as a subframe with low interference power for the users served by the femto-cell. During ABS, the signals that are mainly transmitted are common reference signals (CRS), as well as other mandatory system information. ABSs permit to significantly alleviate the high interference suffered by the femto-cell users that are in the RE area. This implies that the femto-cell can extend its coverage area during ABSs because these are not more dominated by the macro-cell interference. This essentially means that using ABS at macro makes possible to increase the offload of traffic to the small-cell layer. To exploit ABSs, the femto-cell has to be aware of the ABS muting pattern used by the interfering macro-cells. In this way, the femto eNB can schedule the critical UEs (the users in the Range Extended area) during the ABSs while the others are scheduled during the no-ABSs. The ABS muting pattern is characterized by the position of the ABSs in the frame and by the ratio among the ABSs and the total number of subframes called ABS period or ABS muting rate. The ABS pattern is periodical with period equal to 40 subframes for the FDD mode. The ABS muting pattern is not specified by the standard, but it is let to the operator implementation. It can be changed dynamically in order to find the configuration that maximizes the overall system performance while the Quality of Service (QoS) of the users

is satisfied. Dynamic configuration requires an information exchange among the cells by using X2 interface.

New releases of the LTE-A standard are evaluating the opportunity to introduce further enhancements to the eICIC. Advanced solutions, capable to suppress the residual interference from signaling in ABSs, are proposed for the UE receiver and thus ideally not interfered from the macro eNB. In addition, the definition of the ABS becomes more general, including also subframes in which the macro-cell eNB is not muted but transmits data with reduced power. These subframes are called Reduced Power SubFrame (RPSF). RPSFs are introduced in order to offer a higher flexibility to the system and to permit a better balancing among the femto-cell gain and the macro-cell loss.

3.2.1 Considered Scenario

In this study we consider a system where N small-cells are overlapped and share the same resources of a macro-cell. The i-th small-cell is uniformly distributed in the macro-cell area with distance d_i. Values of d_i under 250 meters have not been considered because when the small-cell is too close to the macro-cell the benefits of the small-cell are strongly reduced, due to the power unbalancing. In addition, below this threshold, the macro-cell can still serve users with a maximum Modulation and Coding Scheme (MCS), therefore the amount of required resources is minimal. In order to consider realistic traffic situations, each user performs a different service request in terms of Physical Resource Block (PRB). The considered traffic classes are four:

- VoIP: characterized by a request equal to 16 Kibit s^{-1};
- Gaming: characterized by a request equal to 17.5 Kibit s^{-1};
- Video: characterized by a request equal to 160 Kibit s^{-1};
- FTP: characterized by a best-effort request.

The total number of users U and their arrangement in each class varies in order to have a sufficient "traffic mixture". The resources are allocated

following a Proportional Fair algorithm [75,143]. The users are classified in three groups:

- FUEs are the UEs that are always connected with the femto-cells either if eICIC and CRE are used or not. In general FUEs are the UEs in close vicinity of the femto-cell eNB and, in particular, the UEs that measure a SINR on the reference signal sent by the macro-cell (γ_{dB}^{m}) lower than the SINR measured on the reference signal sent by the i-th femto-cell ($\gamma_{i}{}_{dB}^{f}$) without REB. $\mathcal{F}$ is the total number of these UEs, and $\mathcal{F}_i$ is the number of FUEs in the i-th femto-cell;

- MUEs are the UEs that are always connected with the macro-cell either if eICIC and CRE are used or not. For these users $\gamma_{dB}^{m} \geq \gamma_{i}{}_{dB}^{f} \ \forall i = 1, \cdots, N$. $\mathcal{M}$ is the total number of these UEs.

- REUEs (Range Extended UEs) are the UEs that are connected with the macro-cell in absence of REB/eICIC and with the femto-cell when eICIC/REB is used; $\mathcal{R}_e$ is the total number of these UEs. For these users the SINR values measured in absence of REB satisfy the following conditions: $\gamma_{dB}^{m} \geq \gamma_{i}{}_{dB}^{f} \ \forall i = 1, \cdots, N$ and at least for one value of i we have that $\gamma_{dB}^{m} - \gamma_{i}{}_{dB}^{f} \leq \lambda_{idB}$.

Denoting with R_i^m and $R_{i,j}^f$ the bandwidth request of user i-th MUE and of i-th FUE of the j-th femto-cell, respectively, we can define the following load factors

$$M = \frac{\sum_{j=1}^{\mathcal{M}} R_j^m}{B} \tag{3.4}$$

$$F_i = \frac{\sum_{j=1}^{\mathcal{F}_i} = R_{j,i}^f}{B} \tag{3.5}$$

where M represents the macro-cell load factor and F_i is the i-th femto-cell load factor. Finally, B represents the amount of available PRBs in the system.

The users are uniformly distributed within the cells and the Okumura-Hata model is selected as path-loss model to describe the average signal

propagation in urban areas and large cities. For what concerns the REB value λ_{idB}, we impose a value that permits to the REUEs to achieve the highest MCS[1] in any case. Hence, λ_{idB} has to satisfy two conditions:

$$\begin{cases} \gamma_{i\ dB}^{f} + \lambda_{idB} \geq \gamma_{dB}^{m} \\ \gamma_{i\ dB}^{f\ ABS} \geq \gamma_{dB}^{m} \end{cases} \tag{3.6}$$

where $\gamma_{i\ dB}^{f\ ABS}$ is the SINR measured during the ABS. In addition we have that

$$\Gamma_{dB} = \gamma_{dB}^{m} - \gamma_{dB}^{m\ ABS} \gamma_{i\ dB}^{f\ ABS} = \gamma_{i\ dB}^{f} + \Gamma_{dB} \tag{3.7}$$

Hence, a value that satisfies both conditions in (3.6) is:

$$\lambda_i = \lambda = \Gamma_{dB} \tag{3.8}$$

As ABS muting ratio, three possible values, considered in the first 3GPP evaluations [145], are assumed:

- 1 ABS: the macro-cell schedule its traffic load on 7/8 of frame resources keeping blank[2] one subframe.

- 2 ABS: the macro-cell schedule its traffic load on 6/8 of frame resources keeping blank two subframe.

- 1 ABS + 1 RPSF (called RPSF in the following): the macro-cell schedule normally its traffic load on 6/8 of frame resources keeping blank one subframe and transmitting on the others with reduce power.

It is important to stress that the proposed method can be easily extended to different values of the ABS muting ratio.

[1]The MCS is changed according to the SNR value [144].
[2]Only PDCCH is sent.

3.2.2 Enhanced Inter-Cell Interference Evaluation

In this section, the different eICIC configurations are analysed and an adaptive algorithm based on the current traffic load distribution is proposed. The performance of each configuration is evaluated for different macro-cell load.

In particular, when $M \leq 6/8$, the macro-cell has at least two idle subframes, which can be used by any eICIC technique, without affecting macro performance. On the other hand, $6/8 < M \leq 7/8$ represents an interesting range of load. Indeed, the macro-cell can use the empty subframe for the 1-ABS eICIC configuration, which allows a limited improvement of femto-cells performance. Alternatively, the macro-cell needs to give up a partially used subframe in order to exploit the 2-ABS configuration. Finally, the RPSF may allow an efficient use of the partially used subframe. When $7/8 < M \leq 1$, the macro-cell can not reserve any idle subframe to support REUEs. For these reasons, it is interesting to evaluate the different eICIC configurations for $M = \{6/8, 7/8, 1\}$, when the mean load of each femto-cell varies.

The performance in terms of throughput can be derived for the case of absence of eICIC (all the users in RE area are served by the macro eNB) as

$$T_{no-eICIC} = M + \min\left(1 - M, \sum_{i=1}^{N} F_i\right) \tag{3.9}$$

where the $\min(x, y)$ operation is used to describe the saturation of the macro-cell.

For what concerns the 1-ABS and 2-ABS techniques, it is possible to derive a lower bound of the performance. Indeed, the bandwidth required by a REUE to the macro-cell is always greater than or equal to the bandwidth required to the nearest femto-cell since $\lambda = \Gamma_{dB}$. By considering equal bandwidth requests, that is a worst case analysis, the performance of i-ABS configuration, with $i = 1, 2$, can be expressed as

$$T_{i-ABS} = \min\left(\frac{8-i}{8}, M\right) + N \min\left(\frac{i}{8}, F\right) \tag{3.10}$$

where the addends represent the throughput of the macro-cell and the femto-cells, respectively, and $F = \frac{1}{N}\sum_{i=1}^{N} F_i$ is the mean traffic load of the femto-cells. It is straightforward to note that (3.10) describes the performance for any $i \in [1, 8]$.

The performance analysis of RPSF is more complex, because it has to take into account the detrimental effect of the simultaneous transmissions from macro and femto-cells. In particular, the transmission power reduction of the macro-cell involves a SINR reduction for the MUEs, with a possible increase of the required bandwidth. At the same time, the low power transmission of the macro-cell entails the increase of interference for the REUEs connected to the femto-cell, and hence a reduction of the performance.

According to the aforementioned remarks, RPSF performance can be written as

$$\begin{aligned} T_{RPSF} = &\left[\min\left(M, \frac{6}{8}\right) + f_1(M)\right] + \\ &+N\left[\min\left(\frac{1}{8}, F\right) + f_2(F)\right] \end{aligned} \tag{3.11}$$

where $f_1(M)$ and $f_2(F)$ represent the throughput of macro-cell and femto-cells during the RPSF subframe, respectively. In particular, $f_1(M)$ and $f_2(F)$ should take into account the loss of throughput due to the concurrent transmission of macro and femto-cell. Assuming the knowledge of λ, Γ_{dB} and the SINR of every user in Range Extension area, it is possible to quantify this loss at the expense of a high computational cost. Hence, for a given scenario, it is possible to identify the convenience region of each technique, that is where a particular eICIC configuration provides the best performance. Alternatively, an analytical model based on parameters derived by simulations can be obtained. Taking into account a simple linear model, we have

$$f_1(M) = 2A_M\left[\left|M - \frac{6}{8}\right| - \left|M - \frac{8}{8}\right| + \frac{2}{8}\right] \tag{3.12}$$

$$f_2(F) = 2A_F\left[\left|F - \frac{1}{8}\right| - \left|F - \frac{3}{8}\right| + \frac{2}{8}\right] \tag{3.13}$$

where A_M and A_F represent the percentages of maximum loss for the macro-cell and the femto-cell, respectively.

Eqs. (3.9), (3.10) and (3.11) can be used to choose the most suitable configuration for a given M and F. In the next section, the three considered configurations will be evaluated by means of simulations and the adaptive algorithm will be presented.

3.2.3 Performance Analysis

A simulation campaign has been done in order to verify the behaviour of different eICIC configurations (presented in Sec. 3.2.2) as a function of the traffic load. In particular, in Sec. 3.2.2 a theoretical approach is provided that can be used when many information are known. Referring to the scenario described in Sec. 3.2.1 a lot of simulations have been done in three different load configurations: $M < 6/8$, $6/8 < M < 7/8$ e $7/8 < M < 1$. The provided results have been averaged on several runs, each one with a random distribution of the femto-cells and the users. The results are expressed in terms of throughput percentage gain respect to no-eICIC case, as a function of the femto-cell mean load[3] (F_i).

From the obtained results we can note that, until the system is in saturation (i.e., $M + \sum_i F_i = 1$), there is not any gain by introducing eICIC and REB when the macro-cell load is low (Figs. 3-1 and 3-2). The 2-ABS and RPSF configurations present better performance compared to the 1-ABS case when the network saturation point is exceeded, because with only one ABS the resources are not fruitfully exploited. The behaviours of RPSF and 2-ABS are almost the same because the network load is low and it is possible to allocate two ABS frame without interfering with the macro-cell scheduling.

Figs. 3-3 and 3-4 show the performance of the network with a higher macro-cell traffic load, that is $6/8 < M < 7/8$. From these figures it is possible to state that for low femto-cell load the best configurations are RPSF as well as 1-ABS. As the femto-load grows the 1-ABS solution is

[3] We have assumed an uniform distribution of the load among the femto-cells.

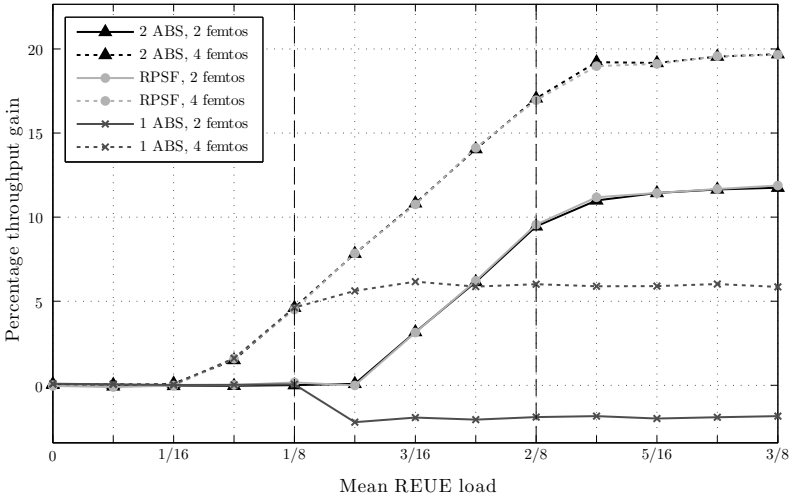

Figure 3-1: Percentage throughput gain of different eICIC configurations when the macro-cell load is $M = 6/8 - 1/16$, with 2 (continuous lines) and 4 (dotted lines) femto-cells.

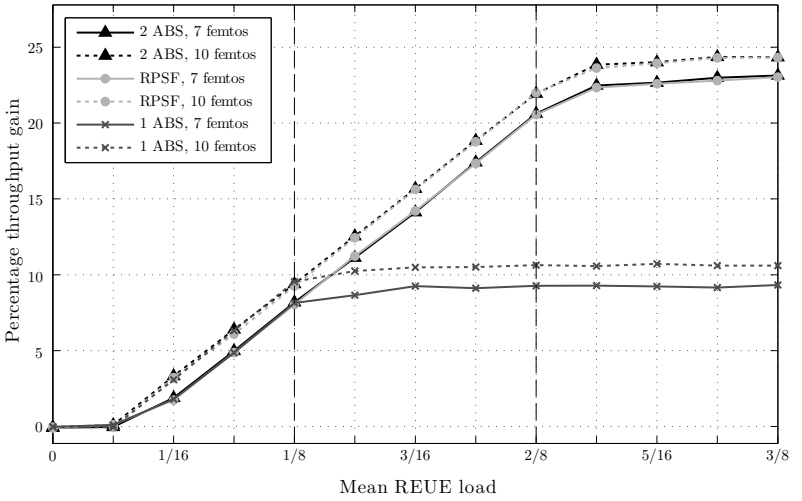

Figure 3-2: Percentage throughput gain of different eICIC configurations when the macro-cell load is $M = 6/8 - 1/16$, with 7 (continuous lines) and 10 (dotted lines) femto-cells.

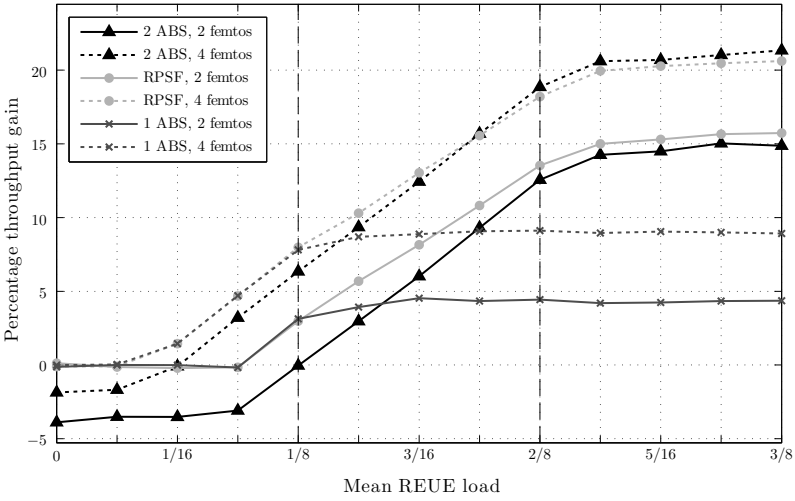

Figure 3-3: Percentage throughput gain of different eICIC configurations when the macro-cell load is $M = 7/8 - 1/16$, with 2 (continuous lines) and 4 (dotted lines) femto-cells.

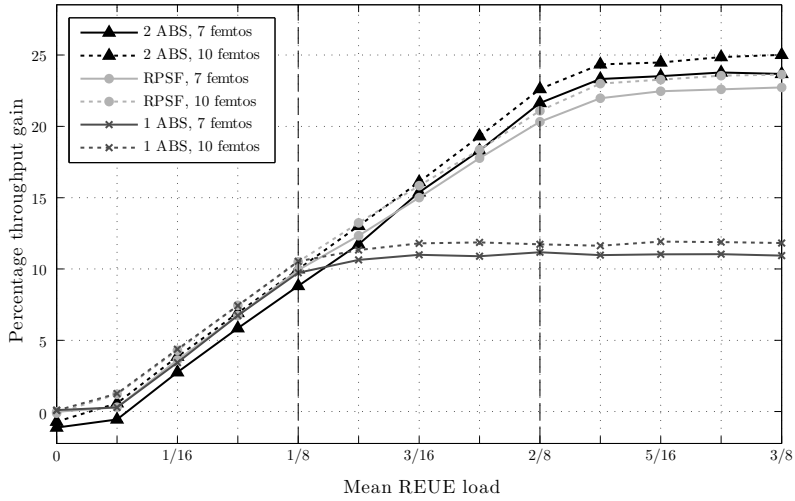

Figure 3-4: Percentage throughput gain of different eICIC configurations when the macro-cell load is $M = 7/8 - 1/16$, with 7 (continuous lines) and 10 (dotted lines) femto-cells.

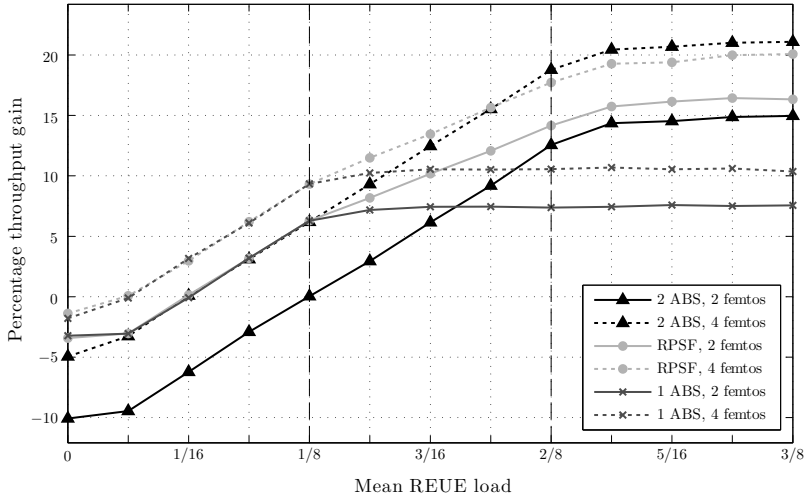

Figure 3-5: Percentage throughput gain of different eICIC configurations when the macro-cell load is $M = 8/8 - 1/16$, with 2 (continuous lines) and 4 (dotted lines) femto-cells.

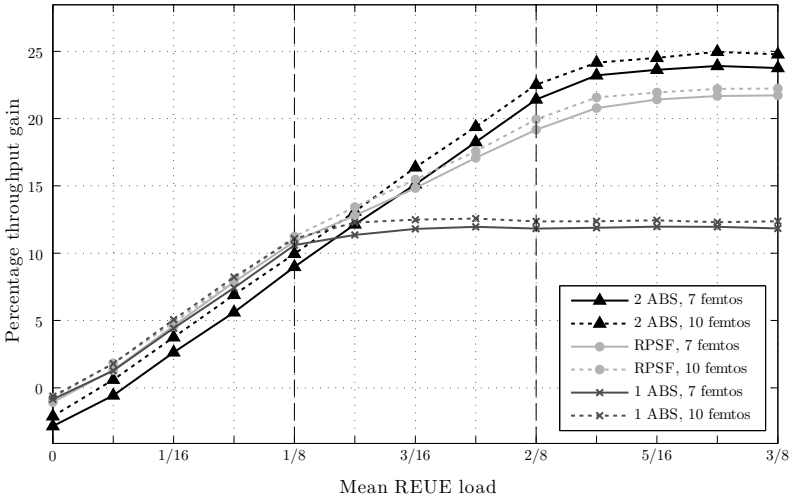

Figure 3-6: Percentage throughput gain of different eICIC configurations when the macro-cell load is $M = 8/8 - 1/16$, with 7 (continuous lines) and 10 (dotted lines) femto-cells.

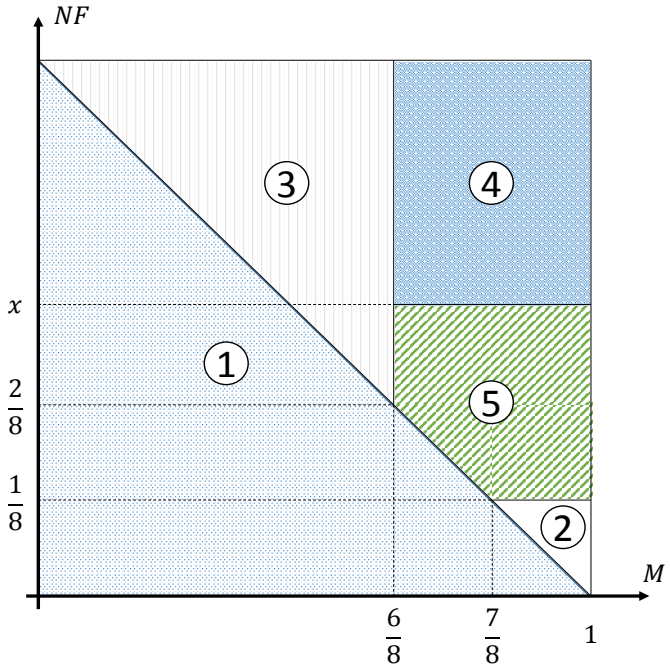

Figure 3-7: Proposed adaptive interference management configuration criterion.

no longer optimal, advantaging the RPSF technique. For higher femto-cell traffic values, and for $N \geq 3$, the best solution becomes the 2-ABS configuration, due to the throughput loss of the femto-cells during the simultaneous transmission of RPSF.

Finally, Fig. 3-5 and Fig. 3-6 show the network performance when the macro-cell is almost saturated, with $7/8 < M < 8/8$. The results are similar to those presented in Figs. 3-3 and 3-4, but it is possible to see that the best eICIC configuration leads to a performance deterioration for low femto-cell traffic loads.

Fig. 3-7 sketches the proposed adaptive criterion based on the aforementioned results. In particular, region **1** represents those traffic load values that do not require any CRE or eICIC technique, because the

macro-cell is able to serve MUEs and REUEs guaranteeing zero outage, since the total requests do not exceed the available resources. Within region **2**, eICIC would have a detrimental effect, hence macro-cell has to serve all the REUEs even if some outage has to be tolerated. In region **3** the low macro-cell traffic load allow the effective use of RPSF or 2-ABS configurations. Regions **4** and **5** are characterized by high macro and femto traffic loads. Hence, RPSF and 2-ABS represent the best choice, especially when the number of femto-cells is high. The two configurations give similar performance, however it is always possible to identify a femto-cell load value, x, which separates the region where RPSF has better performance, that is region **5**, from the region with highest load, i.e., region **4**, where 2-ABS technique is the best solution. The value of x depends on the number of femto-cells N, and an approximated value is reported in Table 3.1.

Table 3.1: Switching values of REUE load as a function of the number of femto-cells.

Femto-cells number (N)	≤ 2	3-5	6-8	9-11	≥ 12
REUE load (x)	N/A	7/32	6/32	5/32	4/32

3.3 Coordinated scheduling and beamforming scheme for HetNet exploiting DOA

This section focuses on a LTA-Advanced HetNet where a small cell is overlapped to a macro cell sharing the same spectrum resources. Without loss in generality, we consider U_M and U_S users served by the macro eNB (MeNB) and the small eNB (SeNB), respectively. Both systems are modeled according to the 3GPP LTE-A standard [108], considering FDD (Frequency Division Duplexing) mode. In order to take into account the worst interference condition, we suppose the two systems operate with the same carrier frequency, f_0, and bandwidth. We assume that there is coordination among the cells, and hence it is possible to exploit a CS/CB CoMP approach to manage the interference: the

two cells can use simultaneously the same time-frequency resources by adopting suitable beamforming techniques and jointly selecting the UEs that can share the same resources with a limited reciprocal interference. In particular, the allocation is performed on a Physical Resource Block (PRB) basis. The PRB represents the smallest element that can be allocated in a LTE-A system. A PRB is made up of twelve subcarriers over seven consecutive OFDM symbols.

The CS/CB scheme proposed here is based on the knowledge of the DoA of the UEs signals. Hence, we assume that both eNBs are equipped with a linear array with L elements spaced of $d = \lambda/2$. Each eNB can estimate the DoA of the signals received either by the small cell UEs (SUEs) or the macro cell UEs (MUEs) (as pictured in Fig.3-8) by using suitable techniques known in the literature as the MuSIC algorithm [121]. The DoA estimates are exchanged via backhaul link between the two eNBs to perform the proposed joint scheduling algorithm. Then the DoA information is used to adapt the transmission by using suitable beamforming schemes. In particular we consider two well known beamforming techniques that are briefly described below.

Conventional Beamforming

The Conventional Beamforming (CVB) technique [54] steers the transmission beam in a target direction, Θ. This allows the maximization of the signal-to-noise ratio (SNR) on direction Θ but does not take into account the interference generated in the other directions.

Let us to assume that the eNB transmits towards a UE whose DoA represents the target direction, Θ. The informative signal is precoded through the weight vector $\mathbf{w}$, whose element w_l, $l = 0, \cdots, L-1$ multiplies the signal on the l-th antenna.

In particular the weights of the CVB are defined as

$$\mathbf{w}_{CVB}(\Theta) = \frac{1}{\sqrt{L}}\,\mathbf{s}(\Theta) \tag{3.14}$$

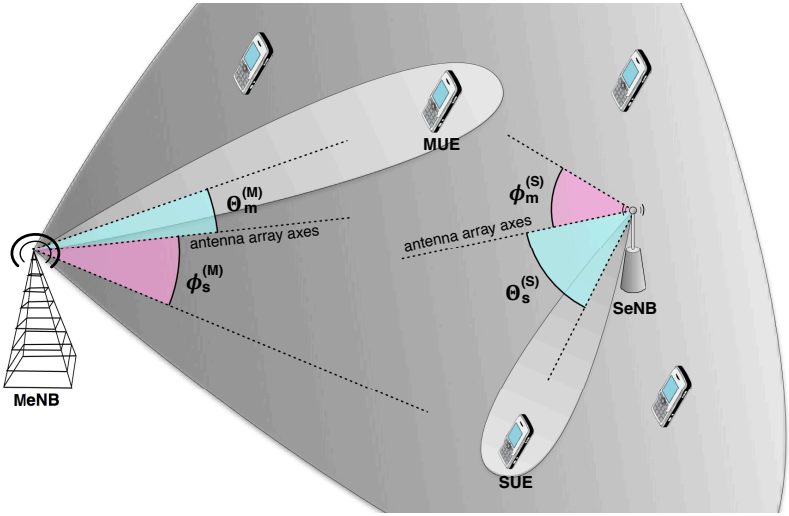

Figure 3-8: MeNB and SeNB equipped with a linear array.

where $\mathbf{s}(\Theta)$ indicates the steering vector on the Θ direction whose element $s_l(\Theta) = e^{j\pi l \sin\Theta}$ (with $l = 0, \cdots, L-1$) takes into account the signal phase rotation due to the transmission from L different antenna elements. These weights compensate the phase offset on each antenna, so the signal can be summed coherently. On the target direction, the beamforming gain is $G_{CVB}(\Theta) = L$. Conversely the CVB gain in the direction ϕ of an interfering user, can be expressed as:

$$I_{CVB}(\Theta, \phi) = \left|\mathbf{w}^H(\Theta)\mathbf{s}(\phi)\right|^2 = \frac{1}{L}\left|\sum_{l=1}^{L} e^{j\pi(l-1)[\sin\phi - \sin\Theta]}\right|^2 .$$

Hence, CVB may cause a detrimental effect on a concurrent UE. The interference amount depends on the received power and the difference among the two DoAs (i.e., Θ and ϕ).

Zero-Forcing Beamforming

Zero-Forcing Beamforming (ZFB) exploits DoA information for nulling the antenna pattern in a specified[4] direction ϕ_{null} trying to maximize the gain in a target direction, Θ. Considering the matrix A whose column are the steering vectors on the target and the null directions, i.e., $A = [\mathbf{s}(\Theta), \mathbf{s}(\phi_{null})]$, the beamforming weights can be calculated as

$$\mathbf{w}^H = \mathbf{s}^H(\Theta) \left(AA^H\right)^{-1} \tag{3.15}$$

where $(X)^{-1}$ indicates the pseudo-inverse matrix of X.

The ZFB gain in the target direction Θ when the null is placed in the direction ϕ_{null} can be expressed as

$$G_{ZFB}(\Theta, \phi_{null}) = \left|\mathbf{s}^H(\Theta) \left(AA^H\right) \mathbf{s}(\Theta)\right|^2. \tag{3.16}$$

The interference generated towards the direction ϕ_{null} can be assumed to be equal to zero

$$I_{ZFB}(\Theta, \phi_{null}) = I_{ZFB}(\phi_{null}) = 0. \tag{3.17}$$

In the target direction Θ the ZFB does not guarantee the maximization of the SNR. Indeed, when Θ is too close to the null direction, the gain offered on Θ may assume small values.

3.3.1 Problem Formulation

The objective of the CS/CB scheme we propose is to maximize the joint exploitation of the available resources. In particular we want to maximize the system throughput, but taking into account the fairness among the two cells. In order to formulate the optimization problem we define the normalized capacity of the PRB p-th as

$$C_p^{(x)} = \log_2\left(1 + \gamma_p^{(x)}\right) \tag{3.18}$$

[4]ZFB can place up to $L - 1$ nulls. However, in this section we are interested in only one null directions.

where x can be S or M if referred to the SUE or the MUE, and where $\gamma_p^{(x)}$ represents the SINR experienced by the SUE (MUE). In particular, this is a function of several variables. To simplify the notation we refer here to the $\gamma_p^{(S)}$ experienced by the SUE[5], that is

$$\gamma_p^{(S)}\left(s, m, t_p^{(S)}, t_p^{(M)}\right) = \frac{P_s^{(S)} G_{t_p^{(S)}}\left(\Theta_s^{(S)}, \phi_m^{(S)}\right)}{N + P_s^{(M)} I_{t_p^{(M)}}\left(\Theta_m^{(M)}, \phi_s^{(M)}\right)} \tag{3.19}$$

where

- $s = 1, ..., U_S$ and $m = 1, ..., U_M$ are the SUE and the MUE served on the same PRB
- $P_s^{(S)}$ and $P_s^{(M)}$ are the power of the signal received by the user s from the SeNB and the MeNB, respectively
- N is the power of the thermal noise, assumed equal for all the UEs
- $\Theta_s^{(S)}$, represents the DoA of the user s respect to and served by the SeNB, as pictured in Fig. 3-8. $\Theta_m^{(M)}$ is defined accordingly
- $\phi_m^{(S)}$ represents the DoA of the user m (served by the MeNB) respect to the SeNB, as pictured in Fig. 3-8. $\phi_s^{(M)}$ is defined accordingly
- $G_{p,t_p^{(S)}}$ represents the useful beamforming gain produced by the SeNB towards its desired UE, and, is a function of the selected beamforming technique $t_p^{(S)}$ that can be CVB or ZFB, as well as the DoAs of the SUE and the MUE, $\Theta_s^{(S)}$ and $\phi_m^{(S)}$
- $I_{p,t_p^{(M)}}$ represents the interfering beamforming gain produced by the MeNB in the direction of the concurrent SUE, in general, is a function of the DoAs of the SUE and the MUE, $\Theta_m^{(M)}$ and $\phi_s^{(M)}$, as well as the selected beamforming technique $t_p^{(M)}$ that can be CVB or ZFB.

[5]The same expression can be easily derived for the MUE.

The goal of the optimization function is to maximize the joint capacity taking into account the fairness among MUEs and SUEs. For this reason we resort to proportional fairness between the SUE and the MUE that communicate on the same PRB. This is equivalent to maximize the product of the capacities (here called *composite throughput*) of SUE and MUE (i.e., $C_p^{(S)} \cdot C_p^{(M)}$) [146]. In doing that we assume that a first phase of resource amount calculation has been already performed for each user and it is denoted by $\mathbf{a}^{(M)}$ for the MUEs and $\mathbf{a}^{(S)}$ for the SUEs (i.e., $a_i^{(S)}$ represents the number of PRBs to be assigned to the i-th SUE).

The optimization problem can be stated as follows,

$$\max_{\substack{\mathbf{\Omega}^{(S)},\mathbf{\Omega}^{(M)},\\ \mathbf{t}^{(S)},\mathbf{t}^{(M)}}} \left\{ \sum_{p=1}^{P} \sum_{s=1}^{U_S} \sum_{m=1}^{U_M} \Omega_{p,s}^{(S)} \Omega_{p,m}^{(M)} \cdot \log_2 \left(1 + \gamma_p^{(S)}(s, m, t_p^{(S)}, t_p^{(M)})\right) \cdot \log_2 \left(1 + \gamma_p^{(M)}(m, s, t_p^{(M)}, t_p^{(S)})\right) \right\} \tag{3.20}$$

$$s.t. : \sum\nolimits_{m=1}^{U_M} \Omega_{p,m}^{(M)} \leq 1 \qquad p = 1, \cdots, P \tag{3.21}$$

$$\sum\nolimits_{s=1}^{U_S} \Omega_{p,s}^{(S)} \leq 1 \qquad p = 1, \cdots, P \tag{3.22}$$

$$\sum\nolimits_{p=1}^{P} \Omega_{p,m}^{(M)} = a_m^{(M)} \qquad m = 1, \cdots, U_M \tag{3.23}$$

$$\sum\nolimits_{p=1}^{P} \Omega_{p,s}^{(S)} = a_s^{(S)} \qquad s = 1, \cdots, U_S \tag{3.24}$$

where $\mathbf{\Omega}^{(M)}$ and $\mathbf{\Omega}^{(S)}$ are the scheduling matrices. The generic element of $\mathbf{\Omega}^{(S)}$, $\Omega_{p,s}^{(S)}$, is equal to one if the p-th PRB is allocated to the s-th user, zero otherwise. The elements of $\mathbf{\Omega}^{(M)}$ are defined similarly. The constraints expressed in (3.33)-(3.36), guarantee that each PRB is exclusively allocated to only one MUE and one SUE, and that each UE receives the required number of PRBs.

3.3.2 Proposed Scheme

The optimization problem formulated in the previous section is too complex to be solved, hence it is needed to resort to sub-optimal solutions. In particular, we propose to separate in two steps the solution of the Coordinated Beamforming (CB) and the Coordinated Scheduling (CS) problems. First, the best CB technique is analysed for a random pair of concurrent users. Then, according to the first step conclusions, a suitable UEs coupling algorithm is proposed.

Coordinated Beamforming selection

As stated before we consider two beamforming techniques that can be used either by the SeNB or the MeNB. Hence, we have four possible Coordinated Beamforming schemes:

(1) both SeNB and MeNB use CVB

(2) both SeNB and MeNB use ZFB

(3) SeNB uses CVB and MeNB uses ZFB

(4) MeNB uses CVB and SeNB uses ZFB.

For a given user pair (a SUE and a MUE) that share the same PRB, the optimum CB scheme is the one that maximizes the composite throughput. It requires the knowledge of all the parameters expressed in (3.19), and, hence, each eNB must have an estimate of the amount of interference that it produces on the user of the other cell. In order to reduce the computational complexity we propose a sub-optimal method based on the difference between the DoAs of the users. The beamforming technique selection is performed separately at the SeNB and the MeNB side. The method is based on the observation that the ZFB is able to guarantee almost zero interference on the concurrent UE direction and almost maximum gain in the target UE direction, if the difference among the two DoAs is sufficiently high, as pictured in Fig.3-9a. The figure represents the ZFB gain for two values of ϕ_{null} as

a function of the target direction Θ. We can observe that, if the angle separation between ϕ_{null} and Θ is higher than a certain critical value, θ_C, ZFB is the best choice. We define the critical angle as the angular difference between the null and the first maximum gain, as shown in Fig.3-9a. The θ_C value varies depending on the null position as pictured in Fig.3-9b. Thus, starting from a sampling of that curves each TP can separately determine the critical angle for each pair of users selected by the CS. We denote with $\Delta_{s,m}^{(M)}$ and $\Delta_{s,m}^{(S)}$ the angular distance between the small cell user s and the macro cell user m, respect to MeNB and SeNB, respectively.

We propose to map the four cases before in four angle conditions:

- (CB1): $\Delta_{s,m}^{(M)} \geq \theta_C$ and $\Delta_{s,m}^{(S)} \geq \theta_C$
- (CB2): $\Delta_{s,m}^{(M)} \geq \theta_C$ and $\Delta_{s,m}^{(S)} < \theta_C$
- (CB3): $\Delta_{s,m}^{(M)} < \theta_C$ and $\Delta_{s,m}^{(S)} \geq \theta_C$
- (CB4): $\Delta_{s,m}^{(M)} < \theta_C$ and $\Delta_{s,m}^{(S)} < \theta_C$.

We have omitted the dependence of θ_C on the value ϕ_{null} for simplicity. This proposed sub-optimum CB selection achieves performance near to the optimum, as shown in Sec.2.4.2.

Coordinated Scheduling

This section describes the CS algorithm proposed here. The basic idea is similar to the one assumed for the CB scheme: using ZFB allows to maximize the spectral efficiency because it permits to lower the interference and at the same time to achieve a gain near to the maximum if there is sufficient separation among the UEs. Hence, the selection of the concurrent MUE and SUE, is made with the aim of maximizing the number of pairs that satisfy the condition (*CB1*) defined in the previous section. In means that the purpose of the proposed iterative scheduling algorithm is to maximize the number UEs pairs for which ZFB can be

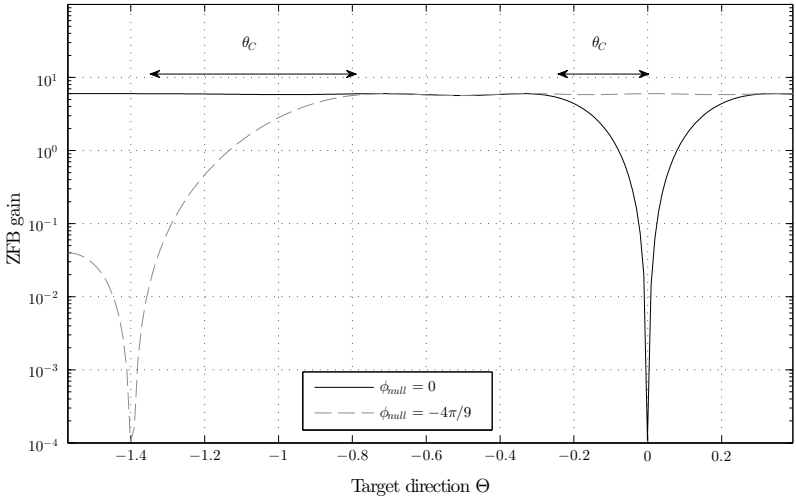

(a) ZFB gain as a function of the target direction for different null directions.

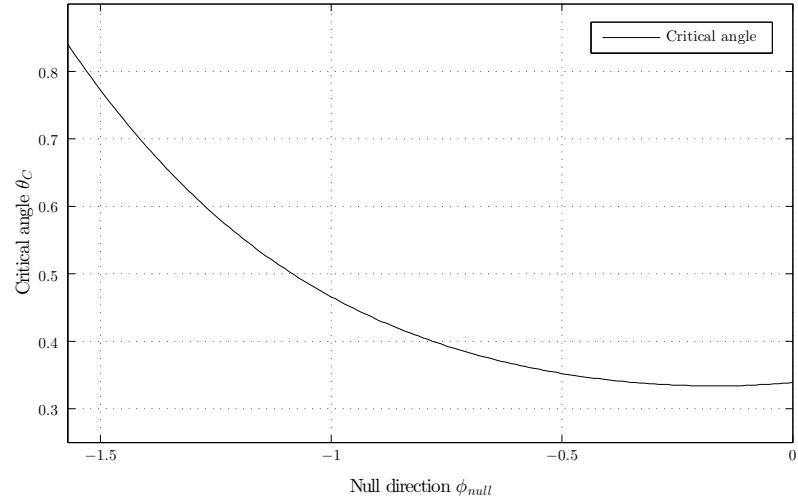

(b) Critical angle trend as a function of the null direction.

Figure 3-9: Critical angle analysis.

used at both sides (SeNB and MeNB). The following procedure is repeated iteratively for each PRB taking into account only the UEs that have not jet received the total amount of requested PRBs ($a_s^{(S)}$ or $a_m^{(M)}$).

Let us consider the iteration p-th and $U_S^p \leq U_S$ SUEs and $U_M^p \leq U_M$ MUEs that need to receive additional resources. SeNB and MeNB calculate for each possible user pair the reciprocal angular distance $\Delta_{s,m}^{(S)}$, $\Delta_{s,m}^{(M)}$. Then each eNB calculates its matrix, $\mathbf{\Delta}^{(S/M)}$, with dimension $(U_S^p \times U_M^p)$ and whose element (i,j) is 1 if $\Delta_{i,j}^{(S/M)} \geq \theta_C$, 0 otherwise.

The CS algorithm operates a logical "*and*" between the two matrices $\mathbf{\Delta}^{(S/M)}$ obtaining a matrix $\mathbf{Z}^p$. The elements that are equal to 1 in $\mathbf{Z}^p$ correspond to the UEs pairs that satisfy the condition (*CB1*). Hence, the algorithm first selects the UE (among all the SUEs with $s = 1, \cdots, U_S^p$ and all the MUEs with $m = \cdots, U_M^p$) that has smallest[6] number of possibilities to satisfy the condition (*CB1*), that is

$$\min \left\{ \min_m \left\{ \sum_{s=1}^{U_S^p} Z_{s,m} \right\}, \min_s \left\{ \sum_{m=1}^{U_M^p} Z_{s,m} \right\} \right\} \tag{3.25}$$

Without loss of generality, we can assume that the selected UE is served by the macro cell ($\bar{m}$), the correspondent SUE forming the new pair is selected among the SUEs listed in the $\bar{m}$ column of $\mathbf{Z}^p$. It is the one that has the smallest number of possibilities to satisfy the condition *CB1* that is

$$\min_{s=1,\cdots,U_S^p} \left\{ \sum_{m=1}^{U_M^p} Z_{s,m} \right\} \tag{3.26}$$

$$s.t.: \qquad Z_{s,\bar{m}} \neq 0 \tag{3.27}$$

The same procedure holds if the first selected user belongs to the small cell. The complexity grows linearly with the product between U_S and U_M, since it is necessary to compute every angular distance between the users of the macro and the small cell. The selection algorithm has

[6] Excluding zero entries.

a finite number of steps, whose complexity depends on the sum of U_S and U_M.

3.3.3 Numerical Results

This section presents some numerical results in order to assess the effectiveness of the proposed CS/CB scheme. As a first step we want to validate the CB selection criterion proposed in Sec. 3.3.2. Fig. 3-10, 3-11 and 3-12 shows the mean user throughput as a function of the total number of users in the system. In particular, Fig. 3-10 shows the performance of different CB methods when the UEs pairs are randomly chosen (referred as random allocation - RandAll). The sub-optimal CB method (SOM) is compared with the optimum method (OM) and with a benchmark transmission that uses ZFB for any pair of MUE-SUE. The SOM reaches midway performance between OM and ZFB. In particular, it is possible to see that the SOM represents a good approximation of the OM.

The performance of the proposed CS/CB scheme (SmAll-SOM) is shown in Fig. 3-11. The CB selection (SOM) is integrated with the proposed CS method based on a smart allocation (SmAll) of the PRBs to the users pairs. From this figure we can notice the throughput gain that is achieved in comparison with a random selection of the UEs pairs. While in Fig. 3-12 it is possible to see that the CB SOM and the CB OM reach roughly the same performance when the SmAll CS is used. This allows to reduce the complexity of the algorithm maintaining unchanged the high values of throughput.

Finally, the SmAll functioning is shown in Fig. 3-13 where the percentage of user pairs belonging to the different CB cases is depicted for the RandAll and the SmAll scheduling. While the RandAll distributes almost uniformly the UEs pairs, the proposed scheme maximizes the *CB1* case, reducing the others drastically. This allows the improvement shown in Figs. 3-11, 3-11 and 3-12.

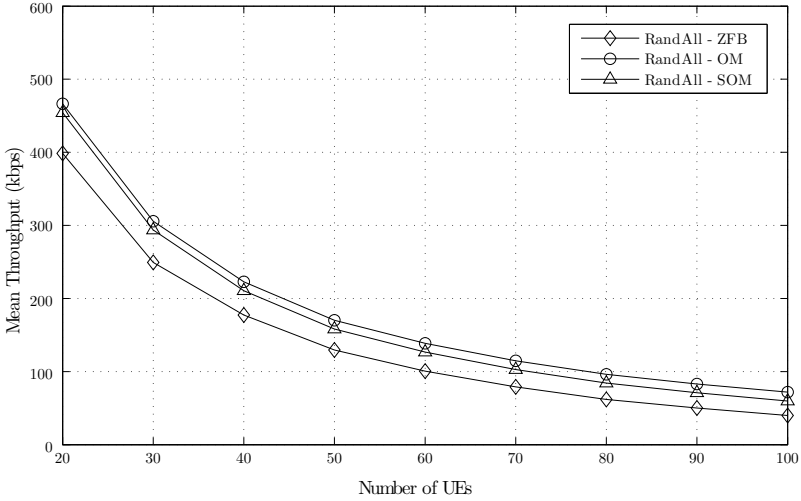

Figure 3-10: Throughput performance for random user pairs and different CB techniques.

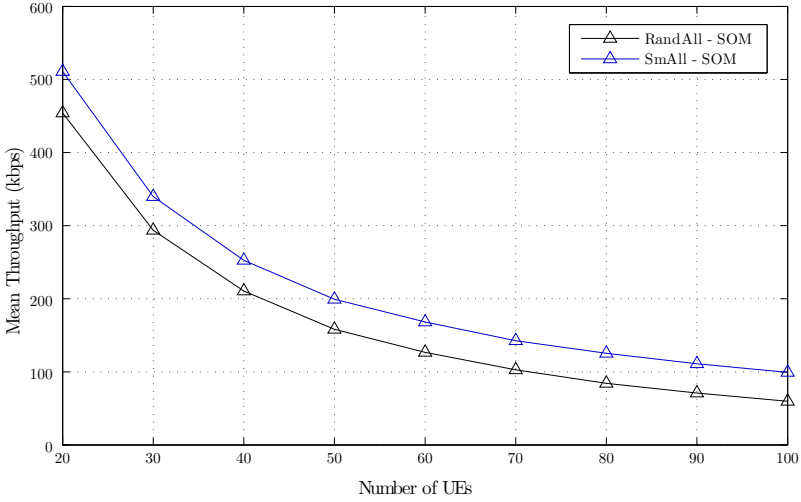

Figure 3-11: Throughput comparison between the RandAll and the SmAll using the proposed SOM.

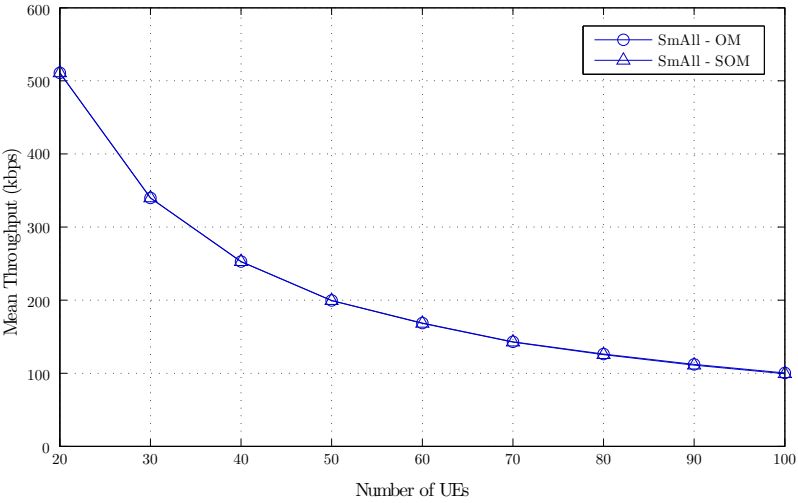

Figure 3-12: Comparison between OM and the proposed SOM using SmAll.

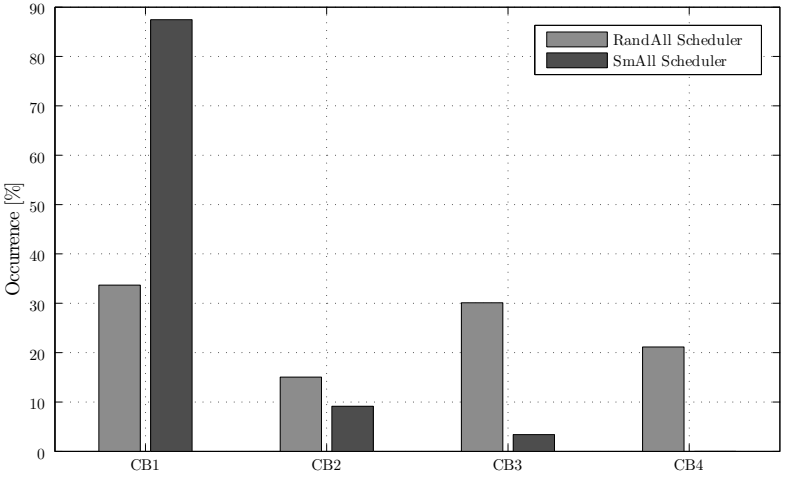

Figure 3-13: Pair distribution according to the considered four cases for the proposed method and a random coupling.

3.4 Optimized JT-CoMP transmission for HetNet using eICIC

This section focuses on an Orthogonal Frequency Division Multiple Access (OFDMA) two layer network where a macrocell is overlapped by a small cell layer in a co-channel deployment scenario. We focus on a dense deployment scenario where many small cell nodes are densely deployed to support huge traffic over a relatively wide area [147].

The number of small cells, S, and the number of UEs, U are chosen following a Spatial Poisson Point Process (SPPP) that is extensively used for modeling heterogeneous networks [148–150]. We neglect the inter-macrocell interference assuming that it is mitigated through suitable frequency allocation schemes, hence the total number of cells is $C = S + 1$. UEs and small cells are randomly placed in the macrocell area following an uniform distribution. In particular we indicate

- the set of UEs as $\boldsymbol{\Upsilon} = \{1, \cdots, U\}$;
- the set of Resource Blocks (RBs) available in each frame period (that is assumed equal to 10 ms) as $\boldsymbol{\Lambda} = \{1, \cdots, K\}$;
- the set of communication data rates requested by the UEs as $\boldsymbol{\Psi} = \{R_1^{req}, \cdots, R_U^{req}\}$;
- the set of cells as $\boldsymbol{\Omega} = \{1, \cdots, C\}$.

eICIC parameters

As stated before eICIC performance depends on the REB and the muting ratio values. However, the choice of these parameters strongly depends on the particular scenario, and a general optimum selection criterion cannot be defined. In addition, while the ABS muting pattern is fixed by the macrocell, the REB value could be defined independently by each small cell leading to possible inefficiencies. However, a dynamic use of the CoMP on top of a basic eICIC approach can limit the problems related to a no-optimal choice of the eICIC parameters.

We refer to [151] for the choice of the REB value of cell, c, assuming the Equal Path Loss (EPL) method, that has been demonstrated to be

$$\lambda^c{}_{dB} = 10log_{10}\frac{G_M P_M^T}{G_c P_c^T} \tag{3.28}$$

where P_c^T and P_M^T are the transmitting powers of the c-th small cell and the macrocell, respectively, and G_c and G_M represent the transmitting antenna gains, at the c-th SBS and at the MBS, respectively.

The muting ratio is chosen in order to minimize the mean UEs service outage. In particular, as shown in Sec. 3.4.2 we have resorted to computer simulations in order to optimize this value. It will be shown that for a dense small cell networks the optimal muting ratio does not vary substantially when the number of small cells and UEs vary. In addition, setting a suboptimal value does not affect significantly the performance.

SINR distribution

Each UE measures the DL SINR value received by different cells, then feedbacks these measures to its serving cell periodically (once a frame). The UE can be served in an ABS or in a noABS subframe, depending if the UE is in CRE area or not. In the ABSs the macrocell transmits only signaling, hence it transmits with a reduced power level. The proposed system takes into account that a UE, u, could be served simultaneously by more than one TP (either small or macro cells). In order to express the average SINR of the UE served with JT-CoMP we introduce two three-dimensional matrices, $\mathbf{M}^{ABS}$ and $\mathbf{M}^{noABS}$, whose dimensions are $(U \times C \times X)$ and $(U \times C \times (K-X))$, respectively and where X represents the number of RBs in the ABS part of the frame. For both matrices the element (u, c, k)-th (i.e, $m_{u,c,k}^{ABS}$ and $m_{u,c,k}^{noABS}$) is equal to 1 if the k-th RB is allocated by the c-th cell to the u-th user, 0 otherwise. Hence, the resulting average SINR of the u-th UE measured on the k-th RB in

an ABS or noABS subframe can be written as

$$\Gamma_{u,k}^{ABS} = \frac{\sum_{c=1}^{C} m_{u,c,k}^{ABS} P_c^R}{\sum_{c=1}^{C} \sum_{\substack{p=1 \\ p \neq u}}^{U} m_{p,c,k}^{ABS} P_c^R + P_C^R D + N} \tag{3.29}$$

$$\Gamma_{u,k}^{noABS} = \frac{\sum_{c=1}^{C} m_{u,c,k}^{noABS} P_c^R}{\sum_{c=1}^{C} \sum_{\substack{p=1 \\ p \neq u}}^{U} m_{p,c,k}^{noABS} P_c^R + N} \tag{3.30}$$

where:

- P_c^R represents the received power[7] per RBs of the c-th cell;
- D is the macrocell power level reduction in ABS subframes;
- N is the AWGN noise power;
- without loss in generality we assume that cell-index $c = C = S+1$ represents the macrocell.

User data rate

The communication data rate of the UEs depends on the amount of allocated RBs and the experienced SINR. The u-th UE that is served on the $z = ABS$ or $z = noABS$ frame portion has a resulting data rate equal to

$$R_u^z = \sum_{k=1}^{Q} g\left(\sum_{c=1}^{C} m_{u,c,k}^z\right) N_S \log_2\left(1 + \Gamma_{u,k}^z\right) \tag{3.31}$$

where N_S represents the number of data subcarriers per RB, $g(x)$ is a function defined as: $g(x) = 1$ if $x > 0$, $g(x) = 0$ otherwise and $Q = X$ if $z = ABS$ or $Q = (K - X)$ if $z = noABS$.

Benchmark solutions

The performance of the proposed system described in the next section will be compared with several benchmark solutions. First of all we

[7] This value takes into account also the transmitting and receiving antenna gains and the pathloss.

propose an heuristic to solve the optimization problem with an affordable computational complexity, hence, we compare the results of the proposed method with those of the numerical solution to validate the goodness of the heuristic.

Then the standard eICIC solution will be considered for comparison. Finally, we will refer to the joint use of CoMP and eICIC proposed in [141]. Indeed, similarly to this work the authors in [141] proposed a dynamic JT-CoMP to be used on top of a semi-static eICIC approach, limiting the use of CoMP to a set of small cell UEs (SUEs) in order to maintain affordable the signaling overhead. The goal is to increase the average UEs throughput and the cell-edge UEs throughput. In particular the work presented in [141] fixes a REB value and then divides the CRE area in two fixed rings. All the SUEs in the CRE area are scheduled in the ABSs, but only the SUEs in the most external CRE ring are served with JT-CoMP. The TPs can be two small cells or a small cell and the macro cell that transmits with reduced power in the ABS. We name this method as eICIC with 2nd ring JT (eICIC+2ndJT).

3.4.1 Proposed System

This section proposes a coordinated scheduling policy that wants to optimize the use of CoMP on top of a basic eICIC. Hence, in the initial phase each UE selects the serving cell as in a basic eICIC approach considering the REB to offload UEs from the MBS. Then, the problem is to determine dynamically which UEs must be served with JT-CoMP and which cells must act as TPs with the goal to minimize the service outage. The problem takes into account the UEs and the small cells positions, the UEs data rate requests and the cells total load. In addition, the proposed solution aims to limit the signaling overhead introduced by CoMP and to distribute the overhead signaling load on different backhaul links. Hence, JT is performed only for a set of UEs that is adaptively chosen, and all the cells can participate in JT, thus limiting to concentrate the complexity and the signaling overhead on the macrocell as in previous proposed solutions [140, 141].

Optimal problem formulation

After the initial basic eICIC configuration, the objective is to minimize the mean serving outage, intended as the inability to satisfy the UEs data requests, selecting the most appropriate JT combinations among UEs and cells. The problem can be formulated as

$$\min_{\substack{\mathbf{M}^{ABS} \\ \mathbf{M}^{noABS}}} \frac{1}{U}\sum_{u=1}^{U} R_u^{req} - (R_u^{ABS} + R_u^{noABS}) \cdot \\ \cdot \; g \;\; (R_u^{ABS} + R_u^{noABS}) \tag{3.32}$$

$$s.t. : \mathbf{m}_{u,c}^{z} \oplus \mathbf{m}_{u,s}^{z} = \mathbf{0} \quad c \in \mathbf{\Omega}; u \in \mathbf{\Upsilon} \tag{3.33}$$

$$\sum_{u=1}^{U}\sum_{k=1}^{X} m_{u,c,k}^{ABS} \leq X \quad c \in \mathbf{\Omega} \tag{3.34}$$

$$\sum_{u=1}^{U}\sum_{k=1}^{K-X} m_{u,c,k}^{noABS} \leq (K-X) \quad c \in \mathbf{\Omega} \tag{3.35}$$

$$\sum_{c=1}^{S}\sum_{k=1}^{K-X} m_{u,c,k}^{noABS} \cdot \sum_{c=1}^{S}\sum_{k=1}^{X} m_{u,c,k}^{ABS} = 0 \quad u \in \mathbf{\Upsilon} \tag{3.36}$$

$$R_u^z \leq R_u^{req} + N_S \log_2(1+\Gamma_u^z) \quad u \in \mathbf{\Upsilon} \tag{3.37}$$

where in (3.33) $z = ABS$ or $z = noABS$ depending on the belonging area of the UE; $\mathbf{m}_{u,c}^{z}$ is a vector of length X if $z = ABS$ or $(K-X)$ if $z = noABS$ obtained by matrix $\mathbf{M}^z$ by fixing the user and the cell indices; $\mathbf{0}$ is a zero vector, with dimension defined accordingly. The constraints impose that:

- in (3.33) - the RBs allocated to the u-th UE are the same for all the serving cells (TPs);
- in (3.34) and (3.35) - each cell cannot allocate more that the available RBs in the frame;
- in (3.36) - a UE cannot be served either in the ABS or in the noABS frame portion;

- in (3.37) - the maximum data rate that can be assigned to a UE.

Sub-optimal problem

The optimal problem has a prohibitive complexity to be solved, hence, we have first defined a sub-optimal problem formulation and then we have resorted to a suitable heuristic with affordable computational complexity, to derive numerical results.

Sub-optimal problem formulation: We can reduce the optimal problem complexity by assuming a detrimental condition on the interference: each RB is used by all the cells (except for the RBs in the ABS that are not used by the macrocell) and as a consequence the SINR value in (3.29)-(3.30) becomes independent on the specific RB (i.e., $\Gamma^z_{u,k} = \Gamma^z_u$ $\forall k \in \Lambda$). This permits to substitute the three-dimensional matrices, $\mathbf{M}^{ABS}$ and $\mathbf{M}^{noABS}$, with two new two-dimensional matrices, $\bar{\mathbf{M}}^{ABS}$ and $\bar{\mathbf{M}}^{noABS}$, whose dimensions are $(U \times C)$ and whose element $m^z_{u,c}$ is equal to the number of RBs that the c-th cell has assigned to the u-th user, in the ABS ($z = ABS$) or in the noABS ($z = noABS$) frame portion. Hence the UE, u, communicates on a number of RBs equal to

$$N^{u,z}_{RB} = \begin{cases} \frac{\sum_{c=1}^{C} \bar{m}^z_{u,c}}{\sum_{c=1}^{C} g(\bar{m}_{u,c})} & if \quad \sum_{c=1}^{C} \bar{m}^z_{u,c} \neq 0 \\ 0 & otherwise \end{cases} . \tag{3.38}$$

and (3.31) becomes

$$R^z_u = N^{u,z}_{RB} N_S \log_2 (1 + \Gamma^z_u) \tag{3.39}$$

Finally the utility function can be rewritten as

$$\min_{\substack{\bar{\mathbf{M}}^{ABS} \\ \bar{\mathbf{M}}^{noABS}}} \frac{1}{U} \sum_{u=1}^{U} R^{req}_u - (R^{ABS}_u + R^{noABS}_u) \cdot \\ \cdot \; g \;\; (R^{ABS}_u + R^{noABS}_u) \tag{3.40}$$

$$s.t. : \bar{m}^z_{u,c} = \bar{m}^z_{u,s} \quad c, s \in \mathbf{\Omega}; u \in \mathbf{\Upsilon} \tag{3.41}$$

$$\sum_{u=1}^{U} \bar{m}^{ABS}_{u,c} \leq X \quad c \in \mathbf{\Omega} \tag{3.42}$$

$$\sum_{u=1}^{U} \bar{m}^{noABS}_{u,c} \leq (K - X) \quad c \in \mathbf{\Omega} \tag{3.43}$$

$$\sum_{c=1}^{S} \bar{m}^{noABS}_{u,c} \cdot \sum_{c=1}^{S} \bar{m}^{ABS}_{u,c} = 0 \quad u \in \mathbf{\Upsilon} \tag{3.44}$$

$$R^z_u \leq R^{req}_u + N_S \log_2(1 + \Gamma^z_u) \quad u \in \mathbf{\Upsilon} \tag{3.45}$$

In Section 3.4.2 it will be shown that, differently from (3.32), this worst interference condition problem can be solved numerically, but only for a limited number of variables. Hence, neither this numerical solution can be used for actual scenarios, especially in the context of a dense small cell deployment as considered in this section. For this reason in what follows we propose an heuristic to solve the problem in an actual scenario, while the numerical solution will be used only to validate the heuristic accuracy in a scaled scenario.

Proposed heuristic: As already stated the proposed system considers an initial phase based on a classical eICIC approach, then the heuristic procedure is used. It is applied independently either for the UEs in the CRE area or not. The only difference is that in ABS subframes only the small cells can cooperate, while in the $noABS$ subframes also the macrocell can participate to JT-CoMP. Hence, we generalize the following expressions using z as index (i.e., $z = ABS$ or $noABS$ depending on the considered area).

The procedure is recursive, hence we add a iteration index, i, to the SINR values, $\Gamma^z_u(i)$.

At the begin each BS determines the amount of RBs requested by its UEs in each frame portion (i.e., ABS or noABS) taking into account their received SINR values $\Gamma^z_u(0)$ when a single cell transmission is active. Assuming that initially the serving cell s-th has $U^z_s(0)$ UEs in the frame portion z, the total outage in this area expressed in terms of RBs

is

$$O_s^z(0) = \sum_{u=1}^{U_s^z(0)} \frac{R_u^{req}}{N_S \log_2(1+\Gamma_u^z(0))} - Q \tag{3.46}$$

where $Q = X$ if $z = ABS$ or $Q = K - X$ if $z = noABS$.

If $O_s^z(0) > 0$ the cell is not able to satisfy the data requests of all its UEs in area z, hence it looks for possible cooperating neighbor cells in a recursive manner. The goal is to increase the SINR of the UEs in order to reduce the amount of requested RBs and, hence to reduce the congestion. However, we want to limit the signaling overhead due to JTs and the risk to overload the neighbor cells. Differently form [141] JT-CoMP is not performed on a predetermined group of UEs in the CRE area, but it is limited to the UEs that achieve the highest gain from JT-CoMP. It means that, for each UE, u, the procedure selects the neighbor cell, c_u^1 with $c_u^1 \in \mathbf{\Omega}$ and $c_u^1 \neq s$, that is received with the highest SINR (without considering REB) and is not already overloaded (i.e, it has free resources to be allocated). Then the new SINR value, $\Gamma_u^z(1)$, for user u-th is calculated taking into account the joint transmission from cells s and c_u^1. For that UE, the CoMP gain expressed in terms of RBs that could be saved is

$$G_u^z(1) = \frac{R_u^{req}}{N_S \log_2(1+\Gamma_u^z(0))} - \frac{R_u^{req}}{N_S \log_2(1+\Gamma_u^z(1))}. \tag{3.47}$$

Finally, the UEs are listed in descending order depending on their JT-CoMP gain, $G_u^z(1) \geq G_{u+1}^z(1)$, and the first $P_s^z(1)$ UEs are effectively selected for CoMP transmission from cells s and c_u^1.

$P_s^z(1)$ is a value in the range $[0, \cdots, U_s^z(0)]$ that satisfies the condition

- $\sum_{p=1}^{P_s^z(1)} G_p^z(1) \geq O_s^z(0)$ and $\sum_{p=1}^{P_s^z(1)-1} G_p^z(1) < O_s^z(0)$

or in alternative the most relaxed condition

- $\sum_{p=1}^{P_s^z(1)} G_p^z(1) > \sum_{p=1}^{P_s^z(1)-1} G_p^z(1)$.

First condition assures that the number of UEs that use JT-CoMP, $P_s^z(1)$, is increased up to the cell s-th is not more congested. If it is not

possible, the second more relaxed condition is considered. It permits to limit the number of UEs that use CoMP to those that achieve an actual benefit in terms of requested resources. However, if only condition two is satisfied, the cell still remain congested. Hence, the algorithm is repeated by adding another neighbor cell as TP in the next iteration.

Generalizing the procedure we have that at the end of iteration $(i-1)$-th the outage of cell s is

$$O_s^z(i-1) = \sum_{u=1}^{U_s^z(i-1)} \frac{R_u^{req}}{N_S \log_2(1+\Gamma_u^z(i-1))} - Q \tag{3.48}$$

If $O_s^z(i-1) > 0$, for each UE an additional possible serving cell is selected as the i-th strongest received cell with free resources, c_u^i, and the CoMP gain is calculated as

$$G_u^z(i) = \frac{R_u^{req}}{N_R \log_2(1+\Gamma_u^z(i-1))} - \frac{R_u^{req}}{N_R \log_2(1+\Gamma_u^z(i))} \tag{3.49}$$

The UEs are ordered following a decreasing gain and, finally $P_s^z(i)$ UEs are effectively selected to be served also by the additional cell c_u^i.

$P_s^z(i)$ can assume values in the range $[0, \cdots, U_s^z(i-1)]$, and must satisfy the condition

- $\sum_{p=1}^{P_s^z(i)} G_p^z(i) \geq O_s^z(i-1)$ and $\sum_{p=1}^{P_s^z(i)-1} G_p^z(i) < O_s^z(i-1)$

or in alternative the most relaxed condition

- $\sum_{p=1}^{P_s^z(i)} G_p^z(i) > \sum_{p=1}^{P_s^z(i)-1} G_p^z(i)$

The procedure stops when all the cells are able to satisfy all the UEs requests or when additional CoMP operations do not add any benefit that is

$$\sum_{c=1}^{C} O_c^z(i) = \sum_{c=1}^{C} O_c^z(i-1) \tag{3.50}$$

It is important to stress that in the recursive procedure the offloaded small cells do not participate in new CoMP clusters to help other congested small cells in order to avoid further congestions. The neighbor

Table 3.2: Simulation parameters

Parameter	**Value**
macrocell area	3 km^2
Mean n. of small cells	[20-30]
Mean n. of UEs	[200-300]
RBs per frame	520
MBS TX power	30dB
SBS TX power	20dB
MBS antenna gain	11dBi
MBS antenna gain	0dBi
ABS power reduction	13dB
UEs data rates	35% VoIP 16Kb/s; 25% Gaming 17,5Kb/s; 15% Image 160Kb/s; 25%HD video 460Kb/s;

cells that can be selected as additional TPs at the new iteration are those that have free resources and have not been congested in previous iterations. More UEs can select the same cell as additional TP on a given iteration and it could result in the congestion of the helping cell. However, in general with few iterations the network congestion is solved, because at each iteration the traffic load is spread on a higher number of cells increasing the chances to solve all the congestion problems. We have verified that in average the algorithm stops after 2-3 iterations.

3.4.2 Numerical Results

This section presents the numerical results derived to validate the proposed method. Our focus is on a dense small cell deployment scenario and the parameters used to derive the results are summarized in Table 3.2.

The simulation results have been obtained by averaging several realizations of the scenario, to have results not dependent on one particular distribution of the UEs and the small cells.

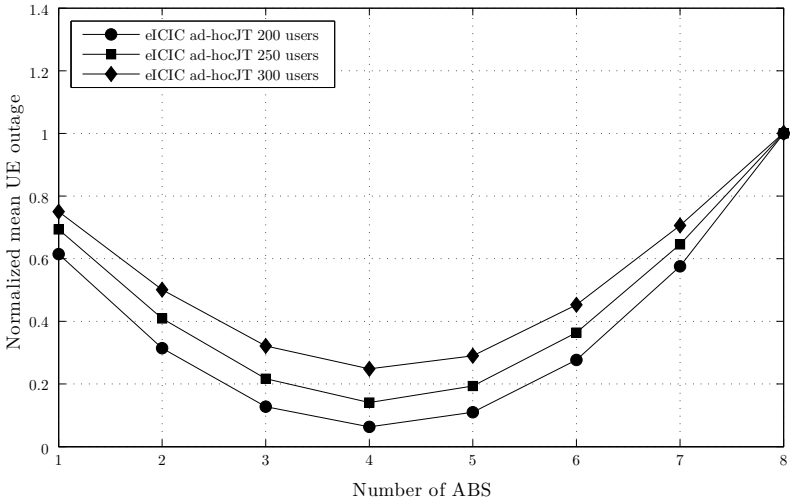

Figure 3-14: Mean UE serving outage, as a function of the muting ratio, for a mean number of small cells equal to 20.

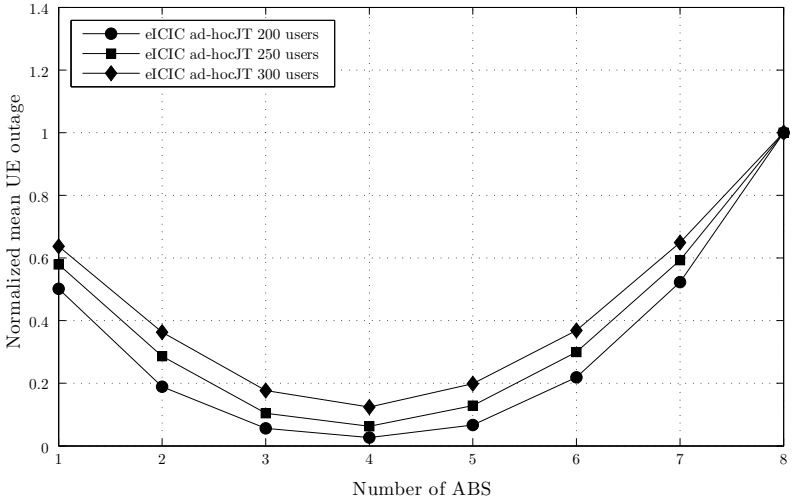

Figure 3-15: Mean UE serving outage, as a function of the muting ratio, for a mean number of small cells equal to 30.

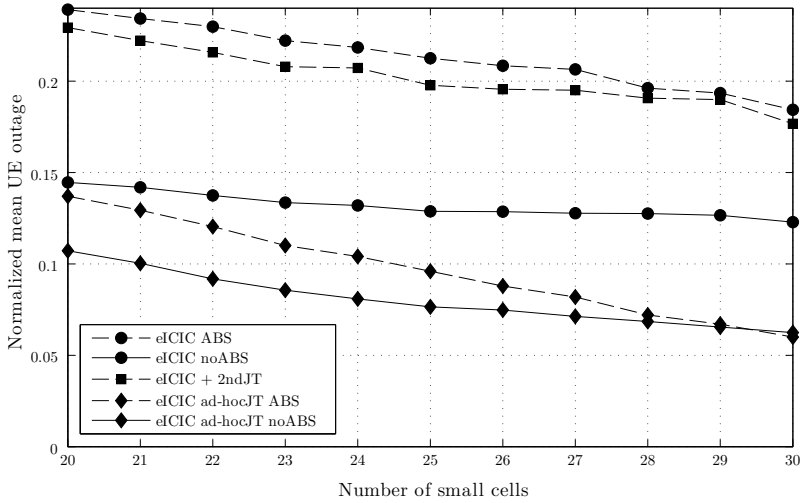

Figure 3-16: Mean serving outage of the proposed heuristic for a mean number of UEs equal to 250.

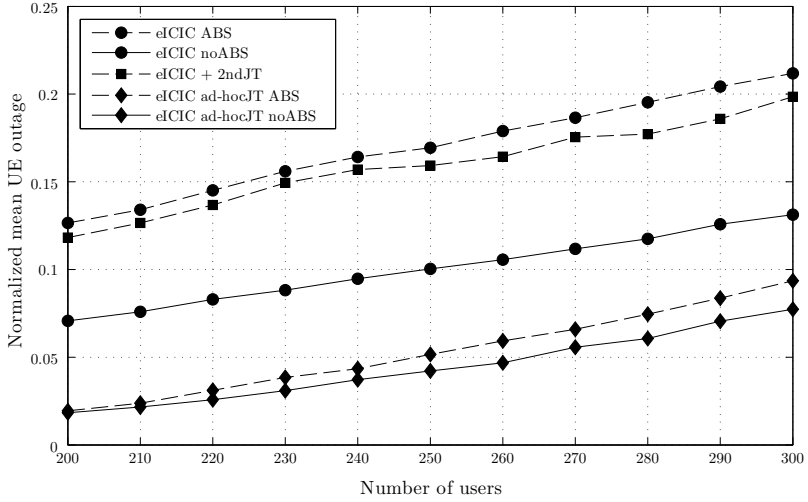

Figure 3-17: Mean serving outage of the proposed heuristic for a mean number of small cells equal to 25.

Firstly we have to optimize the ABS pattern. Figs. 3-14 and 3-15 shows the mean UE service outage, normalized to the data service requests, for different values of the muting ratio assuming a frame composed of 8 subframes. In particular Figs. 3-14 and 3-15 show the results for a variable mean number of UEs, assuming 20 and 30 small cells in the area, respectively. These figures point out the existence of an optimum value of the muting ratio, however, we can note that this value slightly changes with the UEs or small cells number. In addition a near-zero slope around the minimum is evident, suggesting that a not perfect optimization does not affect notably the performance of the method. In what follows the muting ratio is fixed at 4/8.

Before to show the results in an actual scenario, we want to prove the goodness of the proposed heuristic. Hence the simulation results obtained for the proposed heuristic are compared with those obtained by solving numerically the analytical problem as defined in (3.40) by using an open source optimization software [152]. However, due to the high complexity of the numerical solution, only for these results, we have limited the problem dimension considering only a sector of 90 deg of the macrocell area. Table 3.3 shows the accuracy of our method expressed as the difference between of the total serving outage derived by the numerical solution and by the proposed heuristic computer simulations, normalized to the total requested data rate, for different mean number of UEs. We can note that the difference slightly increases with the number of UEs but still remain very limited, thus showing the good approximation of the proposed heuristic.

Table 3.3: Difference between the numerical solution and the proposed heuristic.

Users	10	20	30	40	50
Service outage gap in ABS (%)	0.0028	1.5092	1.8809	2.1415	2.2524
Service outage gap in noABS (%)	0.0017	0.6514	1.0374	1.3703	1.5493

Then, the proposed heuristic (named eICIC ad-hocJT) has been evaluated in terms of the mean service outage normalized to the UEs data rate requests, as a function of the mean number of UEs and the small cells in the whole macrocell area (Figs. 3-16 and 3-17). The performance has been compared with that of a basic eICIC approach (eICIC) and with that of the method proposed in [141] and named here eICIC+2ndJT. In particular the results are provided separately for the UEs served in the ABS or noABS[8] frame portions. For the method eICIC+2ndJT we derive only the total average outage of the UEs in the CRE area because the paper [141] does not consider the UEs in the cell centre, that are served as in a basic eICIC approach.

We can see that the proposed method outperforms the benchmark solutions providing a significant reduction of the service outage. As expected, the serving outage increases with the number of UEs. Conversely, by increasing the number of small cells, the network is able to provide a higher throughput, hence there is a reduction of the total serving outage. The only exception is represented by the UEs in noABS area served with basic eICIC that do not benefit of a higher number of small cells, but on the contrary suffer for a higher interference. This problem is solved in our method because interference is constructively exploited with CoMP.

Another interesting comparison is in terms of consumed energy. The curves presented in Fig. 3-18 are referred to the UEs in the CRE area in order to have a comparison with the eICIC+2ndJT approach. We can see that despite the significant reduction of the service outage shown before, our method has a comparable energy consumption. In particular it permits to lower the consumption of energy respect to eICIC+2ndJT if the number of UEs in the area is not too high. Indeed, the proposed method optimizes the CoMP operations to those more efficient and needed. When the number of UEs increases our method has a higher energy consumption because more JT operations are activated. Obviously the basic eICIC method in which CoMP transmissions are

[8]Macrocell UEs are computed in the noABS portion.

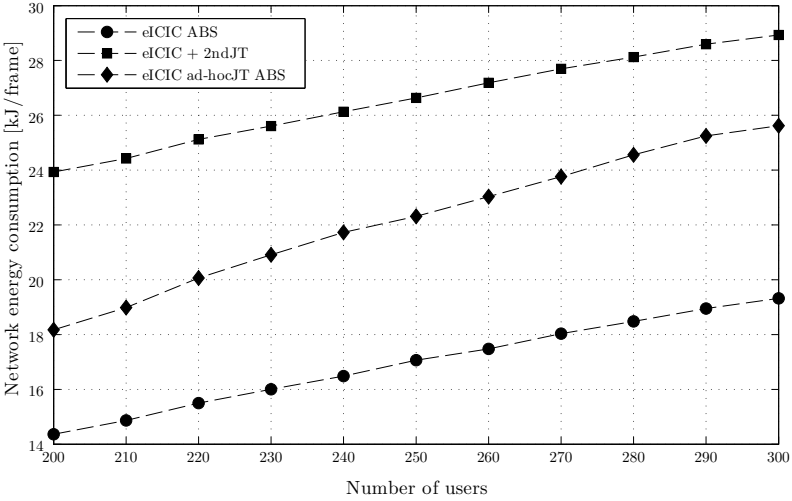

Figure 3-18: Energy consumption as a function of the mean UEs number.

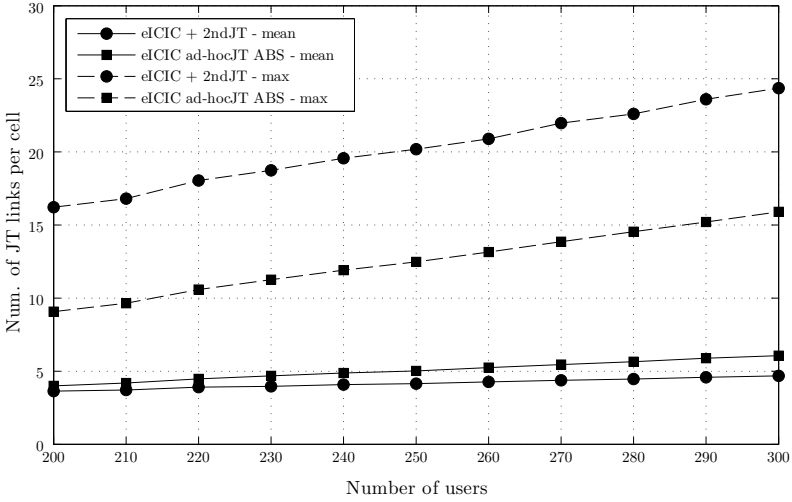

Figure 3-19: Number of JTs links per cell.

not performed permits to save energy but at the cost of a significant higher serving outage.

Finally, the proposed method permits to distribute the CoMP operations among all the cells in the area, avoiding to concentrate the signaling overhead on few cells, and in particular of the macrocell. This results in a reduced capacity requested to the backhaul links, that can be roughly assumed proportional to the number of JT transmissions in which a cell is involved. Fig. 3-19 shows the mean number of JT links (i.e., number of JT-CoMP transmissions) per cell and the value of the maximum number of JT links activated by a single cell. As before we refer to the CoMP operations in the CRE area to compare our results with the benchmark solution. We can note that even if the mean number of JTs for cells in the two methods is almost the same, the maximum value of our proposed method is significantly lower, because the load is more fairly distributed, while in the eICIC+2ndJT approach there is a bias towards the macrocell.

Chapter 4

Conclusion

This thesis addressed the problem of interference in next-generation wireless telecommunication systems. Many solutions, increasingly effective, are proposed in several standards in order to limit the interference and the fading effects. Most of these proposals consider homogeneous networks scenarios, often with structured deployment. Despite this, the heterogeneous scenarios can be an effective solution to meet the growing data-rate demand and the difficulty of offering coverage in specific situations.

The Chapter 1 introduced the problem of interference, then described the main techniques used in 4G and 5G systems. Then, the heterogeneous scenarios were introduced as an effective solution for next-generation wireless networks. Here, new interference issues arise. In fact, heterogeneous networks require specific interference management, not addressed in the standards. In this context, the multi-antenna techniques play a crucial role: the main characteristics and their contribution in the management of interference were described. Particular attention was focused on beamforming, able to steer the transmitted power by digitally changing the pattern through a suitable pre-processing.

The new cells deployment within the access network can be performed by users or by the operator. In the first case, the introduced

small-cell will not have access to the signaling exchanged by the macrocellular systems and therefore there will be not any coordination with them. In this context, the only solution is a cognitive approach, where the computational load of the different solutions lies on the secondary systems. Chapter 2 dealt with the cognitive approach. Through the use of antenna systems compatible with the small size of a small-cell, the beamforming and other techniques based on arrays of antennas allowed to perform effective interference reduction routine. In particular, the main problems were highlighted and subsequently some solutions were proposed to solve them.

In contrast, the coordinated approach addresses the interference issue from the opposite point of view. The new cells, placed in the scenario, have access to a set of control information exchanged with macrocells. In this way, the performance can be greatly improve and the computational load was shifted to the primary systems or even to the core network. Chapter 3 dealt with the coordinated approach. It described the principles and proposed different solutions for the different degrees of coordination discussed in literature.

Bibliography

[1] T. Farley, "Mobile telephone history," *Telektronikk*, 2005.

[2] I. 802.16m, "System requirements document (sdd)," IEEE, Tech. Rep. 09/0002r10, Jan 2010.

[3] ——, "Evaluation methodology (emd)," IEEE, Tech. Rep. 09-0004r5, 2009.

[4] I. P802.16m/D4, "Advanced air interface," IEEE, Tech. Rep., Feb 2010.

[5] 3GPP, "Physical layer aspects for evolved utra," 3GPP, Tech. Rep. TR 25.814, Sep 2006.

[6] ——, "X2 protocol specification," 3GPP, Tech. Rep. TS 36.423, Sep 2014.

[7] ——, "Physical layer procedures," 3GPP, Tech. Rep. TS 36.213, Sep 2014.

[8] C. G. Gerlach, I. Karla, A. Weber, L. Ewe, H. Bakker, E. Kuehn, and A. Rao, "Icic in dl and ul with network distributed and self-organized resource assignment algorithms in lte," *Bell Labs Technical Journal*, vol. 15, no. 3, pp. 43–62, Dec 2010.

[9] B. Bandemer, A. Gamal, and Y.-H. Kim, "Simultaneous nonunique decoding is rate-optimal," in *Communication, Control, and Computing (Allerton), 2012 50th Annual Allerton Conference on*, Oct 2012, pp. 9–16.

[10] F. Baccelli, A. El Gamal, and D. Tse, "Interference networks with point-to-point codes," in *Information Theory Proceedings (ISIT), 2011 IEEE International Symposium on*, July 2011, pp. 435–439.

[11] M. Akdeniz and S. Rangan, "Optimal wireless scheduling with interference cancellation," in *Information Theory Proceedings (ISIT), 2013 IEEE International Symposium on*, July 2013, pp. 246–250.

[12] V. Leung, "Internetworking wireless terminals to local area networks via radio bridges," in *Wireless Communications, 1992. Conference Proceedings., 1992 IEEE International Conference on Selected Topics in*, Jun 1992, pp. 126–129.

[13] D. Lopez-Perez, G. de la Roche, A. Valcarce, A. Juttner, and J. Zhang, "Interference avoidance and dynamic frequency planning for wimax femtocells networks," in *Communication Systems, 2008. ICCS 2008. 11th IEEE Singapore International Conference on*, Nov 2008, pp. 1579–1584.

[14] V. Chandrasekhar, J. Andrews, and A. Gatherer, "Femtocell networks: a survey," *Communications Magazine, IEEE*, vol. 46, no. 9, pp. 59–67, September 2008.

[15] M. Yavuz, F. Meshkati, S. Nanda, A. Pokhariyal, N. Johnson, B. Raghothaman, and A. Richardson, "Interference management and performance analysis of umts/hspa+ femtocells," *Communications Magazine, IEEE*, vol. 47, no. 9, pp. 102–109, September 2009.

[16] D. Hong, S. Choi, and J. Cho, "Coverage and capacity analysis for the multi-layer cdma macro/indoor-picocells," in *Communications, 1999. ICC '99. 1999 IEEE International Conference on*, vol. 1, 1999, pp. 354–358 vol.1.

[17] H. Yanikomeroglu and E. Sousa, "Power control and number of antenna elements in cdma distributed antenna systems," in *Communications, 1998. ICC 98. Conference Record. 1998 IEEE International Conference on*, vol. 2, Jun 1998, pp. 1040–1045 vol.2.

[18] T. Wirth, L. Thiele, T. Haustein, O. Braz, and J. Stefanik, "Lte amplify and forward relaying for indoor coverage extension," in *Vehicular Technology Conference Fall (VTC 2010-Fall), 2010 IEEE 72nd*, Sept 2010, pp. 1–5.

[19] H. Claussen, "Performance of macro- and co-channel femtocells in a hierarchical cell structure," in *Personal, Indoor and Mobile Radio Communications, 2007. PIMRC 2007. IEEE 18th International Symposium on*, Sept 2007, pp. 1–5.

[20] R. Baines, "The need for wimax picocell femtocells," in *WiMax London 2007*, April 2007, pp. 1–36.

[21] D. Knisely, T. Yoshizawa, and F. Favichia, "Standardization of femtocells in 3gpp," *Communications Magazine, IEEE*, vol. 47, no. 9, pp. 68–75, September 2009.

[22] L. Wang, Y. Zhang, and Z. Wei, "Mobility management schemes at radio network layer for lte femtocells," in *Vehicular Technology Conference, 2009. VTC Spring 2009. IEEE 69th*, April 2009, pp. 1–5.

[23] R. Kim, J. S. Kwak, and K. Etemad, "Wimax femtocell: requirements, challenges, and solutions," *Communications Magazine, IEEE*, vol. 47, no. 9, pp. 84–91, September 2009.

[24] D. Lopez-Perez, A. Juttner, and J. Zhang, "Optimisation methods for dynamic frequency planning in ofdma networks," in *Telecommunications Network Strategy and Planning Symposium, 2008. Networks 2008. The 13th International*, Sept 2008, pp. 1–28.

[25] S. Huan, K. Linling, and L. Jianhua, "Interference avoidance in ofdma-based femtocell network," in *Information, Computing and Telecommunication, 2009. YC-ICT '09. IEEE Youth Conference on*, Sept 2009, pp. 126–129.

[26] Y. Bai, J. Zhou, and L. Chen, "Hybrid spectrum usage for overlaying lte macrocell and femtocell," in *Global Telecommunications Conference, 2009. GLOBECOM 2009. IEEE*, Nov 2009, pp. 1–6.

[27] D. Lopez-Perez, A. Ladanyi, A. Juttner, and J. Zhang, "Ofdma femtocells: A self-organizing approach for frequency assignment," in *Personal, Indoor and Mobile Radio Communications, 2009 IEEE 20th International Symposium on*, Sept 2009, pp. 2202–2207.

[28] S. Hasan, N. Siddique, and S. Chakraborty, "Femtocell versus wifi - a survey and comparison of architecture and performance," in *Wireless Communication, Vehicular Technology, Information Theory and Aerospace Electronic Systems Technology, 2009. Wireless VITAE 2009. 1st International Conference on*, May 2009, pp. 916–920.

[29] D. Choi, P. Monajemi, S. Kang, and J. Villasenor, "Dealing with loud neighbors: The benefits and tradeoffs of adaptive femtocell access," in *Global Telecommunications Conference, 2008. IEEE GLOBECOM 2008. IEEE*, Nov 2008, pp. 1–5.

[30] D. Lopez-Perez, A. Valcarce, G. de la Roche, E. Liu, and J. Zhang, "Access methods to wimax femtocells: A downlink system-level case study," in *Communication Systems, 2008. ICCS 2008. 11th IEEE Singapore International Conference on*, Nov 2008, pp. 1657–1662.

[31] A. Valcarce, D. Lopez-Perez, G. de la Roche, and J. Zhang, "Limited access to ofdma femtocells," in *Personal, Indoor and Mobile Radio Communications, 2009 IEEE 20th International Symposium on*, Sept 2009, pp. 1–5.

[32] Y. J. Sang, H. G. Hwang, and K. S. Kim, "A self-organized femtocell for ieee 802.16e system," in *Global Telecommunications Conference, 2009. GLOBECOM 2009. IEEE*, Nov 2009, pp. 1–5.

[33] C.-K. Han, H.-K. Choi, and I.-H. Kim, "Building femtocell more secure with improved proxy signature," in *Global Telecommunications Conference, 2009. GLOBECOM 2009. IEEE*, Nov 2009, pp. 1–6.

[34] T. Chiba and H. Yokota, "Efficient route optimization methods for femtocell-based all ip networks," in *Wireless and Mobile Computing, Networking and Communications, 2009. WIMOB 2009. IEEE International Conference on*, Oct 2009, pp. 221–226.

[35] J. Yoon, J. Lee, and H. S. Lee, "Multi-hop based network synchronization scheme for femtocell systems," in *Personal, Indoor and Mobile Radio Communications, 2009 IEEE 20th International Symposium on*, Sept 2009, pp. 1–5.

[36] V. Chandrasekhar and J. Andrews, "Spectrum allocation in tiered cellular networks," *Communications, IEEE Transactions on*, vol. 57, no. 10, pp. 3059–3068, October 2009.

[37] T. Zahir, K. Arshad, A. Nakata, and K. Moessner, "Interference management in femtocells," *Communications Surveys Tutorials, IEEE*, vol. 15, no. 1, pp. 293–311, First 2013.

[38] H.-S. Jo, C. Mun, J. Moon, and J.-G. Yook, "Interference mitigation using uplink power control for two-tier femtocell networks," *Wireless Communications, IEEE Transactions on*, vol. 8, no. 10, pp. 4906–4910, October 2009.

[39] A. Golaup, M. Mustapha, and L. Patanapongpibul, "Femtocell access control strategy in umts and lte," *Communications Magazine, IEEE*, vol. 47, no. 9, pp. 117–123, September 2009.

[40] J. Andrews, "Interference cancellation for cellular systems: a contemporary overview," *Wireless Communications, IEEE*, vol. 12, no. 2, pp. 19–29, April 2005.

[41] L. Trichard, J. Evans, and I. Collings, "Large system analysis of linear parallel interference cancellation," in *Communications, 2001. ICC 2001. IEEE International Conference on*, vol. 1, Jun 2001, pp. 26–30 vol.1.

[42] P. Frenger, P. Orten, and T. Ottosson, "Code-spread cdma with interference cancellation," *Selected Areas in Communications, IEEE Journal on*, vol. 17, no. 12, pp. 2090–2095, Dec 1999.

[43] P. Patel and J. Holtzman, "Analysis of a simple successive interference cancellation scheme in a ds/cdma system," *Selected Areas in Communications, IEEE Journal on*, vol. 12, no. 5, pp. 796–807, Jun 1994.

[44] F. van der Wijk, G. Janssen, and R. Prasad, "Groupwise successive interference cancellation in a ds/cdma system," in *Personal, Indoor and Mobile Radio Communications, 1995. PIMRC'95. Wireless: Merging*

onto the Information Superhighway., Sixth IEEE International Symposium on, vol. 2, Sep 1995, pp. 742–746 vol.2.

[45] M. Ghosh, "Co-channel interference cancellation for hdtv receivers," in *Acoustics, Speech, and Signal Processing, 1999. Proceedings., 1999 IEEE International Conference on*, vol. 5, 1999, pp. 2675–2678 vol.5.

[46] R. Karlsson, "Radio resource sharing and capacity of some multiple access methods in hierarchical cell structures," in *Vehicular Technology Conference, 1999. VTC 1999 - Fall. IEEE VTS 50th*, vol. 5, 1999, pp. 2825–2829 vol.5.

[47] T. Zahir, K. Arshad, Y. Ko, and K. Moessner, "A downlink power control scheme for interference avoidance in femtocells," in *Wireless Communications and Mobile Computing Conference (IWCMC), 2011 7th International*, July 2011, pp. 1222–1226.

[48] Y.-Y. Li, M. Macuha, E. Sousa, T. Sato, and M. Nanri, "Cognitive interference management in 3g femtocells," in *Personal, Indoor and Mobile Radio Communications, 2009 IEEE 20th International Symposium on*, Sept 2009, pp. 1118–1122.

[49] M. Şahin, I. Guvenc, M.-R. Jeong, and H. Arslan, "Handling cci and ici in ofdma femtocell networks through frequency scheduling," *Consumer Electronics, IEEE Transactions on*, vol. 55, no. 4, pp. 1936–1944, November 2009.

[50] I. Ashraf, H. Claussen, and L. Ho, "Distributed radio coverage optimization in enterprise femtocell networks," in *Communications (ICC), 2010 IEEE International Conference on*, May 2010, pp. 1–6.

[51] E. J. Hong, S. Y. Yun, and D.-H. Cho, "Decentralized power control scheme in femtocell networks: A game theoretic approach," in *Personal, Indoor and Mobile Radio Communications, 2009 IEEE 20th International Symposium on*, Sept 2009, pp. 415–419.

[52] H.-C. Lee, D.-C. Oh, and Y.-H. Lee, "Mitigation of inter-femtocell interference with adaptive fractional frequency reuse," in *Communications (ICC), 2010 IEEE International Conference on*, May 2010, pp. 1–5.

[53] J. Mietzner, R. Schober, L. Lampe, W. Gerstacker, and P. Hoeher, "Multiple-antenna techniques for wireless communications - a comprehensive literature survey," *Communications Surveys Tutorials, IEEE*, vol. 11, no. 2, pp. 87–105, Second 2009.

[54] L. Godara, "Application of antenna arrays to mobile communications. II. Beam-forming and direction-of-arrival considerations," *Proc. IEEE*, vol. 85, no. 8, pp. 1195–1245, Aug. 1997.

[55] T. Kaiser, A. Bourdoux, M. Rupp, and U. Heute, "Implementation aspects and testbeds for mimo systems," *EURASIP Journal on Advances in Signal Processing*, vol. 2006, no. 1, p. 069217, 2006.

[56] N. Chiurtu, B. Rimoldi, and I. Telatar, "On the capacity of multi-antenna gaussian channels," in *Information Theory, 2001. Proceedings. 2001 IEEE International Symposium on*, 2001, pp. 53–.

[57] G. Foschini and M. Gans, "On limits of wireless communications in a fading environment when using multiple antennas," *Wireless Personal Communications*, vol. 6, no. 3, pp. 311–335, 1998.

[58] G. Stuber, J. Barry, S. McLaughlin, Y. Li, M.-A. Ingram, and T. Pratt, "Broadband mimo-ofdm wireless communications," *Proceedings of the IEEE*, vol. 92, no. 2, pp. 271–294, Feb 2004.

[59] D. Pham, K. Pattipati, P. Willett, and J. Luo, "A generalized probabilistic data association detector for multiple antenna systems," in *Communications, 2004 IEEE International Conference on*, vol. 6, June 2004, pp. 3519–3522 Vol.6.

[60] S. Alamouti, "A simple transmit diversity technique for wireless communications," *Selected Areas in Communications, IEEE Journal on*, vol. 16, no. 8, pp. 1451–1458, Oct 1998.

[61] V. Tarokh, N. Seshadri, and A. Calderbank, "Space-time codes for high data rate wireless communication: performance criterion and code construction," *Information Theory, IEEE Transactions on*, vol. 44, no. 2, pp. 744–765, Mar 1998.

[62] V. Tarokh, H. Jafarkhani, and A. Calderbank, "Space-time block codes from orthogonal designs," *Information Theory, IEEE Transactions on*, vol. 45, no. 5, pp. 1456–1467, Jul 1999.

[63] B. Hassibi and B. Hochwald, "High-rate codes that are linear in space and time," *Information Theory, IEEE Transactions on*, vol. 48, no. 7, pp. 1804–1824, Jul 2002.

[64] J. Winters, J. Salz, and R. Gitlin, "The impact of antenna diversity on the capacity of wireless communication systems," *Communications, IEEE Transactions on*, vol. 42, no. 234, pp. 1740–1751, Feb 1994.

[65] S. Swales, M. Beach, D. Edwards, and J. McGeehan, "The performance enhancement of multibeam adaptive base-station antennas for cellular land mobile radio systems," *Vehicular Technology, IEEE Transactions on*, vol. 39, no. 1, pp. 56–67, Feb 1990.

[66] H. Zhuang, L. Dai, S. Zhou, and Y. Yao, "Low complexity per-antenna rate and power control approach for closed-loop v-blast," *Communications, IEEE Transactions on*, vol. 51, no. 11, pp. 1783–1787, Nov 2003.

[67] G. Jöngren, M. Skoglund, and B. Ottersten, "Combining beamforming and orthogonal space-time block coding," *Information Theory, IEEE Transactions on*, vol. 48, no. 3, pp. 611–627, Mar 2002.

[68] H. Sampath and A. Paulraj, "Linear precoding for space-time coded systems with known fading correlations," *Communications Letters, IEEE*, vol. 6, no. 6, pp. 239–241, June 2002.

[69] S. Zhou and G. Giannakis, "Optimal transmitter eigen-beamforming and space-time block coding based on channel correlations," in *Communications, 2002. ICC 2002. IEEE International Conference on*, vol. 1, 2002, pp. 553–557.

[70] M. Baker, "From LTE-Advanced to the future," *IEEE Commun. Mag.*, vol. 50, no. 2, pp. 116–120, February 2012.

[71] T. Nakamura, S. Nagata, A. Benjebbour, Y. Kishiyama, T. Hai, S. Xiaodong, Y. Ning, and L. Nan, "Trends in small cell enhancements in LTE advanced," *IEEE Commun. Mag.*, vol. 51, no. 2, pp. 98–105, 2013.

[72] D.-C. Oh, H.-C. Lee, and Y.-H. Lee, "Power control and beamforming for femtocells in the presence of channel uncertainty," *IEEE Trans. Veh. Technol.*, vol. 60, no. 6, pp. 2545–2554, 2011.

[73] S. Chen, Z. Feng, Q. Zhang, and P. Zhang, "Interference mitigation and capacity optimization in cooperative public femtocell networks with cognitive enabled multi-element antennas," in *2012 IEEE Globecom Workshops (GC Wkshps)*, 2012, pp. 652–656.

[74] G. Bartoli, R. Fantacci, D. Marabissi, and M. Pucci, "LTE-A Femto-Cell Interference Mitigation with MuSiC DOA Estimation and Null Steering in an Actual Indoor Environment," in *2013 IEEE International Communication Conference (ICC)*, 2013, pp. 1–5.

[75] D. Marabissi, D. Tarchi, R. Fantacci, and A. Biagioni, "Adaptive Subcarrier Allocation Algorithms in Wireless OFDMA Systems," in *IEEE International Conference on Communications*, May 2008, pp. 3475–3479.

[76] G. Bartoli, R. Fantacci, D. Marabissi, and M. Pucci, "Physical Resource Block clustering method for an OFDMA cognitive femtocell system," *Physical Communication, Elsevier*, 2014.

[77] J. Zhang and J. Andrews, "Adaptive spatial intercell interference cancellation in multicell wireless networks," *IEEE J. Sel. Areas Commun.*, vol. 28, no. 9, pp. 1455–1468, 2010.

[78] J. Zhang, R. Chen, J. Andrews, A. Ghosh, and R. Heath, "Networked mimo with clustered linear precoding," *IEEE Trans. Wireless Commun.*, vol. 8, no. 4, pp. 1910–1921, 2009.

[79] Y. Shi, J. Zhang, and K. B. Letaief, "Group sparse beamforming for green cloud radio access networks," in *IEEE Globecom, Atlanta, GA*, December 2013.

[80] F. Rusek, D. Persson, B. K. Lau, E. Larsson, T. Marzetta, O. Edfors, and F. Tufvesson, "Scaling Up MIMO: Opportunities and Challenges with Very Large Arrays," *IEEE Signal Process. Mag.*, vol. 30, no. 1, pp. 40–60, 2013.

[81] T. Marzetta, "Noncooperative Cellular Wireless with Unlimited Numbers of Base Station Antennas," *IEEE Trans. Wireless Commun.*, vol. 9, no. 11, pp. 3590–3600, 2010.

[82] E. G. Larsson, F. Tufvesson, O. Edfors, and T. L. Marzetta, "Massive MIMO for next generation wireless systems," *submitted to IEEE Commun. Mag.*, 2013. [Online]. Available: http://arxiv.org/abs/1304.6690

[83] H. Q. Ngo, E. Larsson, and T. Marzetta, "Energy and Spectral Efficiency of Very Large Multiuser MIMO Systems," *IEEE Trans. Commun.*, vol. 61, no. 4, pp. 1436–1449, 2013.

[84] C. Shepard, H. Yu, N. Anand, E. Li, T. L. Marzetta, Y. R., and L. Zhong, "Argos: practical many-antenna base stations," in *ACM Int. Conf. Mobile Computing and Networking (MobiCom)*, 2012, pp. 53–64.

[85] A. Larmo, M. Lindstrom, M. Meyer, G. Pelletier, J. Torsner, and H. Wiemann, "The LTE link-layer design," *IEEE Commun. Mag.*, vol. 47, no. 4, pp. 52–59, Apr. 2009.

[86] G. Bartoli, R. Fantacci, D. Marabissi, L. Micciullo, and M. Fossi, "An Efficient Subcarrier Allocation Method for AeroMACS Based Communication Systems," *IEEE Trans. Aerosp. Electron. Syst.*, Apr. 2013.

[87] V. Chandrasekhar, J. Andrews, and G. A., "Femtocell networks: a survey," *IEEE Commun. Mag.*, vol. 46, no. 9, pp. 59–67, Sep. 2008.

[88] M. Chowdhury, Y. Jang, and Z. Haas, "Network evolution and QoS provisioning for integrated femtocell/macrocell networks," *Int. Journal Wireless Mobile Networks*, vol. 2, no. 3, pp. 1–16, Aug. 2010.

[89] M. Selim, M. El-Khamy, and M. El-Sharkawy, "Enhanced frequency reuse schemes for interference management in LTE femtocell networks," in *International Symposium on Wireless Communication Systems (ISWCS)*, Aug. 2012, pp. 326–330.

[90] C. Bouras, G. Kavourgias, V. Kokkinos, and A. Papazois, "Interference management in LTE femtocell systems using an adaptive frequency reuse scheme," in *Wireless Telecommunications Symposium (WTS)*, Apr. 2012, pp. 1–7.

[91] A. Attar, V. Krishnamurthy, and O. Gharehshiran, "Interference management using cognitive base-stations for UMTS LTE," *IEEE Commun. Mag.*, vol. 49, no. 8, pp. 152–159, Aug. 2011.

[92] D.-C. Oh, H.-C. Lee, and Y.-H. Lee, "Cognitive radio based femtocell resource allocation," in *International Conference on Information and Communication Technology Convergence (ICTC)*, Nov. 2010, pp. 274–279.

[93] F. Khan and Y.-J. Choi, "Joint subcarrier and power allocations in OFDMA-based cognitive femtocell networks," in *18th Asia-Pacific Conference on Communications (APCC)*, Oct. 2012, pp. 812–817.

[94] D. Tarchi, R. Fantacci, and D. Marabissi, "Proposal of a cognitive based mac protocol for m2m environments," in *24th Annual IEEE International Symposium on Personal, Indoor and Mobile Radio Communications*, 2013, pp. 8–11 September 2013, London, UK.

[95] D. Sun, X. Zhu, Z. Zeng, and S. Wan, "Downlink power control in cognitive femtocell networks," in *International Conference on Wireless Communications and Signal Processing (WCSP)*, Nov. 2011, pp. 1–5.

[96] S. Yiu, C.-B. Chae, K. Yang, and D. Calin, "Uncoordinated Beamforming for Cognitive Networks ," *IEEE Trans. Commun.*, vol. 60, no. 5, pp. 1390–1397, May 2012.

[97] J. Xie, Z. Fu, and H. Xian, "Spectrum sensing based on estimation of direction of arrival," in *International Conference on Computational Problem-Solving (ICCP)*, Dec. 2010, pp. 39–42.

[98] E. Yaacoub and Z. Dawy, "Enhancing the performance of OFDMA underlay cognitive radio networks via secondary pattern nulling and primary beam steering," in *IEEE Wireless Communications and Networking Conference (WCNC)*, 2011, pp. 1476–1481.

[99] J. MacQueen, "Some methods for classification and analysis of multivariate observations," in *Proc. Fifth Berkeley Symp. on Math. Statist. and Prob.* Univ. of Claif. Press, 1967, pp. 281–297.

[100] 3GPP, "Evolved Universal Terrestrial Radio Access (E-UTRA); User Equipment (UE) radio transmission and reception," Third Generation Partnership Project, Standard TS36.101, Settembre 2014.

[101] Q. Spencer, B. Jeffs, M. Jensen, and A. Swindlehurst, "Modeling the statistical time and angle of arrival characteristics of an indoor multipath channel," *IEEE J. Sel. Areas Commun.*, vol. 18, no. 3, pp. 347–360, Mar. 2000.

[102] A. Note, "Theory, Techniques and Validation of Over-the-Air Test Methods for Evaluating the Performance of MIMO User Equipment," Agilent Technologies, Tech. Rep., 2010.

[103] ITU-R, "Guidelines for evaluation of radio transmission technologies for IMT-2000," International Telecommunication Union, Recommendation M.1225, Feb. 1997.

[104] T. Lavate, V. Kokate, and A. Sapkal, "Performance Analysis of MUSIC and ESPRIT DOA Estimation Algorithms for Adaptive Array Smart Antenna in Mobile Communication," in *Second International Conference on Computer and Network Technology (ICCNT)*, Apr. 2010, pp. 308–311.

[105] R. Schmidt, "Multiple emitter location and signal parameter estimation," *IEEE Trans. Antennas Propag.*, vol. 34, no. 3, pp. 276–280, Mar. 1986.

[106] B. Friedlander and B. Porat, "Performance analysis of a null-steering algorithm based on direction-of-arrival estimation," *IEEE Trans. Acoust., Speech, Signal Process.*, vol. 37, no. 4, pp. 461–466, Apr. 1989.

[107] R. Qamar and N. Khan, "Null steering, a comparative analysis," in *IEEE 13th International Multitopic Conference (INMIC)*, Dec. 2009, pp. 1–5.

[108] 3GPP, "Evolved Universal Terrestrial Radio Access (E-UTRA) - Base Station (BS) radio transmission and reception," Third Generation Partnership Project, Standard TS36.104, Sep. 2012.

[109] ——, "Evolved Universal Terrestrial Radio Access (E-UTRA) - FDD Home eNode B (HeNB) Radio Frequency (RF) requirements analysis," Third Generation Partnership Project, Standard TS36.921, Sep. 2012.

[110] A. Jain, M. Murty, and P. Flynn, "Data Clustering: A Review," *ACM Computing Surveys*, vol. 31, no. 3, pp. 264–323, Sep. 1999.

[111] A. K. Jain, "Data clustering: 50 years beyond K-means," *Elsevier, Pattern Recognition Letters*, vol. 31, no. 8, pp. 651–666, Jun. 2010.

[112] S. Johnson, "Hierarchical Clustering Schemes," *Psychometrika, Springer*, vol. 32, no. 3, pp. 241–254, Sep. 1967.

[113] A. Jain and R. Dubes, *Algorithms for Clustering Data*. Prentice Hall, Englewood Cliffs, NJ, 1988.

[114] B. Chen, P. Tai, R. Harrison, and Y. Pan, "Novel hybrid hierarchical-k-means clustering method (h-k-means) for microarray analysis," in *Computational Systems Bioinformatics Conference, 2005. Workshops and Poster Abstracts. IEEE*, 2005, pp. 105–108.

[115] G. Ioannopoulos, D. Anagnostou, and M. Chryssomallis, "A survey on the effect of small snapshots number and SNR on the efficiency of the MUSIC algorithm," in *IEEE Antennas and Propagation Society International Symposium (APSURSI)*, Jul. 2012, pp. 1–2.

[116] L. Huang, G. Zhu, and X. Du, "Cognitive femtocell networks: an opportunistic spectrum access for future indoor wireless coverage," *Wireless Communications, IEEE*, vol. 20, no. 2, pp. 44–51, April 2013.

[117] K. Hugl, K. Kalliola, and J. Laurila, "Spatial reciprocity of uplink and downlink radio channels in fdd systems," *Proc. COST 273 TD(02) 066*, May 2002.

[118] T. Yoo and A. Goldsmith, "On the optimality of multiantenna broadcast scheduling using zero-forcing beamforming," *IEEE J. Sel. Areas Commun.*, vol. 24, no. 3, pp. 528–541, 2006.

[119] K. Hamdi, W. Zhang, and K. Letaief, "Opportunistic spectrum sharing in cognitive MIMO wireless networks," *IEEE Trans. Wireless Commun.*, vol. 8, no. 8, pp. 4098–4109, 2009.

[120] J. Andrews, H. Claussen, M. Dohler, S. Rangan, and M. Reed, "Femtocells: Past, Present, and Future," *Selected Areas in Communications, IEEE Journal on*, vol. 30, no. 3, pp. 497–508, April 2012.

[121] G. Bartoli, R. Fantacci, K. Letaief, D. Marabissi, N. Privitera, M. Pucci, and J. Zhang, "Beamforming for Small Cells Deployment in LTE-Advanced and Beyond," *Comm. Magazine IEEE*, April 2014.

[122] Q. Ye, B. Rong, Y. Chen, M. Al-Shalash, C. Caramanis, and J. Andrews, "User Association for Load Balancing in Heterogeneous Cellular Networks," *Wireless Communications, IEEE Transactions on*, vol. 12, no. 6, pp. 2706–2716, June 2013.

[123] B. Soret, H. Wang, K. Pedersen, and C. Rosa, "Multicell cooperation for LTE-advanced heterogeneous network scenarios," *Wireless Communications, IEEE*, vol. 20, no. 1, pp. 27–34, February 2013.

[124] Y. Wang and K. Pedersen, "Time and Power Domain Interference Management for LTE Networks with Macro-Cells and HeNBs," in *Vehicular Technology Conference (VTC Fall), 2011 IEEE*, Sept 2011, pp. 1–6.

[125] A. Damnjanovic, J. Montojo, J. Cho, H. Ji, J. Yang, and P. Zong, "UE's role in LTE advanced heterogeneous networks," *Communications Magazine, IEEE*, vol. 50, no. 2, pp. 164–176, February 2012.

[126] A. Barbieri, A. Damnjanovic, T. Ji, J. Montojo, Y. Wei, D. Malladi, O. Song, and G. Horn, "LTE Femtocells: System Design and Performance Analysis," *Selected Areas in Communications, IEEE Journal on*, vol. 30, no. 3, pp. 586–594, April 2012.

[127] D. Lopez-Perez, I. Guvenc, G. De la Roche, M. Kountouris, T. Quek, and J. Zhang, "Enhanced intercell interference coordination challenges in heterogeneous networks," *IEEE Wireless Commun.*, vol. 18, no. 3, pp. 22–30, Jun. 2011.

[128] S. Sun, Q. Gao, Y. Peng, Y. Wang, and L. Song, "Interference management through CoMP in 3GPP LTE-advanced networks," *IEEE Wireless Commun. Mag.*, vol. 20, no. 1, pp. 59–66, Feb. 2013.

[129] K. Pedersen, Y. Wang, B. Soret, and F. Frederiksen, "eICIC Functionality and Performance for LTE HetNet Co-Channel Deployments," in *Proc. IEEE 2012 Veh. Technol. Conf. (VTC Fall)*, Sep. 2012, pp. 1–5.

[130] S. Deb, P. Monogioudis, J. Miernik, and J. Seymour, "Algorithms for Enhanced Inter-Cell Interference Coordination (eICIC) in LTE HetNets," *IEEE/ACM Trans. Netw.*, vol. PP, no. 99, pp. 1–1, 2013.

[131] A. Bedekar and R. Agrawal, "Optimal muting and load balancing for eICIC," in *Proc. 2013 11th Int. Symp. Modeling Optimization in Mobile, Ad Hoc Wireless Networks (WiOpt)*, May 2013, pp. 280–287.

[132] K. Somasundaram, "Proportional Fairness in LTE-Advanced Heterogeneous Networks with eICIC," in *Proc. 2013 IEEE 78th Veh. Technol. Conf. (VTC Fall)*, Sep. 2013, pp. 1–6.

[133] S. Lembo, P. Lunden, O. Tirkkonen, and K. Valkealahti, "Optimal muting ratio for Enhanced Inter-Cell Interference Coordination (eICIC) in HetNets," in *Proc. IEEE Int. Conf. Commun. (ICC) Workshops*, Jun. 2013, pp. 1145–1149.

[134] M. Vajapeyam, A. Damnjanovic, J. Montojo, T. Ji, Y. Wei, and D. Malladi, "Downlink FTP Performance of Heterogeneous Networks for LTE-Advanced," in *Proc. IEEE Int. Conf. Commun. (ICC) Workshops*, June 2011, pp. 1–5.

[135] D. Lopez-Perez and H. Claussen, "Duty cycles and load balancing in HetNets with eICIC almost blank subframes," in *Proc. 2013 IEEE 24th Int. Symp. Personal, Indoor Mobile Radio Commun. (PIMRC) Workshops*, Sep. 2013, pp. 173–178.

[136] C. Yang, S. Han, X. Hou, and A. Molisch, "How do we design CoMP to achieve its promised potential?" *IEEE Wireless Commun. Mag.*, vol. 20, no. 1, pp. 67–74, Feb. 2013.

[137] G. Morozov and A. Davydov, "CS/CB CoMP scheme with semi-static data traffic offloading in HetNets," in *Proc. IEEE 24-th Int. Symp. Pers. Indoor Mobile Radio Commun. (PIMRC)*, London, UK, Sep. 2013, pp. 1347–1351.

[138] K. Kwak, H. Lee, H. W. Je, J. Hong, and S. Choi, "Adaptive and Distributed CoMP Scheduling in LTE-Advanced Systems," in *Proc. IEEE 78-th Veh. Technol. Conf. (VTC Fall)*, Sep. 2013, pp. 1–5.

[139] U. Jang, H. Son, J. Park, and S. Lee, "CoMP-CSB for ICI Nulling with User Selection," *IEEE Wireless Commun.*, vol. 10, no. 9, pp. 2982–2993, Sep. 2011.

[140] E. Visotsky, B. Mondal, T. Thomas, N. Mangalvedhe, A. Ghosh, and X. Wang, "Joint Scheduling for CoMP and eICIC in Heterogeneous Network Deployments," in *Vehicular Technology Conference (VTC Spring), 2013 IEEE 77th*, June 2013, pp. 1–5.

[141] Y.-N. R. Li, J. Li, W. Li, Y. Xue, and H. Wu, "CoMP and interference coordination in heterogeneous network for LTE-Advanced," in *Globecom Workshops (GC Wkshps), 2012 IEEE*, Dec 2012, pp. 1107–1111.

[142] W. Luo, Y. Ji, and A. Guo, "An adaptive ABS-CoMP scheme in LTE-Advanced heterogeneous networks," in *Personal Indoor and Mobile Radio Communications (PIMRC), 2013 IEEE 24th International Symposium on*, Sept 2013, pp. 2769–2773.

[143] G. Bartoli, R. Fantacci, D. Marabissi, L. Micciullo, and M. Fossi, "Carrier Allocation Method for AeroMACS System in Airport Channel," *IEEE Trans. Aerosp. Electron. Syst.*, vol. 49, no. 2, pp. 786–797, Apr. 2013.

[144] S. Morosi, D. Marabissi, E. Del Re, R. Fantacci, and N. Del Santo, "A rate adaptive bit-loading algorithm for in-building power-line communications based on dmt-modulated systems," *Power Delivery, IEEE Transactions on*, vol. 21, no. 4, pp. 1892–1897, 2006.

[145] 3GPP, "Evaluations of RSRP/RSRQ measurement," Third Generation Partnership Project, Standard R4-110284, 2010.

[146] T.-D. Nguyen and Y. Han, "A Proportional Fairness Algorithm with QoS Provision in Downlink OFDMA Systems," *IEEE Commun. Lett.*, vol. 10, no. 11, pp. 760–762, Nov. 2006.

[147] 3GPP, "Scenarios and requirements for small cell enhancements for E-UTRA and E-UTRAN," TR36.932 V12.1.0, Tech. Rep., 2013.

[148] V. Chandrasekhar and J. Andrews, "Uplink capacity and interference avoidance for two-tier femtocell networks," *Wireless Communications, IEEE Transactions on*, vol. 8, no. 7, pp. 3498–3509, July 2009.

[149] H. ElSawy, E. Hossain, and M. Haenggi, "Stochastic Geometry for Modeling, Analysis, and Design of Multi-Tier and Cognitive Cellular Wireless Networks: A Survey," *Communications Surveys Tutorials, IEEE*, vol. 15, no. 3, pp. 996–1019, Third 2013.

[150] M. Haenggi, J. Andrews, F. Baccelli, O. Dousse, and M. Franceschetti, "Stochastic geometry and random graphs for the analysis and design of wireless networks," *Selected Areas in Communications, IEEE Journal on*, vol. 27, no. 7, pp. 1029–1046, September 2009.

[151] D. Lopez-Perez, X. Chu, and I. Guvenc, "On the Expanded Region of Picocells in Heterogeneous Networks," *Selected Topics in Signal Processing, IEEE Journal of*, vol. 6, no. 3, pp. 281–294, June 2012.

[152] S. L. Digabel, "Algorithm 909: NOMAD: Nonlinear optimization with the MADS algorithm," *ACM Transactions on Mathematical Software*, vol. 37, no. 4, pp. 1–15, 2011.